University of Southampton

Faculty of Physical Sciences and Engineering

School of Electronics and Computer Science

CHARGE TRAPPING CHARACTERISATION AND ELECTRICAL PERFORMANCE OF THERMALLY AGED POLYMERIC CABLE INSULATION

by

Ziyun Li

A thesis submitted for the degree of Master of Philosophy

September 2020

University of Southampton

Abstract

Faculty of Physical Sciences and Engineering

School of Electronics and Computer Science

Thesis for the degree of Master of Philosophy

CHARGE TRAPPING CHARACTERISATION AND ELECTRICAL PERFORMANCE OF THERMALLY AGED POLYMERIC CABLE INSULATION

by

Ziyun Li

With the growing interest in high voltage direct current (HVDC) transmission systems, the impact of space charge on insulation has attracted more attention recently and the traps in the materials are considered to be one of the dominant factors that affects the electrical performance of the insulation. Meanwhile, in past decades, significant effort has been made to establish the relationship between ageing and the lifetime of electrical insulating materials so that the degree of ageing of insulation can be used to predict its lifetime. Generally, the chemical structure of dielectrics could be affected by ageing, and further electrical performance such as breakdown strength, dielectric loss, and conductivity will change. However, we still cannot use a simple and clear model with few characteristics to connect ageing with chemical and electrical changes to predict insulation lifetime. So, in my research, space charge behaviour is used to explain the ageing process in a HVDC system and the trapping parameters are the key to linking ageing with other electrical properties. In this case, how to use space charge dynamics to estimate the trap parameters, the impact of ageing on trapping, and the relation between trapping and electrical performance are tough problems. The relationship between ageing and trapping parameters will be explored. Hence, the initial trapping parameters and breakdown strength could be used to infer breakdown behaviour after ageing, which means trapping parameters can be used to assess the degree of ageing of the insulation in a HVDC system and predict dielectrics lifetime.

In this thesis, the structure, morphology, and impact on the properties of polyethylene (PE) will be introduced and the thermal ageing mechanisms will be explored. In order to study the innate

character of space charge, the mechanism of charge injection and transport in dielectric materials will be presented. Moreover, previous research on space charge behaviours in polymeric materials is reviewed for clear research direction. The relative space charge and trapping parameters model will also be introduced.

The experimental work focuses on the low-density PE (LDPE) films with different degrees of thermal ageing, its impact on charge trap density, and changes in electrical breakdown strength. The samples were aged in two environments, nitrogen and air, at various temperatures over different lengths of time. The degree of ageing of the samples was characterised using Fourier-transform infrared (FTIR), and differential scanning calorimetry (DSC) was used to investigate the impact of thermal ageing on the internal structure and morphology of PE. Meanwhile, the Raman technique was used to detect the degree of thermal ageing in different layers inside of the films. Space charge dynamics for ageing LDPE were measured using the pulsed electroacoustic (PEA) technique. In addition, the electrical breakdown strength of the aged samples was measured, and breakdown data was processed using the Weibull distribution. DC electrical conductivity was measured to verify the hypothesis about the substantial growth of conductivity in seriously aged LDPE and is the reason a rapid charge decay rate was observed in these samples. The results of a chemical analysis show that thermal ageing in the air leads to a gradual increase in the thermo-oxidative-degree of LDPE. However, the crystallinity of aged films cannot be impacted by the degree of oxidation but the ageing temperature. Nitrogen-aged LDPE, with a notably lower carbonyl index, shows similar trends in DSC tests with air-aged specimens. As for space charge dynamics, traps are introduced into the samples during thermal ageing in the fan oven and deep traps dominate the process. At the early stage of the ageing process, a small number of deep traps in the vicinity of the electrodes can suppress further charge injection, which results in the increase in breakdown strength and the reduction of DC conductivity. During the sustained rise of the degree of ageing, more deep and shallow traps are introduced into the sample, thus higher DC conductivity and lower breakdown strength are detected due to the large amount of charge injection. The space charge behaviours of nitrogen-aged LDPE suggest that deep traps are mainly introduced by oxidation and shallow traps are generated by the thermal effect.

Trapping parameters (injection barrier, trap density, and trap energy level) are evaluated using an improved model. The injection barrier is enhanced by thermal ageing due to surface oxidation. Thermal ageing can introduce traps into LDPE, but the test method for deep ageing samples needs to be modified. The traps introduced by thermal ageing have a higher trap energy level.

Table of Contents

Table of Tables

Table of Figures

Table of Figures

Publications

Journal papers:

1) Li, Z, and Chen, G. *Space charge in thermally aged polyethylene and its electrical performance*. Materials Research Express, vol. 6, no. 3, 2018.

2) Liu, N, Li, Z, Chen, G, Chen, Q, and Li, S. *Space charge dynamics Of CF 4 fluorinated LDPE samples from different fluorination conditions and their DC conductivities*. Materials Research Express, vol 4, no. 7, 2017.

Conference papers:

3) Z. Li, N. Liu, and G. Chen. *Thermal ageing and its impact on charge trap density and breakdown strength in LDPE*. 19th International Symposium on High Voltage Engineering, Pilsen, Czech Republic, August 2015.

4) Z. Li, N. Liu, S. Gabriel and G. Chen. *Thermal ageing and its impact on charge trap density and breakdown strength in Polyethylene*. IEEE Conference on Electrical Insulation and Dielectric Phenomena, Toronto, Canada, October 2016.

5) Z. Li, N. Liu, S. Gabriel and G. Chen. *Thermal Ageing and Its Impact on Charge Trapping Parameters in LDPE*. IEEE Conference on Electrical Insulation and Dielectric Phenomena, Ft, Worth, Texas, United States, October 2017.

Research Thesis: Declaration of Authorship

Print name:	[Your full name]

Title of thesis:	[Thesis title]

I declare that this thesis and the work presented in it are my own and has been generated by me as the result of my own original research.

I confirm that:

1. This work was done wholly or mainly while in candidature for a research degree at this University;
2. Where any part of this thesis has previously been submitted for a degree or any other qualification at this University or any other institution, this has been clearly stated;
3. Where I have consulted the published work of others, this is always clearly attributed;
4. Where I have quoted from the work of others, the source is always given. With the exception of such quotations, this thesis is entirely my own work;
5. I have acknowledged all main sources of help;
6. Where the thesis is based on work done by myself jointly with others, I have made clear exactly what was done by others and what I have contributed myself;
7. Delete as appropriate None of this work has been published before submission or Parts of this work have been published as:

Signature:		Date:	

Acknowledgements

First of all, I would like to present my sincere appreciation and gratitude to my supervisor Professor George Chen. During these years, his erudition, endless patience and professionalism guide me in every piece of my study and research. Whenever I was confused, he gave me enough confidence and motivation to move on in electrical insulation research. I would also like to thank my examiners, Dr. Igor Golosnoy, Dr. James Pilgrim and Dr. Paul Chappell for give my many valuable comments and suggestions to my work.

My special thanks go to my colleague, Dr Ning Liu for a lot of help and advice during my research. I would also like to thank to the technicians in the Tony Davies High Voltage Laboratory for their support on my experimental work.

Finally, thanks to all my friends for their help in Southampton, and thanks to my family for their support and understanding.

Definitions and Abbreviations

AC	Alternating current
AL	Aluminum
ASTM	American Society for Testing and Materials
Au	Gold
CI	Carbonyl index
DC	Direct current
DSC	Differential scanning calorimetry
FTIR	Fourier-Transform Infrared
HDPE	High density polyethylene
HVDC	High voltage Direct current
LDPE	Low-density polyethylene
LIMM	Laser intensity modulation method
LIPP	Laser induced pressure pulse
LLDPE	Linear low-density polyethylene
OIP	Oil-impregnated-paper
PE	Polyethylene
PEA	Pulsed electroacoustic
PWP	Pressure wave propagation
R-square	Coefficient of determination
Sc	Semiconductor
TP	Thermal pulse
TSP	Thermal step pulse
XLPE	Cross-linked polyethylene

Chapter 1 Introduction

Polymers are a category of material with large long-chain macromolecules, composed of many repeated monomer units and branching that are connected by a strong covalent bond. The Nobel laureate, Hermann Staudinger, first proposed this idea in 1920 and laid the foundation for a polymer system[1] after which the application of polymers underwent an explosive development. From the first fully synthetic polymer, Bakelite, in 1909 to the design polymers of today, the research and application of polymers have spanned the fields of biology, physics, chemistry, electrical engineering and others. In many areas, polymers have many different behaviours compared with other solid materials and even provide many irreplaceable technological solutions, especially in electrical insulating applications [2]. Polymers have demonstrated outstanding performance in electrical engineering as polymers used for electrical insulation typically have high dielectric strength and low dielectric loss. LDPE has been widely used as the base material in power cable insulation because of its good electrical performance and stable chemical characteristics. However, in recent years, with the rise of large-capacity and long-distance HVDC transmission systems, the effect of space charge has had a significant impact on insulation selection and design. Space charge has been considered to be both a cause and consequence of ageing in polymeric materials. During high voltage application, particularly for DC conditions, space charge formation in insulation systems can cause an amplification of the electric field in certain locations. As a result, it will accelerate degradation and even lead to an early failure of insulation materials[3].

1.1 Polyethylene

1.1.1 Molecular Structure

Polyethylene (abbreviated PE) is a category of common polymers composed of a monomer unit, ethylene, a gaseous hydrocarbon with the formula C2H2. The molecule consists of a long chain of a number of covalently linked carbon atoms with a pair of hydrogen atoms attached to each carbon [2] that can be viewed as a pair of methylene groups (=CH2) where the chain ends with methyl groups, as shown in Figure 1.1. Thus, the formula of ideal pure PE composed with alkanes is C2nH4n+2, where n is the degree of polymerisation and describes the number of ethylene units polymerised to form the backbone. The typical degree of polymerisation n exceeds 100 and can reach up to 280,000 or even more. The H-C-H bond angle in PE is 112° instead of 90° in ethylene, the C-C angle is 108°, the C-C bond length is 0.18nm, and the C-H bond is 0.11nm [4].

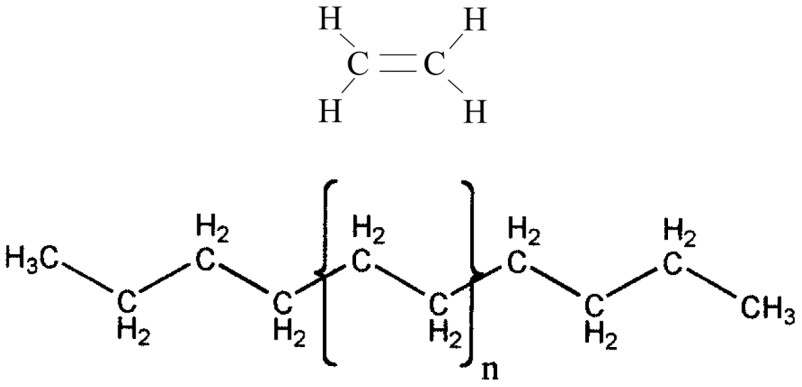

Figure 1.1: Chemical structure of ethylene unit and pure polyethylene[5].

PE is a semicrystalline polymer, which indicates that its molecular chains are arranged in a regular and periodic manner in some regions (i.e. the crystalline region), while the chains in other regions are formed randomly (i.e. the amorphous region). If ν_c is the volume of crystalline material and ν_a is the volume of amorphous region with a sample, then the volume crystallinity $\chi_V = \nu_c/(\nu_a + \nu_c)$ [4]. The volume ratio between the crystalline region and amorphous region will determine the property of the polymer materials, thus the degree of volume crystallinity is established to estimate the crystalline proportion, which is given as χ_V :

$$\chi_V = \frac{\nu_a - \nu_m}{\nu_a - \nu_c} \tag{1.1}$$

where ν_m is the specific volume of certain semicrystalline materials, ν_a is the specific volume of pure amorphous fraction, and ν_c is the crystalline fraction of that material [6]. The PE with few chains defects have a higher degree of crystallinity than those that have many defects. Generally, the polymer with a higher concentration of branches has a lower density, that is, the overall density of the material rises with the increment of crystallinity [2]. Therefore, PE is classified into several different categories based on its density and branching. Different types of PE have different mechanical properties that is strongly dependent on the molecular weight and the extent and degree of branching and crystallinity. There are four typical categories of PE: high-density PE (HDPE), LDPE, linear low-density PE (LLDPE), and crosslinked PE (XLPE).

HDPE is chemically closest to ideal pure PE, as shown in Figure 1.2(a). With an extremely low level of defects to hinder chain arrangement, a high degree of crystallinity can be achieved resulting in a high density that is generally between 0.93 to 0.98g/cm^3, and hence, stronger tensile strength and better resistance to chemical attack but less transparency. LDPE is a type of PE that contains substantial concentrations of branches that hinder crystallisation resulting in relatively lower densities that fall between 0.91 to 0.93g/cm^3, as shown in Figure 1.2(b). Principally, the branches

are composed of ethyl and butyl groups and some long-chain branches. LLDPE resins consist of molecules with linear PE chains to which short alkyl groups are attached at random intervals, as shown in Figure 1.2(c). The branches, in this case, are mainly ethyl, butyl, or hexyl groups that will hinder crystallisation to some extent resulting in a density range from 0.90 to 0.94g/cm^3. XLPE is a type of special PE that has been chemically modified to covalently link adjacent chains, as shown in Figure 1.2(d). Crosslinks are comprised of either direct C-C bonds or bridging species such as siloxanes, resulting in the creation of a gel-like network, which is essentially insoluble and thus makes XLPE a thermosetting material. Because of its unique mechanical properties, XLPE has been widely used in high voltage insulation, especially in high voltage cables [2].

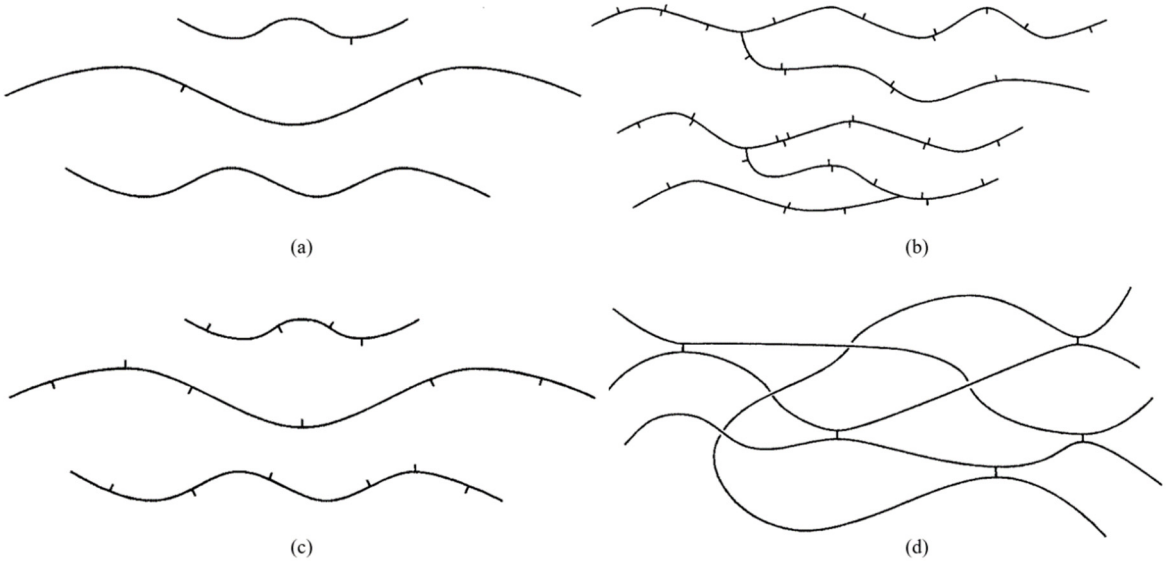

Figure 1.2: Schematic representation of different types of polyethylene. (a) High density polyethylene; (b) Low density polyethylene; (c) Linear low density polyethylene; (d) Cross-linked polyethylene [2].

1.1.2 Morphology

In polymer materials, the morphology is used to describe the arrangement of polymer molecules in a solid or molten state. PE is a semicrystalline polymer that is composed of both crystalline and amorphous parts. In fact, most crystalline polymers are semicrystalline polymers consisting of two or more solid phases, in at least one of which molecular chains are arranged with a regular three-dimensional array and in one or more other phases the chains are disordered. The physical properties of PE products are dominated by the crystalline or noncrystalline phase and their size, shape, orientation, connectivity, etc., with respect to one another [2].

The change in volume with the temperature for amorphous and semicrystalline polymers is represented in Figure 1.3. When semicrystalline polymers are cooled down from a liquid state at the melting point, the specific volume drops very abruptly resulting in the formation of crystalline structures with regularly arranged molecules. As for amorphous polymers, the specific volume declines continuously and linearly as the temperature cools from the melting point to the glass transition point. Yet, both of these categories of polymers are mechanically rubbery at temperatures between the melting and glass transition points, and the specific volume drops at a much slower rate during the glassy state after the glass transition point. For LDPE, the melting temperature is 378K to 388K and the glass transition temperature is about 165K [7].

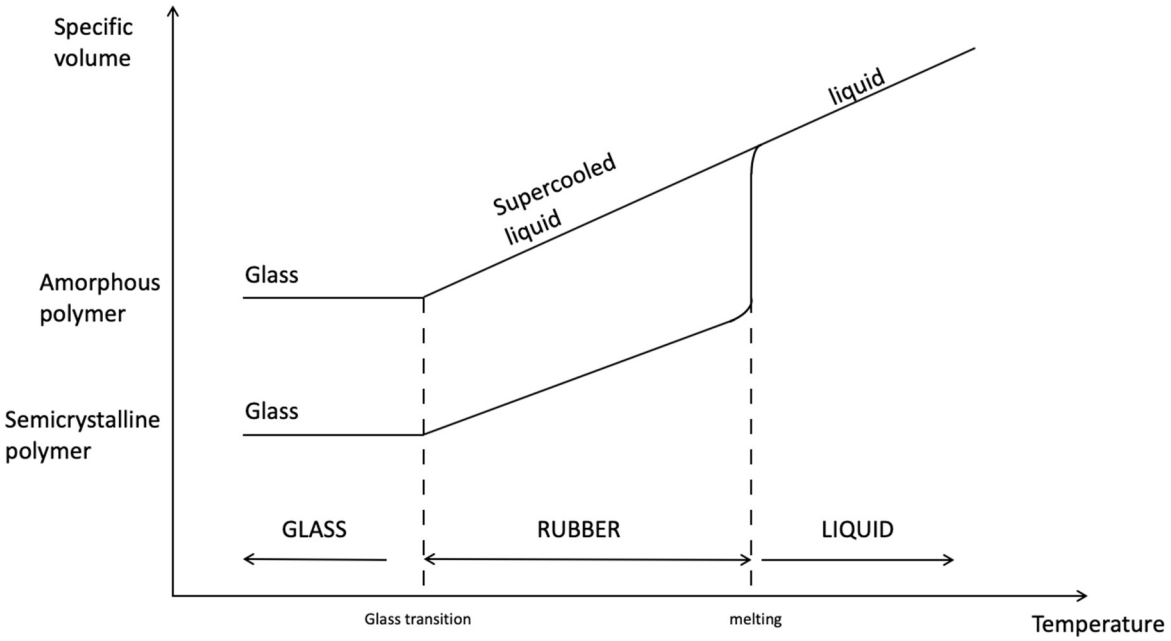

Figure 1.3: A schematic diagram representing the decease of specific volume with temperature for amorphous and semi-crystalline polymers [1].

The most general morphology of PE is that a crystallite's a and b dimensions are much greater than its c dimension, that is, two-dimension crystals grow much bigger than the third dimension, which is termed 'lamellae', as illustrated in Figure 1.4 [2]. The lateral dimensions can vary over several orders of magnitude for crystals grown from a solution to form a crystalline region. Moreover, lamellae will grow outward rapidly from nucleation sites and form 'spherulites', which is the most common large-scale structure of polymers composed of crystalline and noncrystalline regions, as shown in Figure 1.5 [1]. The size of spherulites is restricted by the crystallisation time and the concentration of nucleation sites. The size will also influence the physical properties, such as density and hardness.

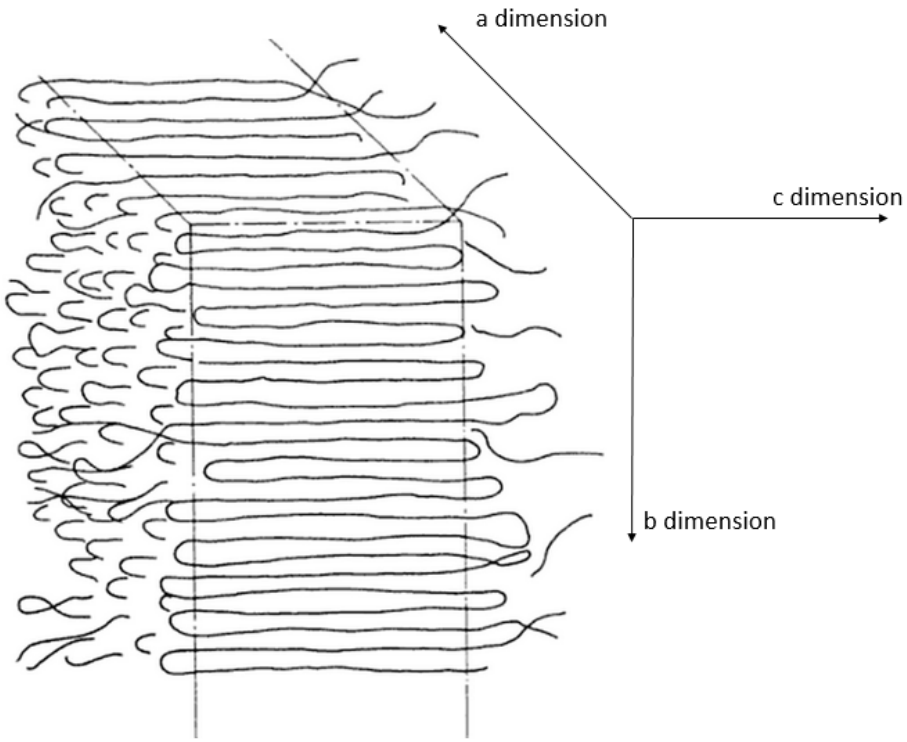

Figure 1.4: Schematic representation of a polyethylene lamella [2].

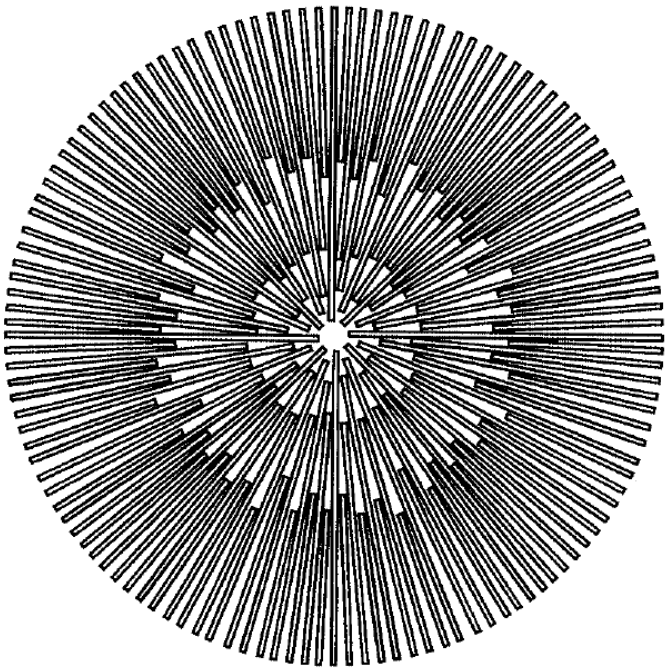

Figure 1.5: Schematic representation of a spherulite [1].

1.1.3 Polyethylene as High Voltage Insulator

The strong bond between electrons and nuclei within the polymer molecule, in which the electrons reside in σ - orbitals and are localised to their bonds, results in a substantial band gap for some

polymers, especially PE as an insulator. Meanwhile, PE has good physical qualities in cracking and moisture resistance. As the XLPE has a unique chain structure, the XLPE-insulated cable is able to operate at up to 90°C, which is higher than the oil impregnated paper (OIP) insulated cable [8]. In fact, compared with a traditional oil-paper insulation system, PE, as a non-polar material, has many advantages as an insulator such as lowering the manufacturing cost, easy installation and handling, high dielectric strength, high electrical resistivity, and low dielectric loss factor. The electrical properties of the three PE types are shown in Table 1.1 [7].

Table 1.1: Electrical properties of typical polyethylene

Parameters	**LDPE**	**HDPE**	**XLPE**
Relative Permittivity $\mathcal{E}_r$ (Test frequency: 1KHZ)	2.28-2.38	2.3-2.38	2.4
Dissipation factor $Tan(\delta)$ （1MHZ）	1-10 x 10^{-4}	10^{-3}	10^{-3}
Breakdown strength (kVmm-1)	20-180	20-180	80
Volume resistivity (Ω·cm)	>1018	>1018	~1018
Arc resistance (sec)	138-180	200-280	-

From the first installation of 228kV cables manufactured with LDPE in France, tonnes of high voltage cables with PE have been put into operation and this electrical transmission solution has undergone rapid development in the past few decades [9]. The improvements in PE manufacture and relative technology allows us to design materials capable of operating at higher voltages of up to 500kV, further distances, and in more complex environments such as the seabed. As the HVDC technique has recognised advantages in large-capacity, long-distance transmission systems, and connection between power grids with different frequencies, HVDC cables with polymeric insulation have been considered to be used for a long time. Furthermore, renewable clean energy, such as wind power, has an indispensable role in energy structure that encourages the development of HVDC cables [10]. However, during HVDC application, charges may be injected and trapped inside of the material. Space charge formation in insulation systems can cause an amplification of the electric field in certain locations, which may lead to an early dielectric failure [3]. Thus, space charge research in polymeric insulation is an urgent task for HVDC insulation selection and design.

1.2 Thermal ageing in polymer insulation

In past decades, significant efforts have been made to establish the relationship between ageing and the lifetime of electrical insulating materials. Generally, the chemical and physical structure of dielectrics can be affected by ageing resulting in the deterioration of their electrical performance (such as breakdown strength, dielectric loss, and conductivity). In this research, thermal ageing is the key factor considered to explore the relationship between ageing and space charge

performance in PE. Therefore, previous research about the chemical impact and morphology changes from high temperatures in polymeric insulation materials are reviewed in this chapter.

1.2.1 Thermal Ageing Impact on chemical properties

PE has been widely used not only in insulation systems but many other areas since the 20th century. Generally, polymer degradation is caused by physical and chemical factors. Physical factors include heat, light, ionising radiation, mechanical processing and others. and chemical factors such as oxygen, ozone, chemicals and polymerisation catalysts. A lot of studies have been conducted on PE degradation in different situations such as radiation, atmospheric oxygen, humidity, rain, sand, wind, and extreme temperatures [11], [12].

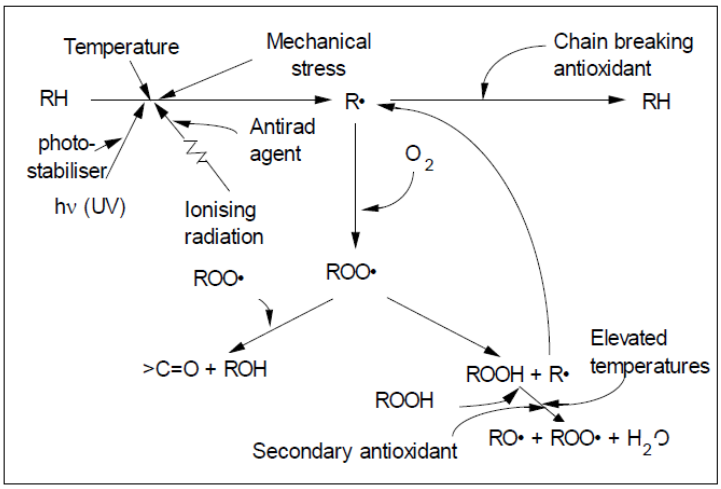

Figure 1.6: Degradation mechanism of polymeric materials [13].

Generally, thermal ageing is a kind of basic degradation process in different fields. In most polymers, the generic oxidation mechanism that controls thermal ageing is the 'Boland mechanism', which acts in three stages: initiation, propagation, and termination [15], [16]. In the first stage, the thermal energy leads to the abstraction of a hydrogen atom from a polymeric chain, and the peroxide (ROO^{o}) is formed from a macroradical (R^{o}) with oxygen. In a further propagation stage, the peroxide abstracts another hydrogen atom to create a hydroperoxide (ROOH). Finally, in the last stage, the different radicals combine and form a variety of groups such as ketones (R=O), hydroperoxides (ROOH), alkyl chains (R-R), and esters (RC(O)-OR) that are illustrated in Figure 1.6.

In [11], commercial LDPE films were aged at 70°C for up to 21 months to analyse their mechanical properties and molecular microstructure. First, according to the Fourier-Transform Infrared Measurement (FTIR) results, it was found that the Carbon-oxygen groups were introduced during ageing; the carbonyl structure in thermally aged PE is shown in Figure 1.7.

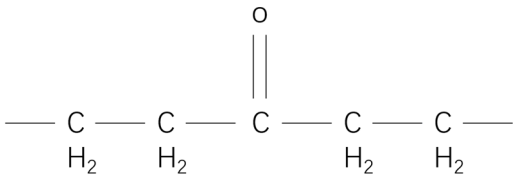

Figure 1.7. Carbonyl structure in thermally aged polyethylene.

Meanwhile, the C13 NMR (nuclear magnetic resonance spectroscopy) result shows that the crosslinks play a secondary role in thermal ageing (shown in Figure 1.8). In the Figure 1.8, it is shown that the Carbon-carbon double bond is broken due to the ageing, and the new Carbon-carbon single bond is formed.

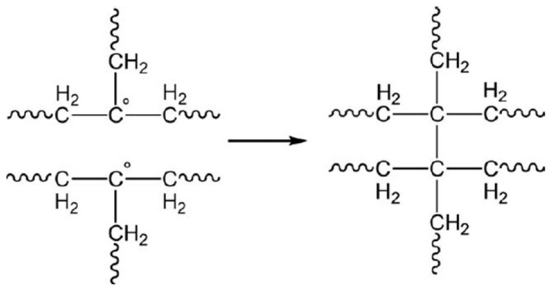

Figure 1.8. Formation of a crosslink between two polymeric chains during thermal ageing [11].

1.2.2 Thermal Ageing Impact on electrical properties

Direct evidence from AC-endurance tests carried out on peelings from XLPE cable insulation at a standard temperature of 383K and field of 80kV/mm has shown that high temperatures during cable stressing ages the insulation [14]. Previous studies of space charge behaviour in cable peeling have shown that ageing results in changes to the density and depth of charge traps [15]. The density indicates the space charge density inside of the insulation, and the charge traps means the energy level or the charge trap. Furthermore, in [16], space charge measurements were applied to insulation peeling taken from a single 90kV AC transmission cable whose segments had been stressed for between 8,000 and 10,000 hours at different temperatures (293K and 383K). The results show that both AC electrical or thermal stressing contributes to the modification of charge trap distribution in XLPE insulation. The two types of cable stress result in a reduced generation of shallow positive charge traps and increases the number density of deep positive charge traps. Meanwhile, the endurance lifetime is reduced in thermally stressed cable segments and it has been associated with the decrease of the amount of shallow-trapped charges and the rise of deep-trapped charges. In crystal, dislocations and intrinsic cationic and anionic vacancy do not contribute so much to trapping, but the substituted defect is one of the most efficient trapping processes. The later defect can be split into two categories, one is called passive trapping centres, associated with

anion vacancies, which can be identified optically by the means of absorption and emission spectra and can be permanently trapped below 200°C. The other category is called active trapping centres and they are associated with substituted cations that are very difficult to identify optically because the electron binding energy must be small. These centres are probably the main source of stress regarding ageing [17]–[19]. Previous research has shown that the injection of electrons from the cathode and the extraction of electrons to the anode (i.e. injection from the anode) are the main mechanisms for the emission of charge in most polymers.

In [20], the XLPE sheet samples were aged at 80°C and 140°C during 5,000 hours, and X-ray diffraction was applied to explore the effect of thermal ageing on the crystallinity of XLPE insulation cables. However, their result shows that thermal ageing does not have any effect on the crystalline phase of XLPE. In [21], LDPE films with different thicknesses, from 30μm to 90μm, were aged in an air oven at 90°C. Following wide-angle X-ray scattering (WAXS) and small angle X-ray scattering (SAXS), this shows that thermal ageing of LDPE in air induces oxidation and scission of molecular chains. Its crystallinity increases and long period decreases, as shown in Figure 1.9. Meanwhile, in the higher temperature ageing sample, the current density becomes larger and the breakdown strength decreases. This is explained by the carbonyl groups in amorphous parts that act as hopping sites for electrons, and the impulse thermal breakdown is considered to dominate due to oxidation after long term thermal ageing.

In [22], the LDPE samples with a thickness of 150μm were thermally aged at 100°C in air, and 180°C, 160°C, 145°C, and 140°C both in air and vacuum conditions. It was found that thermal oxidation has a strong impact on the electrical performance of the LDPE. When the ageing temperature is below the melting point (114°C), the changes in electrical breakdown strength are related to carbonyl groups. At high temperatures, the decrease in breakdown strength is closely associated with oxidation, chain scission, crosslinking, and a reduction in crystallinity. As for the sample aged above 150°C, different degradation mechanisms may be involved.

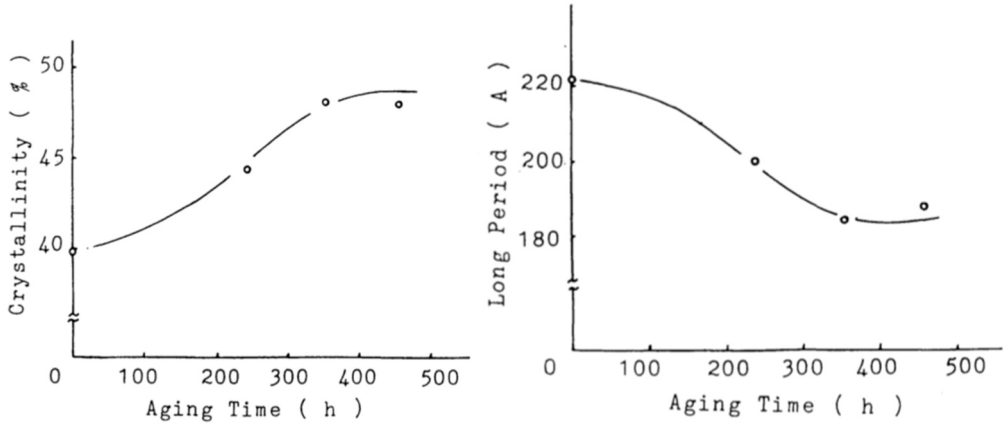

Figure 1.9. Ageing time dependence of crystallinity (left) and long period (right) in PE aged at 90°C in the air[21].

1.3 Research Motivation and Objectives

As discussed above, PE has been widely used as power cable insulation because of its good electrical performance and stable chemical characteristics. However, in recent years, with the increased use of HVDC transmission systems, space charge has become a problem that cannot be ignored, and it has been considered to be both a cause and consequence of ageing in polymeric materials that can lead to local distortions in electric field distribution. Therefore, the first step of this research is to get a better understanding of charge characteristics in dielectrics including charge generation and transportation. Traps, as charge capturing sites inside materials, play an important role in space charge behaviours as they are related to physical and chemical defects [23]. In order to comprehend the space charge state of polymers, research about this trapping and detrapping behaviour is necessary.

It has been reported that ageing leads to an increase in charge trap density. The increase of trap density in polymeric material makes the transport of charge carriers between traps easier. Meanwhile, the deep traps from ageing in the vicinity of the electrodes leads to electric field distortion [24]. In recent years, several space charge ageing models have been proposed to describe the relationship between the charge trap and insulation life, which will hopefully improve insulation design. In previous research [25], the ageing of LDPE film and XLPE film taken from high voltage AC serviced cables, which were in operation for up to 12 years, were used to test a model for using trapping parameters to reflect the degree of ageing quantitatively. Nevertheless, the data collected from the retired cables was affected by several factors such as electrical, thermal, or radiation influence. To modify and simplify the model, a control experiment on the insulation material with fewer influential factors is necessary. Thus, we attempt to design an solution to use the change in charge trap density to characterise the electrical performance of the material, moreover, the ageing status of the material. The solution includes more mature experiments and more accurate simulation calculation.

1.4 Outline of the thesis

This report has been organised into the following chapters.

Chapter 2 Charge transport and space charge studies in polymeric materials: A literature review of charge injection, transport mechanisms, and previous space charge studies is conducted in this chapter. Meanwhile, space charge and trapping parameter models are introduced.

Chapter 3 Sample preparation, thermal ageing, and chemical analysis: The ageing sample preparation process and relative chemical analysis results, that is, the FTIR, DSC, and Raman are introduced.

Chapter 4 Space charge performance in thermal ageing LDPE: The space charge phenomena of different kinds of thermal ageing LDPE were measured by the PEA technique, and the results are shown and analysed in this chapter.

Chapter 5 DC breakdown strength and DC conductivity: In this chapter, the DC breakdown strength and DC conductivity are measured and the results are discussed.

Chapter 6 Thermal ageing and its impact on charge trapping parameters: In this chapter, the trapping parameters of ageing samples estimated by an improved model will be described, and a comparative analysis based on experimental data and simulation results is made. The limitation of this model is also discussed.

Chapter 7 Conclusion and future work: There is a brief conclusion based on current research in this chapter and future work is also discussed.

Chapter 2 Charge transport and space charge research in polymeric materials

Space charge is a concept involving charges such as electrons, ions, and charged particles. It is generally described as trapped charge and occurs when charge is captured and accumulates in the bulk of dielectric materials. It typically happens around the interfaces of impurity, physical defects, chemical clusters, crystal-amorphous areas, or between the chains of polymer molecules. In addition, charges can accumulate at the interfaces between conductors and insulators or at the interfaces between different dielectric materials, such as oil and paper pressboard. The process of enhanced thermal electronic injection from electrodes is considered to be the primary reason for the formation of space charges. Meanwhile, charges can also be generated from dissociation of impurities or additives within insulation materials when applying external electric fields. They can be trapped in capture centres, which are named “traps”; relevant traps may be produced because of contamination during material manufacturing, machining, and usage, etc. Charges with heteropolarity can recombine and then effectively disappear in a process that often results in photonic emission.

2.1 Charge Injection Mechanisms

In an ideal electrode-insulator system, carriers will flow from the conductor to the insulator or from the insulator to conductor until the Fermi levels of electrode and insulator establish the equilibrium, when an insulator contacts with a conductor. Fermi level is defined as the top of the collection of electron energy levers at absolute zero temperature. This process depends on the work function of these two materials and the surface condition of the contact. The nature of the contact surface is complex and can involve the presence of physical and chemical defects such as surface roughness, imperfect contact, chemical impurities including oxidation and moisture, dangling bonds, local polarisation resulting in band bending, donor-acceptor states, and trap states [1]. The potential barrier heights and electrical performance of the contact are heavily impacted by the surface conditions. Generally, three types of electrical contacts occur between electrodes and insulators: neutral contact, blocking contact, and ohmic contact [17]. The two electron-injection mechanisms that are based on the electron energy-band diagram, Richardson-Schottky injection and Fowler-Nordheim injection, are reviewed in the following sections.

2.1.1 Schottky Injection

The potential barrier at the interface between the metal and insulator, which prevents the easy injection of electrons from the metal into the insulator, is assumed to be abrupt (see Fig. 2.1). In this figure, E_f means the original potential barrier height of metal, and the barrier height (eV) comes from the barrier which is formed between two different materials with different conductivity. The primary form of carrier injection, which is Schottky injection, can be customized in many ways and can produce a variety of Schottky-type behaviours, depending on the desired modifications [1][26]. The injection at the metal-polymer interface with the electrode is referred to as a neutral contact.

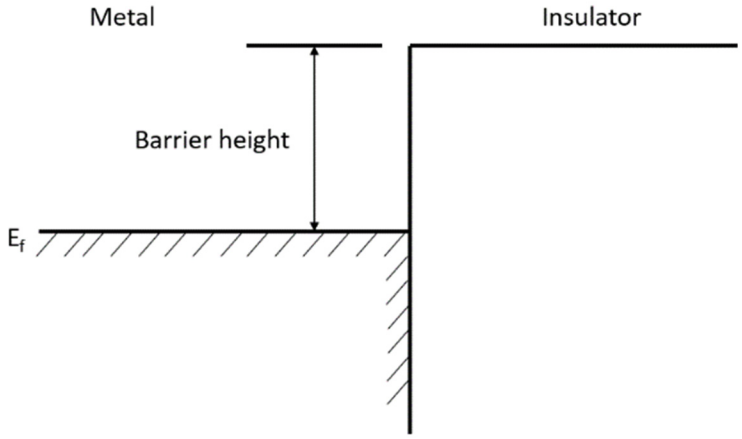

Figure 2.1: The potential barrier at the interface between the metal and insulator.

The original potential barrier height ϕ_B at the interface without external field is determined by the work function of the metal ϕ_m and the electron affinity χ of the insulator, and $\phi_B = \phi_m - \chi$. This barrier height could be reduced by an applied field and the image charge effect, which would enhance the electron injection. This injection model is refined by assuming that the barrier is due to the electrostatic attraction between the electron and the metal. To calculate the attraction between the point charge and the plane, an assumption is made that the plane is replaced by an equal and opposite charge, from symmetry, and the opposite point charge is an equal distance behind the surface of the plane. This is known as the image charge theorem. If x is the distance from the interface, the potential energy of the electron $V(x)$ can be defined as the energy required to take the electron from position x to infinity and is given by Coulomb's law. Furthermore, the potential energy must approach the metal work function, ϕ_m and not $-\infty$, as $x \to 0$. So the $V(x)$ could be given as

$$V(x, image) = -\frac{q^2}{16\pi\varepsilon_o\varepsilon_r x + (q^2/\phi_m)} \tag{2.1}$$

If an external electric field is now applied, and we assume that this is constant in the region of the interface and of magnitude F in the x-direction, then the potential is given by

$$V(x,field) = -qFx \tag{2.2}$$

Meanwhile, Eq. 3.1 can be simplified by assuming $16\pi\varepsilon_0\varepsilon_r x$ is much higher than q^2/ϕ_m. If this were not true, the theory would break down anyway, as $x \to a$, the interatomic spacing, and the influence of particular lattice atoms would predominate. The new potential barrier height $\psi(x)$ is shown by Fig. 2.2 and given by

$$\psi(x) = \phi_m - \chi - \frac{q^2}{16\pi\varepsilon_0\varepsilon_r x} - qFx \tag{2.3}$$

The height of the potential barrier, $V_m = V(x = x_m)$ can be found by differentiating the potential barrier height as a function of distance is zero. So the optimal point x_m is obtained:

$$x_m = \left(\frac{q^2}{16\pi\varepsilon_0\varepsilon_r F}\right)^{1/2} \tag{2.4}$$

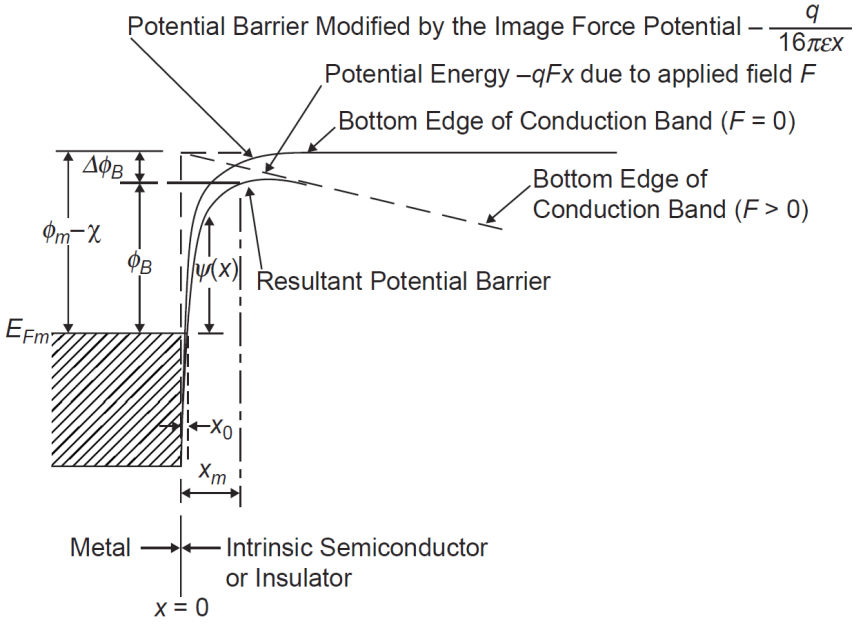

Figure 2.2: The potential barrier lowered by the applied field and image force between a metal and an insulator [17].

Thus, the minimal height of the potential barrier is:

$$\psi = \phi_m - \chi - \left(\frac{q^3 F}{4\pi\varepsilon_0\varepsilon_r}\right)^{1/2} \tag{2.5}$$

In terms of Richardson-Dushman equation, emitted current density J at the absolute temperature T could be expressed:

$$J = A_0 T^2 \exp\left(-\frac{\psi}{k_B T}\right) \tag{2.6}$$

and introducing the expression of the minimal height of the potential barrier, ψ:

$$\begin{aligned} J &= A_0 T^2 \exp\left\{-\frac{\phi_m - \chi - \left(\frac{q^3 F}{4\pi\varepsilon_0\varepsilon_r}\right)^{1/2}}{k_B T}\right\} \\ &= A_0 T^2 \exp\left(-\frac{\phi_B}{k_B T}\right)\exp\left(\frac{1}{k_B T}\left(\frac{q^3 F}{4\pi\varepsilon}\right)^{1/2}\right) \end{aligned} \tag{2.7}$$

where k_B is the Boltzmann constant. In Eq. 3.7, the pre-exponential factor $A_0 = \frac{4\pi q m_e k_B^2 (1-R)}{h^3}$, where h is the Planck constant, m_e is the effective mass of electron and, R is the reflection coefficient of electron interface. A constant term $A = 4\pi q m_e k_B^2 / h^3 = 1.20 \times 10^6 A \cdot m^{-2} K^{-1}$ is often identified.

2.1.2 Fowler-Nordheim Injection

Schottky injection describe a process in which an electron gains enough energy to overpass the potential barrier at the interface between conductor and insulator. In classical mechanics, a particle cannot enter a region in which its total energy is less than the potential energy required. However, the Fowler-Nordheim injection model shows that electrons with insufficient energy do have a finite probability to pass through the barrier. This process, based on the quantum mechanical theory and known as tunnelling, is shown in Fig. 2.3 [27]. The current density of electron tunnelling can be calculated [28]:

$$J(F) = \frac{q^3 m_0 F^2}{8\pi h m_e \phi_B}\exp\left(-\frac{8\pi\sqrt{2m_e}}{3qhF}\phi_B^{3/2}\right) \tag{2.8}$$

where q is the electronic charge, m_0 is the mass of free electron, m_e is the effective mass of tunnelling electron, F is the applied field, h is the Planck constant, ϕ_B is the potential barrier height. If we assume $m_0 = m_e = m$, then the tunnelling current density can be simplified as

$$J(F) = \frac{q^3 F^2}{8\pi h \phi_B}\exp\left(-\frac{8\pi\sqrt{2m}}{3qhF}\phi_B^{3/2}\right) \tag{2.9}$$

This type of carrier injection is expected only to occur at very high fields ($>10^9 V/m$) where the potential barrier at the interface is severely distorted and becomes thin enough to allow tunnelling [1]. The applied fields required for this type of injection surely would be above the observed breakdown strength of LDPE, which is in the range of $10^8 V/m$ [29]. Fowler-Nordheim injection followed by avalanche breakdown has been observed in very thin films of Parylene, in which the conductivity was almost independent of temperature [29].

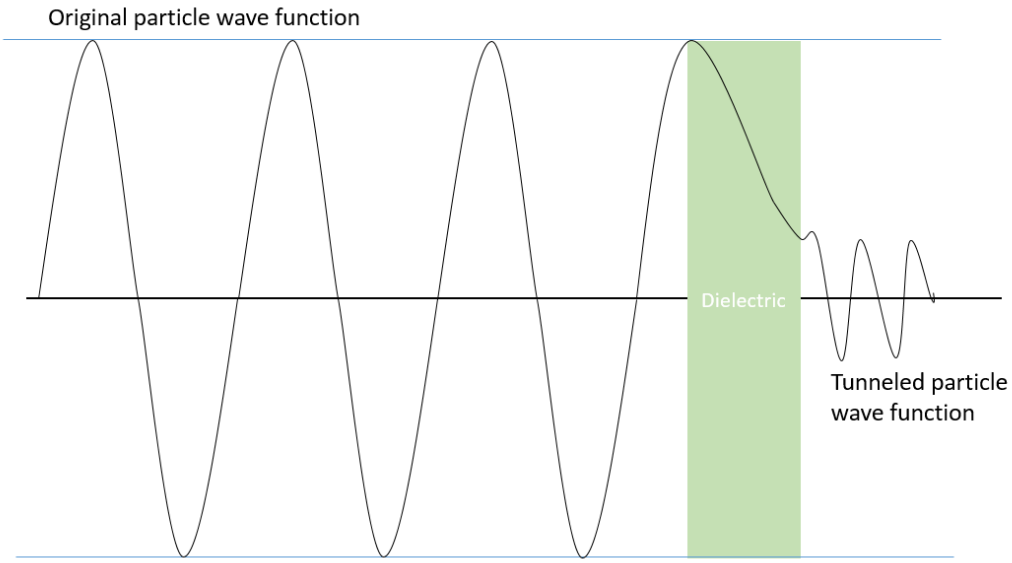

Figure 2.3: The schematic diagram about Fowler-Nordheim Tunnelling.

2.2 Charge Transport Mechanisms

At low electric fields, the voltage-current relation tends to follow Ohm's law, although it is difficult to verify in insulator conditions as currents are usually very small in low electric fields. This occurrence is generally explained in terms of Ohmic conduction. The Ohmic conductivity model always predicts reasonably high mobility, which is not found in insulators. In low fields, a linear voltage-current relation can be easily observed, but in high fields the behaviour becomes different. After being injected into the bulk, it is difficult for charges to move further through the bulk under high fields. Thus, space charges may be accumulated near the electrodes or throughout the bulk, which may limit the further movement of the charge. In high fields, several classic theories describe the conduction process in dielectrics, such as space charge limited current, hopping mechanism, and Poole-Frenkel mechanism. The definition of low and high fields is related to the conductivity of the material.

2.2.1 Space Charge Limited Conduction

Space charge limited current can occur in insulating thin films and is found to be highly dependent on thickness, because space charge accumulation will diffuse into bulk [30]. In a piece of thin insulator which has good contact with the conductor, there may be a very small amount of free charge in the material initially, but more free charge may be injected after application of the electric field. In this theory, it will be assumed that the charge injected into the dielectric is uniformly distributed and that the electric field is constant to simplify the model. Consider an ideal dielectric in which there are no thermally generated carriers, no traps, and only one type of carrier (i.e. electrons or holes). Additionally, the contact between electrode and dielectric is an ohmic contact, which means good injection conditions. In the case of a dielectric without traps, the total current density in the bulk constitutes three parts: drift, diffusion, and displacement current:

$$J = ne\mu F - eD_n \frac{dn}{dx} + \varepsilon_0 \varepsilon_r \frac{dF}{dt} \tag{2.10}$$

where n and μ are the density and mobility of electrons, D_n is the Fick's diffusion coefficient for electrons, and F is the applied electric field. Assuming steady-state electric fields, $dF/dt = 0$. In terms of Poisson's equation, $dF/dx = ne/\varepsilon_0 \varepsilon_r$, the current density is

$$J = \varepsilon_0 \varepsilon_r \mu F \frac{dF}{dx} - \varepsilon_0 \varepsilon_r D_n \frac{d^2 F}{dx^2} \tag{2.11}$$

Because the effect of charge near the injecting electrode dominates the charge accumulation process in dielectrics, the field approaches zero, which would mean the current is a pure diffusion current. However, to simplify the mathematical calculation, the electrons inside the bulk are assumed to be uniformly distributed over the thin thickness, and the diffusion terms are neglected. Thus,

$$J = \varepsilon_0 \varepsilon_r \mu F \frac{dF}{dx} \tag{2.12}$$

Rearranging Eq. 2.11 and integrating both sides, the corresponding F is given by

$$F = \left(\frac{2J}{\varepsilon_0 \varepsilon_r \mu} (x + x_0) \right)^{1/2} \tag{2.13}$$

The relationship between current density and voltage can be calculated by Eq. 3.13, using $V = \int_0^d F dx$. Assuming that x_0 is much smaller than d, the current density is given by

$$J = \frac{9\varepsilon_0\varepsilon_r\mu V^2}{8d^3} \tag{2.14}$$

The charge density, n, in the dielectric is made up of two components, n_0 and n_1, where n_1 is an injection term. So the current density can be thought of as consisting of two parts:

$$J = n_0 e\mu\frac{V}{d} + \frac{9\varepsilon_0\varepsilon_r\mu V^2}{8d^3} \tag{2.15}$$

where the first term is the ohmic conduction and the latter term is the space charge limited conduction. If $n_1 > n_0$, the space charge limited current dominates. The transition voltage, V_{tr} is the voltage at which the space charge limited current begins to dominate over the ohmic current. It can be calculated by equating the ohmic and space charge limited current:

$$V_{tr} = \frac{8en_0d^2}{9\varepsilon_0\varepsilon_r} \tag{2.16}$$

The discussion above is only valid for a trap-free insulator. For an insulator with defects or impurities, the effect of traps on ohmic conduction gives the proportion of electrons $\theta = (n_c/n_t)$, where n_c is free carrier density and n_t is total charge carrier density. If electrons are injected into the dielectric, only the fraction θ will contribute to the current. In this case, the current density and transition voltage is given by

$$\begin{aligned} J &= n_0 e\mu\frac{V}{d} + \theta\frac{9\varepsilon_0\varepsilon_r\mu V^2}{8d^3} \\ V_{tr} &= \frac{1}{\theta}\frac{8en_0d^2}{9\varepsilon_0\varepsilon_r} \end{aligned} \tag{2.17}$$

Note that the above equations are for the case of shallow traps (i.e. $E_{trap} - E_{Fermi}$ is much greater than k_BT). However, when the voltage rises significantly, the number density of injected charge carriers will be approximately equal to the number density of traps, and the Fermi energy level will rise above the trap energy level. In this case, the traps should be considered as deep traps, and all the traps are filled (i.e. space charge is primarily due to traps). Therefore, the current in this case is trap-filled limit current, and the relative transition voltage, V_{TFL}, can be calculated using Poisson's equation[1]:

$$V_{TFL} = \frac{eN_td^2}{2\varepsilon_0\varepsilon_r} \tag{2.18}$$

Where N_t is the number density of traps.

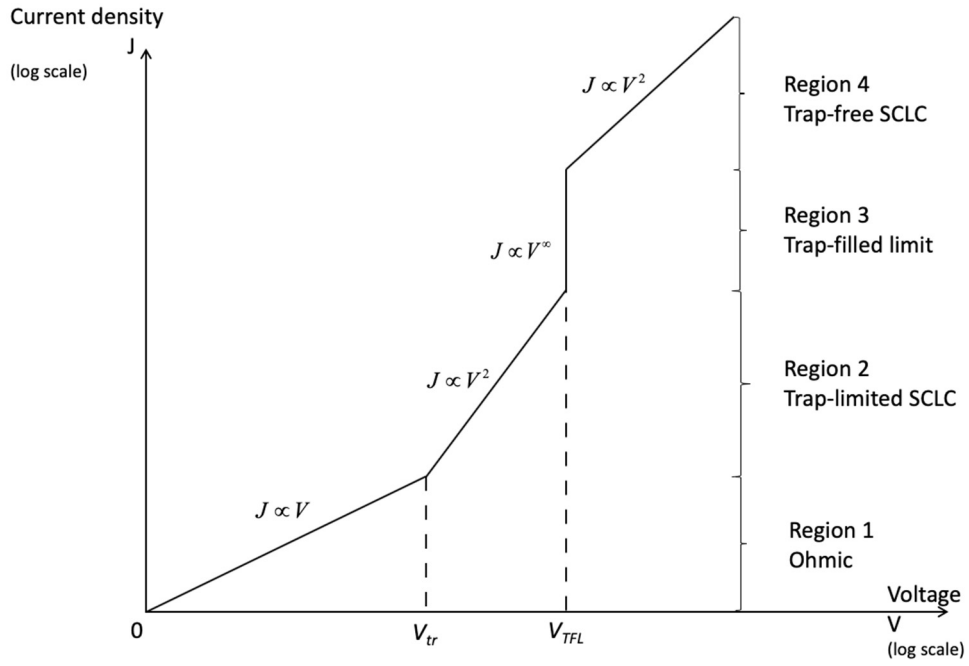

Figure 2.4: Graph showing current density vs. voltage for an ideal case of space-charge limited current [1].

In conclusion, there are four relations between voltage and current density, as shown with schematic $\log(J)$ vs. $\log(V)$ in Figure 2.4:

- Region 1: $0 < V < V_{tr}$, ohmic conduction
- Region 2: $V_{tr} < V < V_{TFL}$, trap-limited space charge limited conduction
- Region 3: $V = V_{TFL}$, all traps at energy level E_t are filled
- Region 4: $V > V_{TFL}$, trap-free space charge limited conduction

2.2.2 Hopping Conduction

In insulators, the Fermi energy level is less than the mobility gap edge; thus, the conduction in insulators can be either by excitation to the mobility edge (although excitation to the mobility edge is unlikely in insulators with large mobility gaps) or by thermally activated transfer between localised sites, which is termed “hopping” [1]. Localised sites here act as trap sites for captured electrons or holes, which exist in forbidden band gaps at various energy levels, as shown in Fig. 2.5. The hopping conduction describes a probability that a carrier, which has occupied a localised site, gains sufficient energy from the thermal vibration and phonon interaction and then travels to a nearby unoccupied site for a small amount of time before being recaptured by another localised state [31]. The local transfer mechanism can proceed by either thermal excitation over a potential barrier, tunnelling through it, or a combination of thermal excitation and tunnelling. Therefore, the overall probability of transfer in this mechanism is a joint probability for the two processes:

$$P(therm) \propto \exp\left\{-\frac{\Delta E(R)}{k_B T}\right\} \tag{2.19}$$

$$P(tun) \propto \exp\{-2\alpha R\} \tag{2.20}$$

where R is the distance between the two localised sites; $\Delta E(R)$ is the difference between the energy levels of the two sites involved; k_B is the Boltzmann constant; and T is the temperature. While assuming all the localised states are at a single level with energy ϕ and considering only the thermal excitation process, the probability of electrons hopping through per unit time is given by

$$P_0 = v \exp\left\{-\frac{\phi}{k_B T}\right\} \tag{2.21}$$

where v is the frequency factor on the order of 10^{12} to 10^{14} s^{-1}. After application of electric field F, a change in barrier height of the localised state is introduced. Then, the influence factor is substituted into Eq. 2.21, which means that the energy required to escape the barrier is reduced in the field direction and increased in the direction against the applied field. Thus, the transfer probability of an electron under an applied field is given by

$$P = v \exp\left\{-\frac{\phi}{k_B T}\right\}\left[\exp\left(\frac{q_e F a}{2k_B T}\right) - \exp\left(\frac{q_e F a}{2k_B T}\right)\right] = P_0\left(2\sinh\left(\frac{q_e F a}{2k_B T}\right)\right) \tag{2.22}$$

where a is the average distance between trap sites.

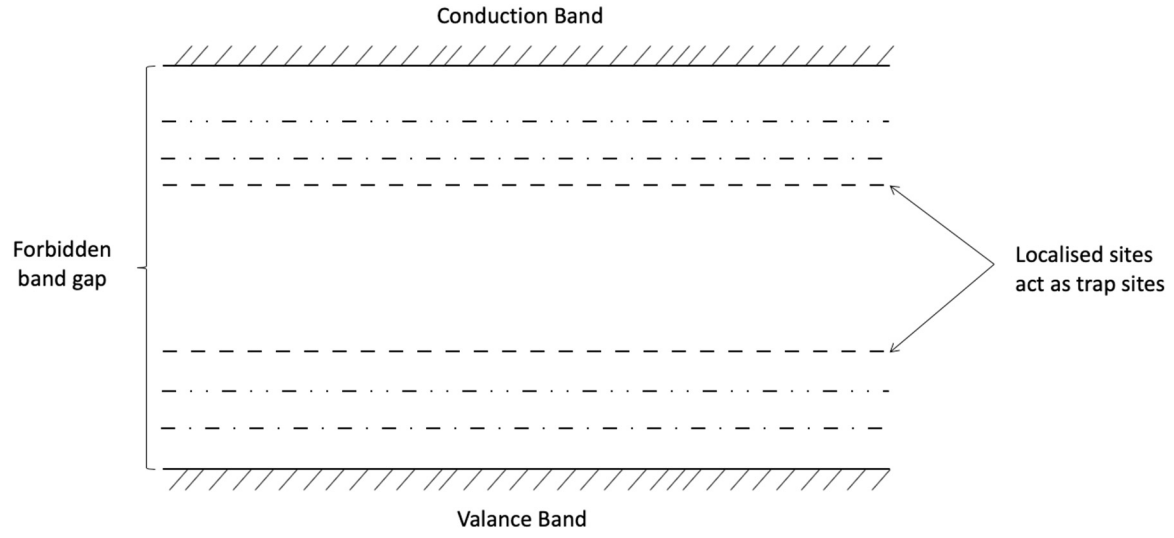

Figure 2.5: Schematic diagram of localised site based on energy band theory in insulator.

Then, two expressions $v_D = Pa$ and $\mu = V_D/F$ are substituted to establish the relation among the drift velocity, mobility of the electrons, and transfer probability. Hence, the hopping mobility is

$$\mu = Pa/F \tag{2.23}$$

Assuming the applied electric field is constant and the distribution of charge carriers is uniform, the current density of this mechanism is

$$J = \sigma F + q_e D_0 \frac{\partial n_c}{\partial x} + \frac{\partial D}{\partial t} = \sigma F = nq\mu F \tag{2.24}$$

where σ is the conductivity, and n is the concentration of charge carriers. Substituting the expression of μ and P, the thermally assisted hopping current density becomes

$$J_{TAH} = 2qnva \exp\left(-\frac{F_t}{k_B T}\right)\left[\sinh\left(\frac{qFa}{2k_B T}\right)\right] \tag{2.25}$$

2.2.3 Poole-Frenkel Mechanism

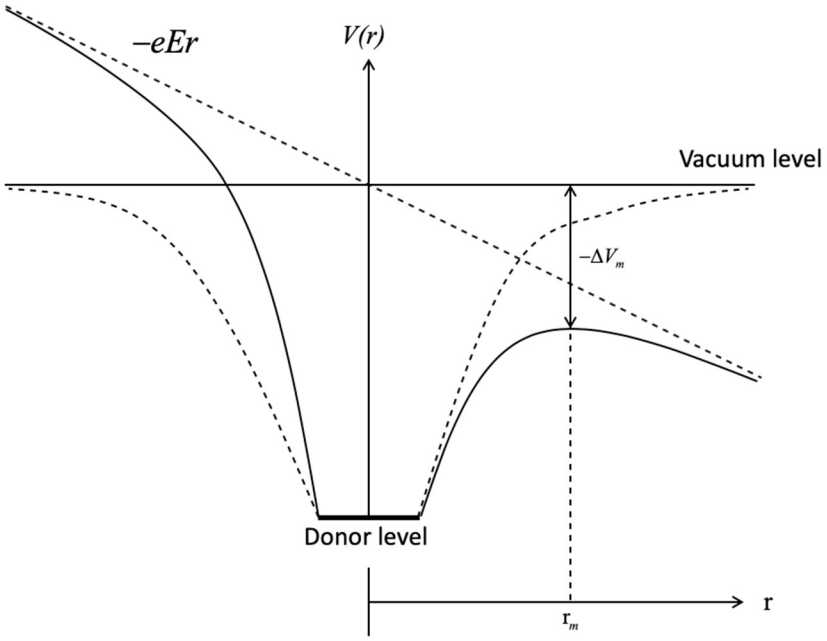

Figure 2.6: Schematic diagram for Poole-Frenkel mechanism.

The phenomenon in which the energy barrier in the bulk of insulators is lowered by the applied electric field is termed “Poole-Frenkel” mechanism [1]. It is an analogue occurring inside of dielectrics that is due to the Schottky effect. The insulator in which the Poole-Frenkel process can occur must have a wide band gap and contain donors or acceptors (i.e. electrons or holes residing in it). In terms of the energy band theory, the donor states are located below the conduction band and the acceptor states are located above the valence band. To simplify analysis, only the donors are considered in this report. Fig. 2.6 represents an electron move from the donor energy level to

the vacuum level under the applied field. As an electron is removed, the Coulombic force between the electron and unoccupied donor is given by

$$F(r) = \frac{-e^2}{4\pi\varepsilon_0\varepsilon_r r^2} \tag{2.26}$$

where r is the distance of separation. Hence, with application of the electric field, the potential energy becomes

$$V(r) = \frac{-e^2}{4\pi\varepsilon_0\varepsilon_r r} - eEr \tag{2.27}$$

Adopting the same procedure as in Schottky injection analysis, the potential energy is differentiated and set to zero, so that the position of the optimal point and corresponding maximum height of the barrier in the field direction is

$$r_m = \left(\frac{e}{4\pi\varepsilon_0\varepsilon_r E}\right)^{1/2} \tag{2.28}$$

$$\Delta V_m = -2\left(\frac{e^3 E}{4\pi\varepsilon_0\varepsilon_r r}\right)^{1/2} \tag{2.29}$$

Then, the Poole-Frenkel expression of electrical conductivity is given by

$$\sigma = \mu n_c q = \sigma_0 \exp\left(-\frac{E_t}{2kT}\right)\exp\left[\frac{q^{3/2}E^{1/2}}{(4\pi\varepsilon_0\varepsilon_r r)^{1/2}k_B T}\right] \tag{2.30}$$

where μ is the mobility of the electron, and σ_0 is a constant [1].

2.3 Space charge behaviours in polymeric insulation

2.3.1 Factors that Affect Space Charge Characteristics in Polyethylene

A good study of the factors that can affect charge formation enables people to improve the electrical performance of materials via proper insulation selection and design. Generally, different materials have diverse space charge behaviours, while some polymers with dissimilar morphology or additives show totally different charge profiles, as impurities or defects play a decisive role in this subject. Meanwhile, it was found that the electrode material also dominates the formation of charge. And as we know, the impact of ageing is crucial for materials and reduces their lifetime and affects the design of insulation. It has been proposed that charge traps are highly correlative with physical and chemical defects in materials, which may introduced by a sufficient degree of ageing

[32]. Space charge performance can be affected by different types of ageing, which has been verified by many experiments on polymer materials from yearly service on aged cables [16]. The results have shown that trap density and trap depth of deep traps in different-year aged XLPE are generally larger than fresh samples [33]. Thus, this section will focus on these factors.

(1) Electrode materials

In previous research, it was confirmed that the electrode materials have a significant effect on the conduction current, activation energy, and space charge distribution [34]. Generally, different insulation materials are attached with different electrode materials in practical application. For instance, XPLE used as cable insulation are loaded with carbon black (i.e. semicon or Sc) to smooth the electric stress profile and achieve a good bonding between XLPE and conductors, as shown in Fig. 2.7. While under laboratory conditions, electrode materials such as gold or aluminium are often coated or evaporated on the sample surface for a good connection with high voltage. Researchers have proposed that semicon (Sc), aluminium (Al), and gold (Au) as electrode materials induce different charge injections in LDPE. From the point of carrier injection, electrons injected from Sc electrodes are more numerous than those from Al electrodes, and Au electrodes inject very little; the number density of holes are injected in the order of Sc>Al>Au. Furthermore, the holes were injected more than electrons in the case for which the Al electrode and Sc electrode condition were reversed [34]. Therefore, choosing a proper type of electrode material, the amount of charge injected into the bulk can be effectively reduced and lead to less degradation of insulation.

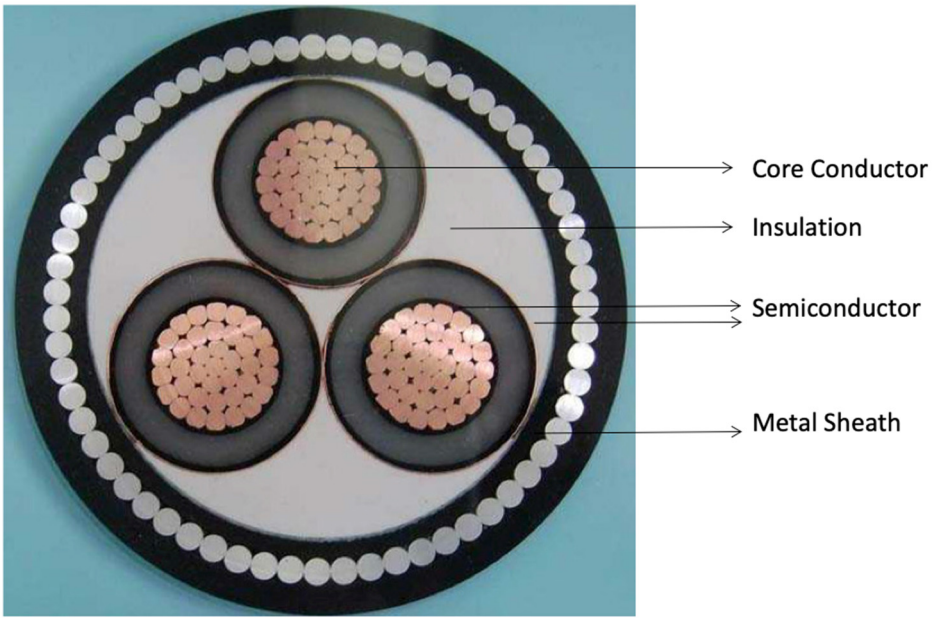

Figure 2.7: Typical structure of XLPE insulated cable.

(2) Thermal ageing

Direct evidence reveals that high temperature during the cable stressing had aged the insulation by ac-endurance tests carried out on peelings from XLPE cable insulation at a standard temperature of 363 K and field of 70 kV/mm [14]. In addition, previous studies of space charge behaviour in cable peeling indicate that ageing results in changes in the density and depth of charge traps [15]. Furthermore in [16], space charge measurements are applied on insulation peeling taken from a single 90 kV AC transmission cable whose segments were stressed for between ~8000 and 10000 hours at either of two temperatures (293 K and 363 K). The results show that both AC electrical and thermal stressing contribute to the modification of charge trap distribution in XLPE insulation. The two types of cable stress result in a reduced generation of shallow positive charge traps and increase the number density of deep positive charge traps. Meanwhile, the endurance life is reduced in thermally stressed cable segments, and it has been associated with a decrease of the amount of shallow trapped charge and a rise of deep trapped charge.

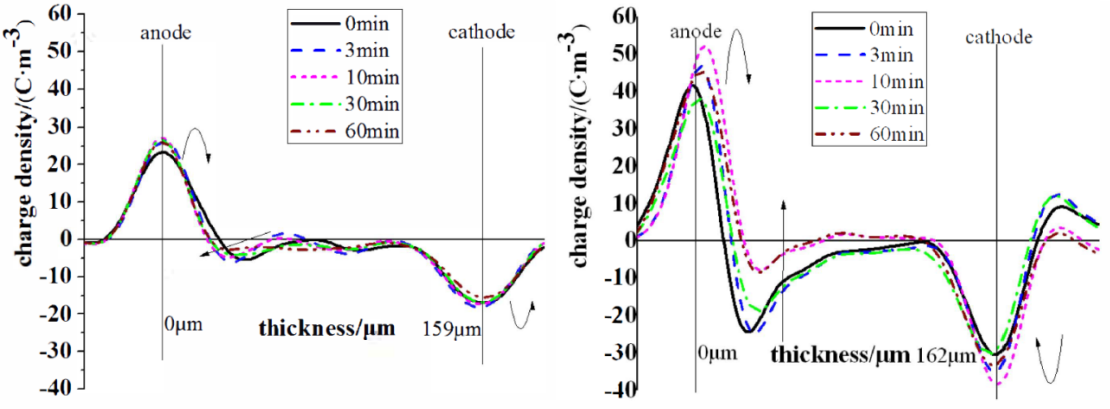

Figure 2.8: Space charge distribution of five-day aged XLPE (left) and 80-day aged XLPE (right) under 50 kV/mm [35].

To explore the sheer impact on polyethylene of thermal ageing, the XLPE samples were thermal aged at 90°C for 5, 30, and 80 days, and relative space charge behaviours were discovered under 50 kV/mm DC electric field in [35]. The results of PEA measurements on XLPE at different ageing stages, shown in Fig. 2.8, can be interpreted as thermal ageing inducing the negative charge traps in samples, and the number of both the deep and shallow charge traps increasing with rise of ageing time. The charge density changes much more significantly at the late stage of thermal ageing (i.e. the space charge properties of insulation increasingly degrade as the ageing time is sustained. However, in this case, it cannot be clearly distinguished whether the changes in charge distribution are caused by the impact of thermal aging on internal additives or by the PE itself.

(3) Radiative ageing

Radiation is also a pivotal factor which affects the electrical properties of polymer insulation, so much research has been done to investigate the correlation between radiative ageing and the space

charge phenomenon. Different charge behaviours in polyethylene might be induced by different sources of radiation, such as ultraviolet, gamma, etc. [36][37][38]. In [36], the LDPE films were aged under a 254 nm, 35 W, fluorescent tube, in three- and seven-day intervals up to 17 days, after which the samples were found to be too fragile for reliable testing. The results indicate that the charges of seven-day UV aged LDPE are difficult to be injected from electrodes, positive and negative respectively, and the accumulated charge is much less and slower in comparison to the virgin sample, which is shown in Fig. 2.9. In addition, the decay results show that the charge remaining in the aged sample decays slowly. This process was explained as follows: deep charge traps are introduced by the increased carbonyl and hydroxyl groups from UV ageing, so charges trapped in deep trapping sites dissipate at a lower rate. Note that a different space charge phenomenon might be observed in samples that irradiated in air and nitrogen. For LDPE irradiated by gamma ray in nitrogen, a shorter high-field transport time for negative carriers was observed, which is sufficient to neutralise positive charge injection at the anode [37].

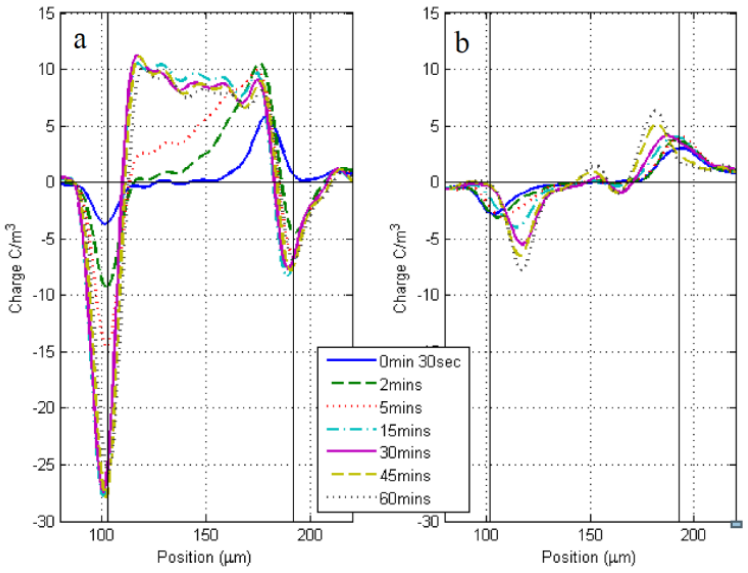

Figure 2.9: Space charge profile of virgin LDPE (left) and seven-day UV aged LDPE (right) during electrical stressing at 60 kV/mm [36].

(4) Electrical ageing

Most space charge research studies are conducted under DC conditions. Space charge can be injected into the bulk of insulation under a DC electric field over the threshold value; however, the effect of AC ageing on space charge formation in insulation cannot be ignored. It was revealed that the space charge under AC conditions is related to the level and duration of the applied field as well as the electrode materials. In previous research [39][40], the charge trapping and mobility of LDPE aged under AC conditions were investigated. In [40], samples were subjected to 50-Hz AC electric stresses up to 50 kV/mm at room temperature for more than 50 hours; then, the charge behaviour

after AC ageing was studied by applying a 50 kV/mm DC field, as shown in Fig. 2.10. The charge in the aged sample decays with a slower rate over a long period of time, compared with the charge in the unaged sample, which dissipates quickly in the first 15 minutes, followed by a slow decay. Combined with the results from the tests on samples with different ageing field levels and durations, it is suggested that stable charge formation in AC aged samples is caused by deep traps that are introduced. These deep traps are believed to form during the AC ageing and be related to injected charge.

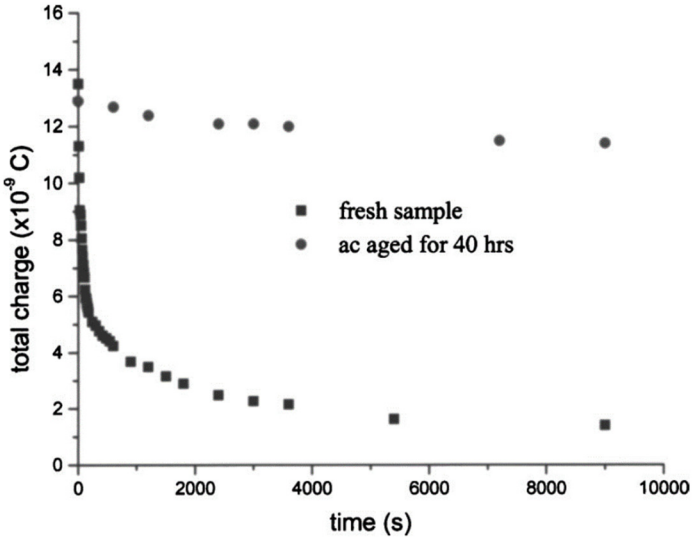

Figure 2.10: Charge decay in AC aged and fresh sample after the removal of DC electric stress [40].

2.3.2 Correlation between Space Charge Build up and Breakdown

The origin of breakdown in polymer insulation has been explained by the effect of space charge build-up and tree growth over the years [41]. The results of many experiments concerning XLPE indicate that space charge modification does occur at steady applied fields. In addition, the increased local stress can cause an electrical tree, which will grow through the insulation and result in dielectric failure, particularly under a long-term applied field [42]. Furthermore, an electric breakdown model was proposed based on the “intrinsic” breakdown strength and the space charge domination [43]. As the accumulation of space charge, the local electric field can be considered consisting with two components: the applied electric field and the field caused by charges.

$$E_{loc} = E_{appl} + E_{sc} \tag{2.31}$$

Although the applied voltage dominates the local field, the impact of space charge on Esc results in the dielectric failure under an applied voltage which is smaller than the intrinsic breakdown strength; thus, the breakdown under DC conditions is governed by internal space charges and injected charges. Furthermore, the electric field distribution due to the presence of space charge

can be estimated based on Poisson's equation, $dE/dx = -\rho(x)/\varepsilon_0\varepsilon_r$. Previous experiments on LDPE showed that the electric field distribution changes with time under steady DC voltage, as illustrated in Fig. 2.11 [44]. Meanwhile, the position of maximum electric field also fluctuates with time, and the electric field enhancement can achieve up to 60% of the applied field. Therefore, it is possible to obtain the applied breakdown strength due to the space charge distribution, especially in polyethylene materials, because a constant local electric breakdown strength is found[45].

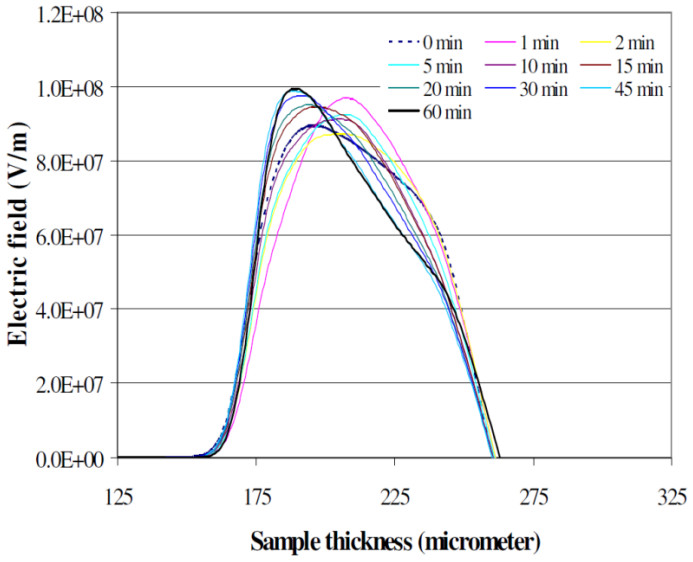

Figure 2.11: The electric field distribution of LDPE when subjected to 76 kV/mm [43].

2.4 Space charge and ageing models

In my research, the ultimate aim focuses on establishing a model to connect ageing and lifetime, and the space charge is the key used. Lifetime indicates the working hours that the insulation can be safely used and meet the requirements. In previous experimental work, described in the last several chapters, the basic experiment work was conducted and the effect of thermal aging on the electrical properties of polyethylene was qualitatively analysed based on the space charge characteristics. As shown in Fig. 2.12, the further research structure, three key factors remain to be done.

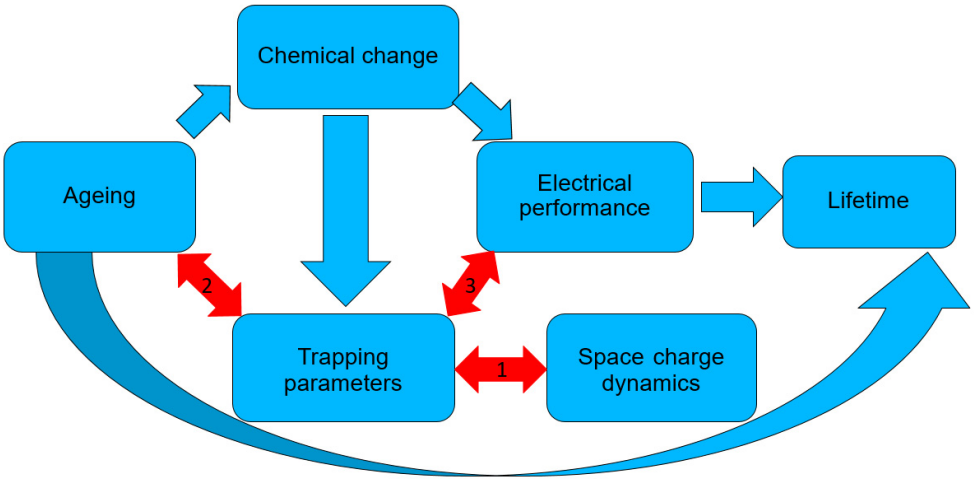

Figure 2.12: The modelling research structure.

First, the trapping parameters of ageing LDPE must be built, based on space charge dynamics; then, the influence of ageing on trapping parameters must be analysed and the regression equation established according to the actual experimental phenomena. Further research can be concentrated on the relationship between trapping parameters and other electrical performance characteristics such as breakdown strength and DC conductivity. Hence, an improved model to estimate trapping parameters in polyethylene will be introduced and parameters estimation work based on our experiment results will be presented next.

2.4.1 Trapping parameters estimation model

In past decades, many approaches have been proposed to establish trapping parameters for different insulation materials to describe the space charge behaviour. Dissado developed a model considering the charge decay process in epoxy resin [46]. In the case of XLPE, trapping parameters have been evaluated based on different-time aged XLPE cable peelings in [47]. In addition, in [23], [24], Chen proposed a trapping and detrapping model based on traps with two energy levels (i.e. shallow and deep traps) in polymer dielectrics, which will be reviewed in next section. Its application in normal and gamma-irradiated polyethylene material was published in [48]. Generally, in previous research, the trapping parameters were built based on the charge decay process, i.e. space charge behaviour after the removal of external fields, as the charges detected by PEA systems in the volts-off process were defined as pure trapped charges, which can reflect the trap distribution clearly [25], [48]. Furthermore, an improved model was developed by Ning in [38], considering both charge depolarization and polarization processes and treating space charge as trapped charge and mobile charge. Meanwhile, the charge neutralization was considered in this model, and the trapping parameters were estimated based on two levels of trap depth (i.e. shallow and deep traps). These traps were revealed to be related to physical and chemical defects introduced by ageing in

polymeric materials. Hence the improved trapping parameter estimation model was used in our further research.

2.4.1.1 Trapping-Detrapping Model Based on Two Energy Levels

As space charge formation has a critical effect on the degradation and even breakdown strength of polymeric materials, it is necessary to study charge generation and tapping and detrapping processes clearly. Meanwhile, many explanations of space charge behaviour in different conditions, such as some works reviewed above, are proposed based on the assumption that there are only two trap energy levels distributed across the sample. So a trapping and detrapping model based on shallow and deep traps is reviewed in this section in terms of [23], and the fundamental models of the charge trapping and detrapping processes are shown in Fig. 2.13. Trapping and detrapping processes have an intimate correlation with the trap distribution in the bulk of insulation materials. Generally, trap energy states in semi-crystalline polymer are not uniform and possibly have several discrete levels or even continuous energy distribution. Because major traps are generated by uncontrollable physical and chemical processes, chaotic energy levels result. To simplify the mathematics, only two trap depths are considered in this model.

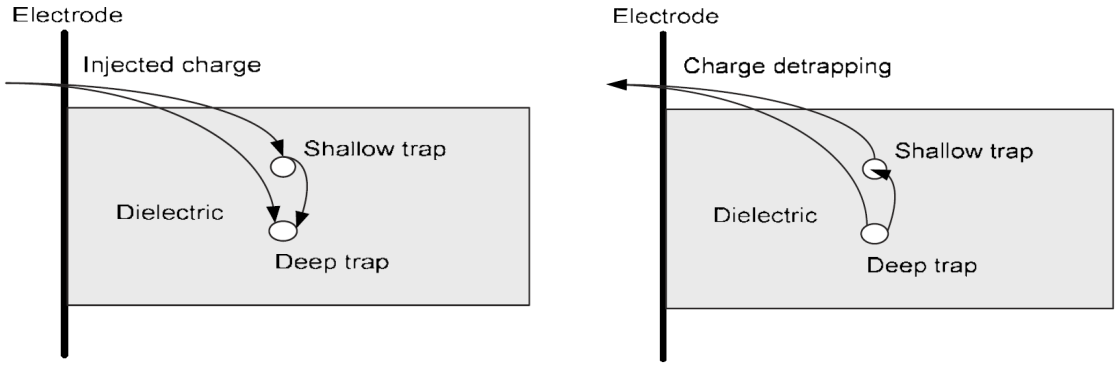

Figure 2.13: Diagrams represent the models of charge trapping and detrapping [23].

First, we assume that all the charges are generated from electrode injection. This assumption is based on previous experimental work [49], which shows that injected charges are the majority of trapped charges. The injected current density is given by

$$J(E,t) = J_0 \exp\left(\frac{E}{E_0}\right)\left[1 - \exp\left(-\frac{t}{\tau}\right)\right] \tag{2.32}$$

where J_0 is the initial current density when the applied field is E_0, E is the applied field, and τ is the time constant related to overall trapping characteristics of the material. In the trapping process, based on the assumption that there is no recombination between injected carriers, and neglecting the trapping process from shallow to deep trap, the charge trapping dynamics are represented by

$$\begin{aligned}\frac{dn_1}{dt} &= \frac{J\sigma_1}{q}(N_1 - n_1)\\ \frac{dn_2}{dt} &= \frac{J\sigma_2}{q}(N_2 - n_2)\end{aligned} \tag{2.33}$$

In this equation set, N_1 and N_2 are the total number of shallow and deep traps, σ_1 and σ_2 are corresponding trapping cross sections for two types of traps, q is the charge amount, and n_1 and n_2 are the trapped charges in the shallow and deep traps, respectively. As for the detrapping process, we only considered thermal detrapping and did not consider the process of detrapping from deep to shallow trap. The mathematical expression is described as

$$\begin{aligned}\frac{dn_1}{dt} &= -k_1 n_1\\ \frac{dn_2}{dt} &= -k_2 n_2\end{aligned} \tag{2.34}$$

where k_1 and k_2 are the thermal detrapping rate constants for shallow and deep traps, respectively, which can be expressed by $k_{th} = N_c v_{th} \sigma \exp\left(-\frac{E}{k_B T}\right)$, where N_c is the effective density of states in the conduction band, v_{th} is the thermal velocity of the charges, E_t is the trap depth, k_B is the Boltzmann constant, and T is the temperature. Then, the boundary conditions are set with both n_1 and n_2 at zero before injection begins. As the rate of change in the density of filled traps equals the summation of the change rate in trapping and detrapping, assuming the injected current depends only on the applied field, the total trapped charge density during the application of the electric field is given as

$$\begin{aligned}n(t) &= n_1(t) + n_2(t)\\ &= \frac{A_1 N_1}{A_1 + k_1}\{1 - \exp[-(A_1 + k_1 t)]\} + \frac{A_2 N_2}{A_2 + k_2}\{1 - \exp[-(A_2 + k_2 t)]\}\end{aligned} \tag{2.35}$$

where A_1 and A_2 can be calculated by $A_n = \frac{J_0 \sigma_2}{q}\exp\left(\frac{E}{E_0}\right)$. Based on Eq. 3.35, assuming $\sigma_1 > \sigma_2$ and the depth of deep trap is larger than shallow trap (i.e. $E_{t2} > E_{t1}$), the time constant for shallow traps is shorter than that for deep traps. A schematic diagram where $\tau_1 = 10s$ and $\tau_2 = 5\tau_1$ is shown in Fig. 2.14 [23].

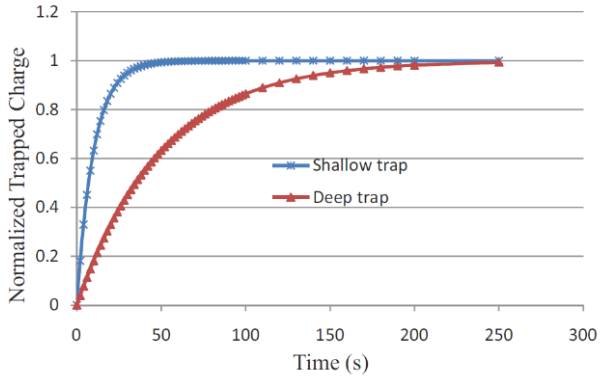

Figure 2.14: Dynamics of charge trapping for trapped shallow and deep traps [23].

After removal of the applied field, the thermal detrapping will be the only process that dominates the charge decay. Identify n_{10} and n_{20} as the initial conditions that can be obtained from the field application process; then, the total trapped charge density after the applied field is removed is given by

$$n(t) = n_1(t) + n_2(t) = n_{10}\exp(-k_1 t) + n_{20}\exp(-k_2 t) \tag{2.36}$$

For detrapping process, with the same assumptions as above, the diagram of trapped charge dynamics after removal of the applied field, where $k_1 = 20s$ and $k_2 = 5k_1$, is shown in Fig. 2.15 [23].

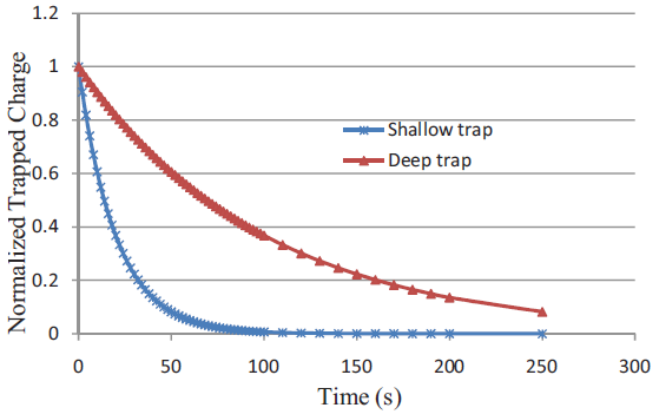

Figure 2.15: Dynamics of trapped shallow and deep traps during decay [23].

In this model, the trapping and detrapping processes are described. In terms of this simplified model, the relative experimental results show that it is easier to fill shallow traps so the effect of trap depth can be easily analysed qualitatively in further research, especially regarding material ageing. On the other hand, trapping parameters n_{10}, n_{20}, k_1, and k_2 based on two trapping levels are built up and provide elementary parameters to describe trap states. However, to simplify the model, the injected charges are assumed in the vicinity of the electrodes, and recombination are neglected. In the actual experiments, the results show that the injected charges can move the bulk forward;

this part of charges cannot be ignored, and neither can the recombination process caused by charge movement. So the further trap parameters model was established, which considers the effect of charge mobility and recombination. The effect of ageing on trap states is one of the main reasons for the change of electrical performance after ageing. Because the relation between ageing and trap states (i.e. trap parameters) has not been established clearly, our research will focus on this part.

2.4.1.2 An Improved Trapping Parameters Estimation Model

In this improved trapping parameters model [38], the injected homocharge in the space charge profile was separated into the charge region of positive and negative, and the thickness of these two zones is equal to d_e and d_h ("e" is electron and "h" is hole), respectively, as shown in Fig. 2.16. Hence, the sum of trapped and mobile charge density can be proposed as

$$n_{h,e} = n_{t_{h,e}} + n_{m_{h,e}} = \frac{Q_{t_{h,e}}}{d_{h,e}A} + \frac{Q_{m_{h,e}}}{d_{h,e}A} \tag{2.37}$$

where n_t and n_m are the trapped charge and mobile charge density in either charge region; Q_t and Q_m represent the total trapped and mobile charge amount; and A is the electrode cross-sectional area. First, an assumption is made that the depth of all traps is on the same energy level, so the changing rate of injected net charge density in positive charge zone under external applied voltage $\frac{dn_h}{d_t}$ can be expressed as

$$\frac{dn_h}{dt} = \frac{J_h}{qd_h} - P_h n_{m_h} - \Delta n_{m_e}{}' \tag{2.38}$$

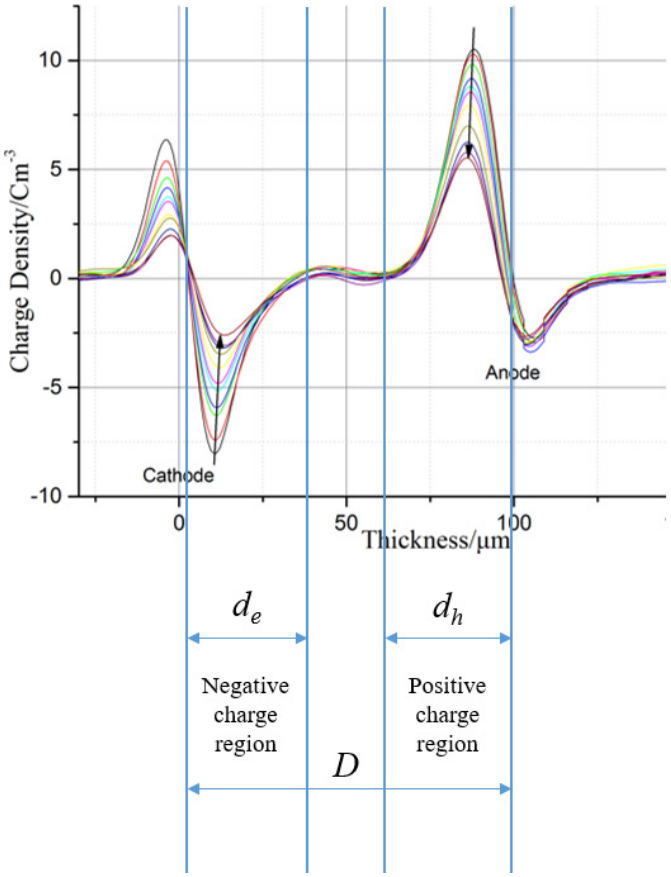

Figure 2.16: Positive and negative charge zones in space charge profile.

In Eq. 2.38, the first term signifies the increasing rate of volumic density of holes injected from the anode under external applied field at the metal-polymer interface by Schottky injection, for which the mechanism was reviewed in last section. The injection current density from anode J_h can be calculated as [1]

$$J_h = A_0 T^2 \exp\left(-\frac{qw_h}{kT}\right)\exp\left(\beta_{sc} E_{i+}^{0.5}\right) \tag{2.39}$$

In Eq. 2.39, A0 is a constant term and can be written as $A_0 = \frac{4\pi q m_e k^3 (1-R)}{h^3}$, where h is the Planck constant, m_e is the effective mass of an electron, and R is the reflection coefficient of the electron interface. A constant term $A = 4\pi q m_e k^2 / h^3 = 1.20 \times 10^6 A \cdot m^{-2} K^{-1}$ is often identified; T is temperature, w_h is the original injection barrier energy level of holes; and E_{i+} is the interfacial electrical field at the anode. Moreover, β_{sc} is Schottky constant, which can be expressed as $\beta_{sc} = \frac{q}{kT}\left(\frac{q}{4\pi\varepsilon_0\varepsilon_r}\right)^{0.5}$, where ε_0 and ε_r represent the vacuum and relative permittivity for the sample, respectively.

In addition, the second term $-P_h n_{m_h}$ in Eq. 3.39 is the decreasing rate of net charge in the zone of positive charge. The reduction of the carrier is ascribed to the outflow of mobile holes from this positive charge region toward the cathode. It was assumed that a certain proportion P_h of mobile holes can flow out of the hole area. In addition, the third term $\Delta n'_{m_e}$ describes the increasing rate of negative mobile charge into the positive charge zone from the opposite region, injected from the cathode. Considering both charge regions, the diagram represents carrier flow dynamics, based on the three terms in Eq. 2.39 (see Fig. 2.17). As can be observed, the mobile charges from two charge regions could be neutralization in the mid region, and the rest of the carriers can flow into other charge regions. As a result, two situations should be considered:

(1) $P_e n_{m_e} > P_h n_{mh}$, so $\Delta n_{m_e}{}' = P_e n_{m_e} - P_h n_{m_h}$ and $\Delta n_{m_h} = 0$

(2) $P_e n_{m_e} > P_h n_{mh}$, so $\Delta n_{m_e}{}' = P_h n_{m_h} - P_e n_{m_e}$ and $\Delta n_{m_e} = 0$

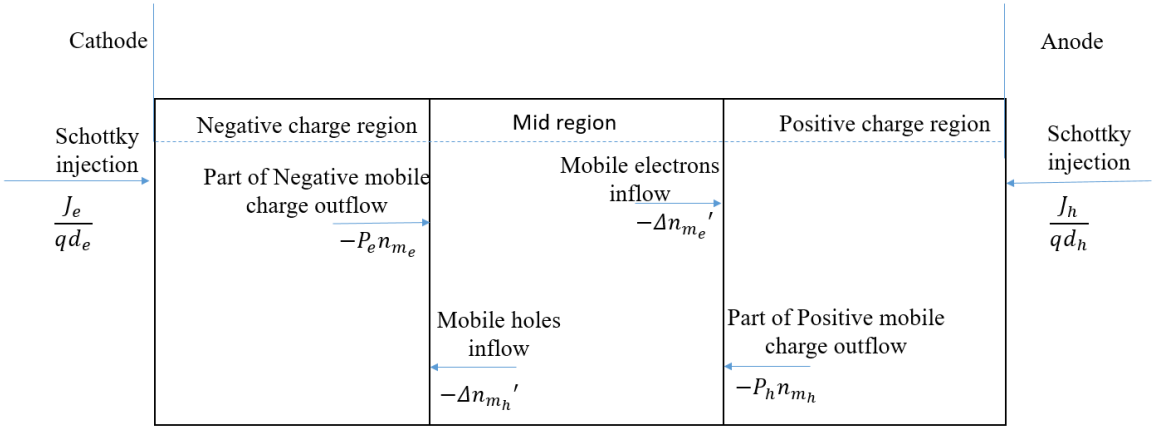

Figure 2.17: Carrier flow diagram under external applied field.

On the other hand, taking the positive charge as an example, the changing rate of the density of trapped holes $\frac{dn_{t_h}}{dt}$ could be expressed as

$$\frac{dn_{t_h}}{dt} = -R_{esc} + R_{cap} - R_{rec} \tag{2.40}$$

$$R_{esc} = n_{t_h} v_0 \exp\left(-\frac{E'_{t_h}}{kT}\right) \tag{2.41}$$

$$R_{cap} = n_{m_h}(N_{t_h} - n_{t_h}) S_h v_{d_h} \tag{2.42}$$

$$R_{rec} = B(n'_{m_e}) n_{t_h} \tag{2.43}$$

In the equation set, Resc, Rcap and Rrec represent the respective charge escaping rate from traps, the charge capturing rate by traps, and the recombination rate of trapped carriers and mobile carriers, which come from the opposite charge zone. In Eq. 2.41, v_0 is the escape attempt frequency, and it is a constant value, which approximates $2\times10^{13}s^{-1}$ at room temperature [1]. E'_{t_h} as modified trap depth can be calculated by $E'_{t_h}=E_{t_h}-\Delta V_{pfh}$, where E_{t_h} is the original trap depth and ΔV_{pfh} is the impact of Poole-Frenkel effect [50], which was reviewed in section 2.2.3. In short, there is Poole-Frenkel effect in the materials with wide band-gap, which represents that the potential barrier height of Coulombic attractive traps can be reduced by Coulombic force between charge trapping centres and carriers [1]. Equation 2.42 can be understood as the following: mobile hole carriers, with an average velocity of v_d, drift pass through empty positive traps with a capture cross section area of S_h, and there is a capturing rate of R_{cap} at which all those positive charges are captured. So N_{t_h} is the total positive trap density and $N_{t_h}-n_{t_h}$ is the number of empty traps of hole carriers. Moreover, assuming the mobile holes move straight along the direction of the local electric field, v_d can be calculated by $v_d=(qE_+a/m_h^*)^{0.5}$, where E_+ is the local electrical field under effect of space charge accumulation in the local charge region, and a and m_h^* represent the trap separation distance and the effective mass of holes in material, respectively. In Eq. 2.43, n'_{m_e} is the mobile electron density in positive charge region and can be expressed by $n'_{m_e}=\int_0^t \Delta n'_{m_e}dt$. Finally, B in the equation is the recombination rate between trapped holes and mobile electrons.

In the charge decay stage, the external voltage is removed, so the term of Schottky injection in Eq. 2.38 could be neglected, as the electric field at electrodes is much lower. Hence, the carrier flow direction diagram is shown in Fig. 2.18. The changing rate of net charge in positive region, after removal of external applied field, could be given by

$$\frac{dn_h}{dt}=-P_h n_{m_h}-\Delta n_{m_e}' \tag{2.44}$$

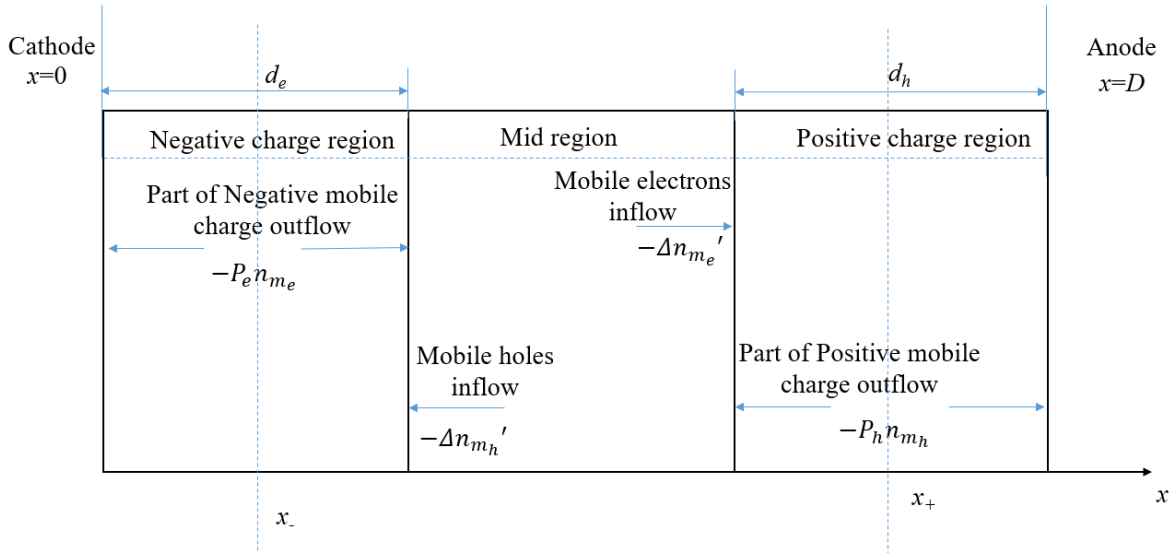

Figure 2.18: Carrier flow diagram after removal of external applied field.

The direction of mobile carrier movement depends on the direction of the local electrical field; hence, the charge should move under the field generated by local space charges, after removal of the external applied field. As shown in Fig. 2.38, a part of holes will decay through the anode, but others will flow toward the cathode. Moreover, Eq. 2.40 to Eq. 2.43 still are suitable in the case of the trapped charge during the decay process, but the field-dependent parameters, Poole-Frenkel reduction and trapping cross section, should be modified.

Furthermore, the model could be extended from a single trap depth to two energy levels of traps (i.e. shallow and deep traps). The second term in Eq. 2.38 becomes $-Pn_{m_e} = -P(n - n_{t_{h1}} - n_{t_{h2}})$, where $n_{t_{h1}}$ and $n_{t_{h2}}$ are the holes trapped in shallow and deep traps. The change rate of shallow and deep trapped charges in the positive charge region could be proposed by Eq. 2.45 and 2.46, respectively.

$$\frac{dn_{t_{h_1}}}{dt} = -n_{t_{h_1}} v_0 \exp\left(-\frac{E_{t_{h_1}} - \Delta V_{pfh_1}}{kT}\right) + n_{m_h}\left(N_{t_{h_1}} - n_{t_{h_1}}\right) S_{h_1} v_{d_h} - B(n'_{m_e}) n_{t_{h_1}} \tag{2.45}$$

$$\frac{dn_{t_{h_2}}}{dt} = -n_{t_{h_2}} v_0 \exp\left(-\frac{E_{t_{h_2}} - \Delta V_{pfh_2}}{kT}\right) + n_{m_h}\left(N_{t_{h_2}} - n_{t_{h_2}}\right) S_{h_2} v_{d_h} - B(n'_{m_e}) n_{t_{h_2}} \tag{2.46}$$

where the subscript 1 and 2 represent the value for shallow and deep traps, respectively.

2.4.2 Model utilization

The early trapping parameters evaluation model proposed by Chen [23] has been used in different normal and ageing samples in previous research [24] [33] [85]. In addition, this model is based on assumption that the polarization process inside the bulk is neglected (i.e. there is no neutralization between positive and negative charges. So the space charge measurements were carried out under

short stressing time, generally no more than 6 minutes, and the space charge dynamics after removal of the external applied field were used to build trapping parameters. In addition, the polyethylene samples used in previous work are generally 180 μm, for the sake of reducing charge neutralization during the volts-on process. However, in the case of the charge injection stage, the PEA tests were performed under 40 kV/mm for 1800 s in our normal and thermal ageing samples with a thickness of ~100 μm, as shown in chapter 5. We would like to explore further space charge injection dynamics and use the work to explain the effect of thermal aging on other electrical performance. In addition, the recombination of different kinds of carriers cannot be ignored in deep thermal ageing polymeric insulation materials with gradually larger mobility of carriers [51]. Hence, the improved model [38] reviewed in the last section is quite suitable for our analysis. Furthermore, the space charges are treated as trapped and mobile charges separately here, and combined with the trapping parameters, the mobile charge dynamics and trapped charge behaviour can be shown clearly, as illustrated in Fig. 2.19. That could be useful to verify the conjecture about the charge behaviours in deep thermal ageing LDPE. On the other hand, the energy level of traps was divided into shallow and deep (i.e. dual-level model), which could be meaningful in our ageing research, as it was suggested that shallow and deep traps can be correlated with different defects introduced by ageing in polymer materials [51], [88], [52].

Generally, care should be taken with the assumption when dealing with a model, particularly a model based on actual experiment results. Notably, in the charge depolarization aspect, it was assumed that charges are uniformly distributed in either charge region for simplicity. In the case of our deep air thermal ageing, the effect of thermo-oxidation was seen throughout the entire film sample, so it could be assumed that the distribution of trapped charges is uniform. In addition, nitrogen ageing samples might be suitable as well, as the difference in space charge behaviour in the vicinity of the electrodes and inside the bulk was not large. However, for slightly air aged samples, space charge dynamics, DC breakdown strength, and electrical conductivity were in close correlation with surface thermo-oxidation. The non-uniform distribution of deep traps introduced by oxidation on the surface was proposed to explain this electrical performance. Generally, the purpose of our research was to investigate the destruction of electrical properties of materials by thermal aging and try to explain them with space charge characteristics, and then build up the connection model. However, the slightly ageing LDPE affected by thermo-oxidation achieved an improved electrical behaviour. So first, trapping parameters based on the improved model could be evaluated in deep air thermal ageing and nitrogen ageing samples. In addition, to explore the influence of thermal ageing on trapping parameters in LDPE more clearly and build a model, specimens with greater degrees of deep ageing should be made. On the other hand, the effect of

surface thermal oxidation should be further investigated, and the inflection point of surface effect should be confirmed as well.

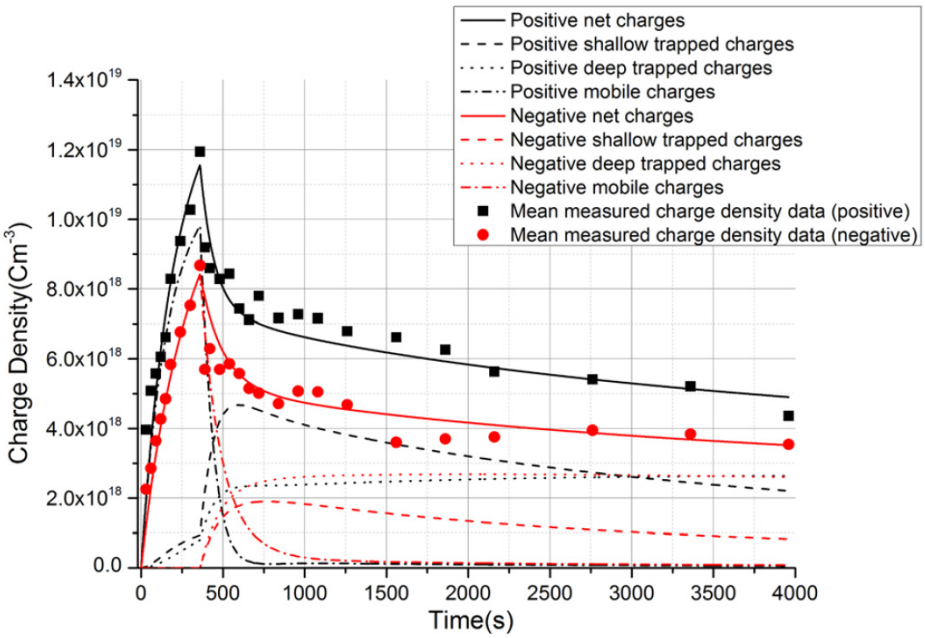

Figure 2.19: Simulated curve fitting with PEA data of normal LDPE, based on dual-level improved model [38].

In addition, the MATLAB software could be used to calculate trapping parameters, with the goal of finding the best curve fitting to match the experimental data. But the charge density of thermal ageing samples, calculated by PEA results, features a non-negligible volatility, which can affect the curve fitting results.

Chapter 3 Sample Preparation, Thermal ageing and Chemical Analysis

Our research aims to establish the relationship between space charge characteristics and lifetime of polymeric insulation, with a focus on thermal ageing. The polymer materials used in insulation systems are mainly cross-link polyethylene (XLPE), and previous research into the thermal ageing process of polymeric insulation cables was conducted on XLPE samples [14], [35]. However, to reduce the number of factors that could affect the results and explore the essence of the impact of thermal ageing on the space charge phenomenon, the sample selected was the type of additive-free LDPE that has less impurities introduced by the manufacturing process compared with XLPE with additives. As a result, the impact on polyethylene itself from thermal ageing can be explored. Therefore, our experimental works focus on the additive-free LDPE films with different degrees of thermal ageing and study its impact on charge trap density and change in electrical breakdown strength. The ageing degrees of the samples were characterized using Fourier-transform infrared (FTIR) spectroscopy, and breakdown strength and space charge dynamics were measured using the pulsed electroacoustic (PEA) technique. In addition, differential scanning calorimetry (DSC) was carried out to measure the crystallinity of LDPE samples, while a microscope was used to observe the surface change of the ageing sample; DC conductivity was measured as well. In this chapter, the sample preparation process and relative chemical analysis results are introduced.

3.1 Sample Selection and Preparation

The original and aged samples used for the experiment were commercially available additive-free LDPE, which was purchased from Goodfellow Cambridge Limited Company. The specific properties of different commercial polymers from different production lines is uncontrollable, so we used specimens from the same batch, which maintains the same thickness to obtain more accurate results. Meanwhile, the thickness of samples measured in our PEA system should be no less than $100\mu m$ for better results with less reflection interference. Additionally, the limit voltage of our DC breakdown test system is 65 kV, so the thickness of LDPE, for which the DC breakdown strength is about 500 kV/mm[7], should be lower than $120\mu m$. As a result, the thickness of LDPE samples was chosen to be $100\mu m$, which is suitable for every measurement in the plan.

Considering a melting temperature of LDPE at about 112°C [7] and accelerating aging, first samples were aged using a typical fan oven at 90°C and 100°C; the different degrees of aging are shown in Table 4.1. We tried to age LDPE films at 110°C, but the uncontrollable deformation made it difficult

to obtain uniform thickness, and the melting of specimen leads to one side cannot be uniformly thermal aged. To get a stable and uniform thermal ageing degree in the fan oven, the LDPE films were held and covered by aluminium foils with vent holes. This enabled us to achieve a higher stable operating temperature [53].

Table 3.1: The ageing conditions of LDPE samples in the air

90°C	1 day	5 days	10 days	15 days	20 days
100°C	1 day	5 days	10 days	15 days	20 days

In addition, previous work shows that the thermal-oxidation on LDPE has a big impact on its electrical properties. However, in actual conditions, PE insulation always operates in an anti-oxidation environment, so thermally ageing PE in an oxidation-isolation condition is necessary. To create a thermal ageing environment which is isolated from oxygen and maintain the same temperature and air pressure, a vacuum oven filled with nitrogen was used. For isolating the effect of oxygen in the air as much as possible, a vacuum oven and balloon were employed (see Fig. 3.1).

First, a state of slight over pressure inside of the oven was created using a balloon filled with nitrogen to retard the impact from the oven leaking during ageing. Then, before heating the LDPE samples, the vacuum oven was vacuumed and filled with nitrogen twice to fully remove oxygen impact inside of the oven. Two balloons filled with nitrogen were connected to both the input and output of the vacuum oven tightly, and they were refilled every eight hours. In addition, specimen films were sandwiched with aluminium foils without vent holes in order to reduce the effect of leaking oxygen. Meanwhile, over time, ageing will inevitably introduce leaking and oxidation, so the ageing time is one day and five days. The FTIR technique was used to detect the oxidation degree to confirm that the thermal ageing environment was successful. This technique is shown in the next section.

Figure 3.1: Thermal ageing installation in nitrogen in vacuum oven.

3.2 Fourier-Transform Infrared Measurement

The Fourier-Transform Infrared (FTIR) technique was applied to reveal the chemical properties for original and aged LDPE films. The spectrum was observed by IR absorption in the range of 440~ 4000 cm^{-1} through LDPE film using an IR Prestage-21 spectrometer. The spectrum was observed over 32 scans accumulation, and the resolution was 4 cm^{-1}. Before the experiment, samples were cleaned using alcohol and then dried to avoid the influence of surface impurity and alcohol.

The general scheme of the polymeric material thermos oxidation indicates the radical character of the thermo-oxidation process, as shown in Fig. 3.2 [13].

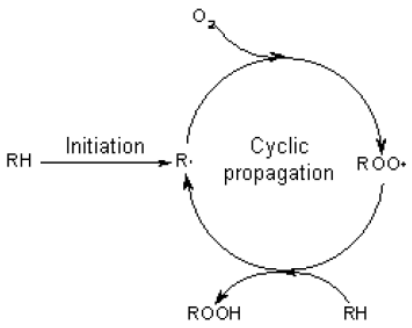

Figure 3.2: Thermo-oxidation process in a polymer [13].

The organic radical reacts with the polymeric substrate which result in a peroxy radical and further to a hydroperoxide accompanied with a macromolecular radical. The chain reaction processes are:

$$R\text{-}H + I\cdot \rightarrow R\cdot + IH$$

$$R\cdot + O_2 \rightarrow ROO\cdot$$

$$ROO\cdot + RH \rightarrow ROOH + R\cdot$$

As samples were aged in a typical fan oven, the major impact on LDPE is oxidation. According to the IR absorption frequencies, shown in Table 3.2 [54], special attention has been paid in the range of 1690~1800 cm^{-1}, as the carbonyl group peaks due to thermal ageing should be observed in that range [55]. The carbonyl index was calculated by a ratio between the oxidation peak A_{ox} and the area of invariant peak A_j [56]. In other words, the carbonyl index (CI) R is

$$R = \frac{A_{ax}}{A_j} \tag{3.1}$$

Table 3.2: The IR absorption frequencies of common functional groups

Functional group	Alkyl C-H	Carboxylic Acid O-H	Amine N-H	Aldehyde C=O
Absorption (cm^{-1})	2950-2850	3000-2500	3500-3200	1740-1690
Functional group	Ester C=O	Carboxylic Acid C=O	Amide C=O	Ketone C=O
Absorption (cm^{-1})	1750-1735	1780-1710	1690-1630	1750-1680

Fig. 3.3 shows the change in FTIR spectra of LDPE due to thermo-oxidative treatment at 90°C and 100°C. The carbonyl index was calculated with Eq. 3.1 by taking the ratio of absorption bands at 1710 and 2020 cm^{-1}. The temperature in the fan oven used for thermal ageing was controlled by the upper and lower limit value of the temperature, so the real temperature in the oven fluctuated. Thus, the ageing temperature and time cannot be used to determine the ageing degree. However, the carbonyl index shows the overall condition of thermal ageing in air.

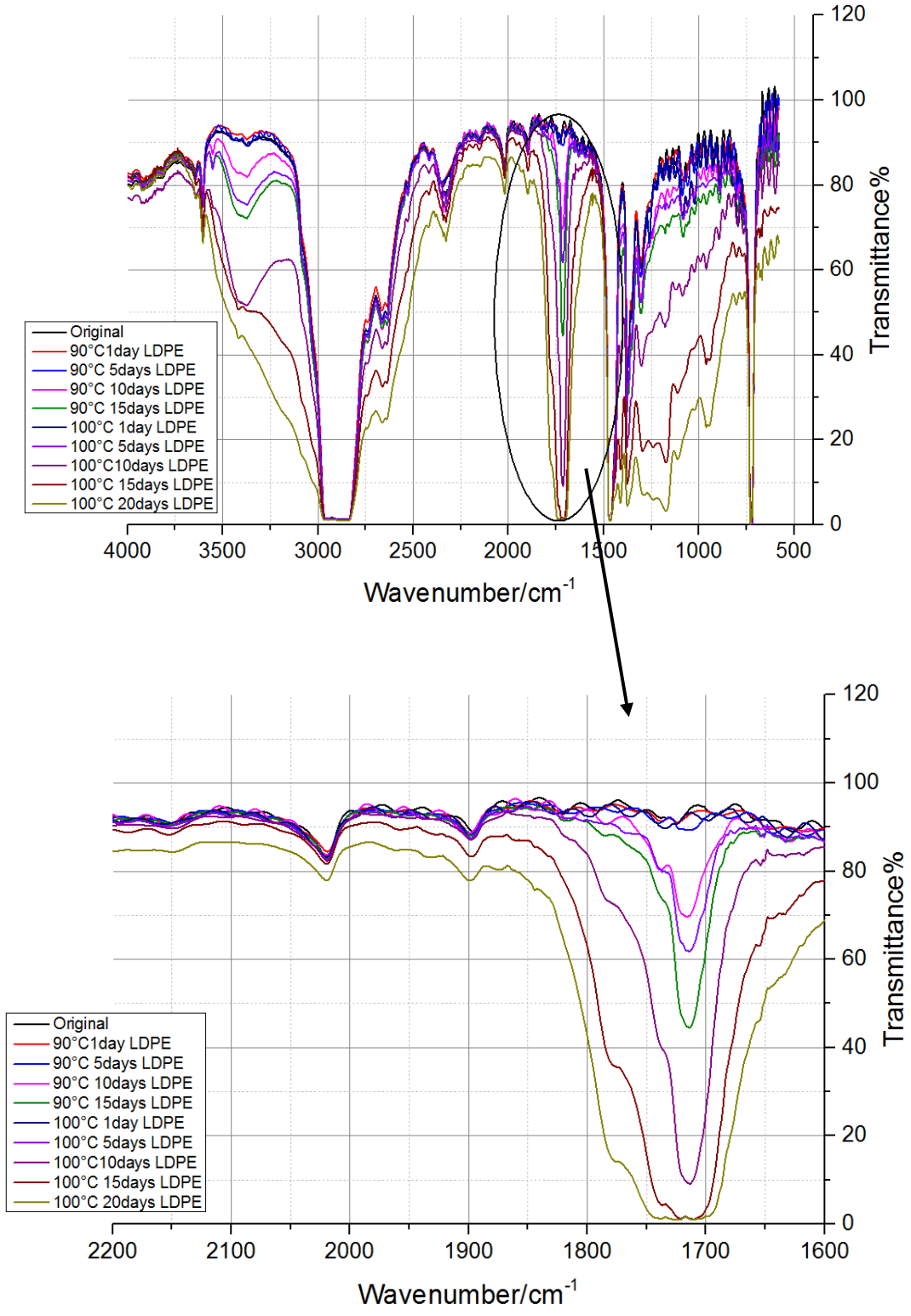

Figure 3.3: FTIR spectrum of original, 90°C aged, and 100°C aged samples with zoom-in peaks within region 1600-2200 cm^{-1}.

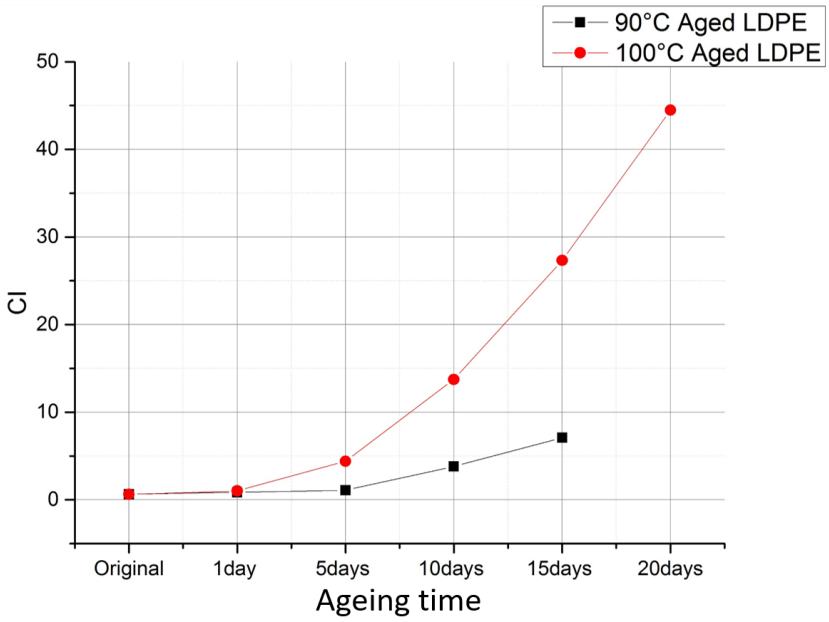

Figure 3.4: Change in the CI of 90°C aged and 100°C aged samples obtained from FTIR spectrum.

Figure 3.4 shows the change in the CI as a function of thermo-oxidation time. It can be seen that the CI increases exponentially after 1 day. Meanwhile, the CI rising rate for 100°C aged LDPE is faster than the index for 90°C aged LDPE after one day.

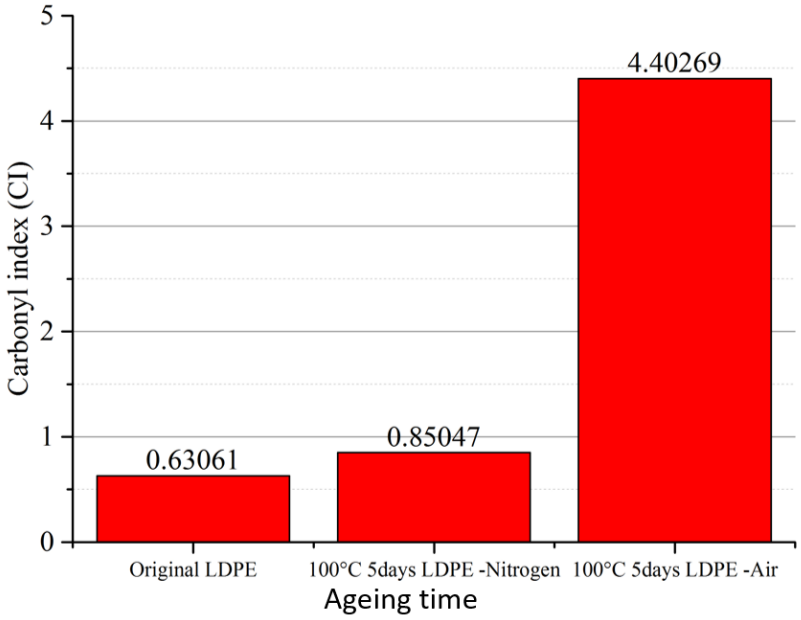

Figure 3.5 Carbonyl index (CI) of original and 100° C five-day thermal ageing in nitrogen and air for LDPE.

The LDPE specimens ageing in nitrogen in the vacuum oven were measured in the FTIR system as well. The carbonyl index (CI) results are shown in Fig. 3.5. In this figure, the carbonyl index of samples which were aged in nitrogen are obviously lower than those of samples aged in air, but the

oxidation cannot be totally removed. Despite that, the LDPE sample aged in our oxidation-isolation condition can be used to compared with the air-ageing sample.

3.3 Differential Scanning Calorimetry Measurement

3.3.1 Experimental Details

The ageing we focus on is thermal ageing, and when dealing with polymeric materials, there are three important thermal processes that should be considered: crystallisation, melting, and glass transition [57]. Thermal ageing beyond the threshold temperature commonly has a significant effect on the thermal behaviours of polymers [58]. Therefore , the impact of thermal ageing on the internal structure and morphology of polyethylene should be investigated. It may be used to establish the connection between the change of trapping parameters and the variation of polyethylene structure in thermal ageing specimens. Therefore, thermal analysis based on crystallinity and melting temperature was conducted by the differential scanning calorimetry (DSC) technique. In a DSC system which is shown in Fig. 3.6, sample and reference are heated, and the energy is supplied to keep the sample and reference temperatures constant. As a result, heat flow as a function of temperature or time of sample can be plotted, based on the electrical power difference between sample and reference [59]. The sample is contained by one of the sealed pans, and the other pan contains nothing and serves as reference. Compared with other thermal analysis methods, DSC has the advantage of being simple and quick.

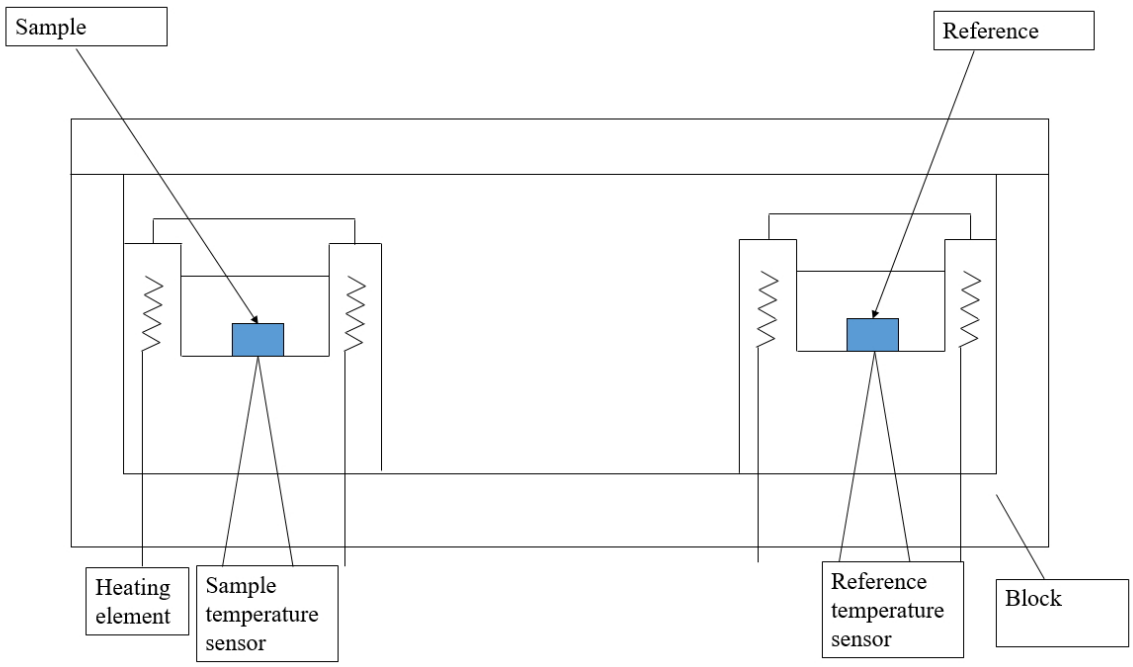

Figure 3.6: Schematic representation of differential scanning calorimetry measuring cell [59].

A Perkin Elmer DSC 7, which is controlled by Pyris software, was utilised to carry out thermal analysis. After setting the nitrogen at 0.5 bar and before beginning the test, the bath was set to 10°C for 30 minutes to ensure that the bath temperature was stabilised. High-purity indium was used for calibration; its reference melting point and melting enthalpy are 156.6°C and 28.45 g/J, respectively. As noted in the literature review earlier in this chapter, the melting point of LDPE is approximately 104°C, so the scanning temperature was from 30°C to 140°C and the heating rate was 10°C/min. Meanwhile, the quality of ageing samples for one set of measurements was 5.0 ± 0.5 mg, and samples were measured in the aluminium pans. Showing the test results, the DSC curve of the virgin LDPE sample is presented in Fig. 3.7.

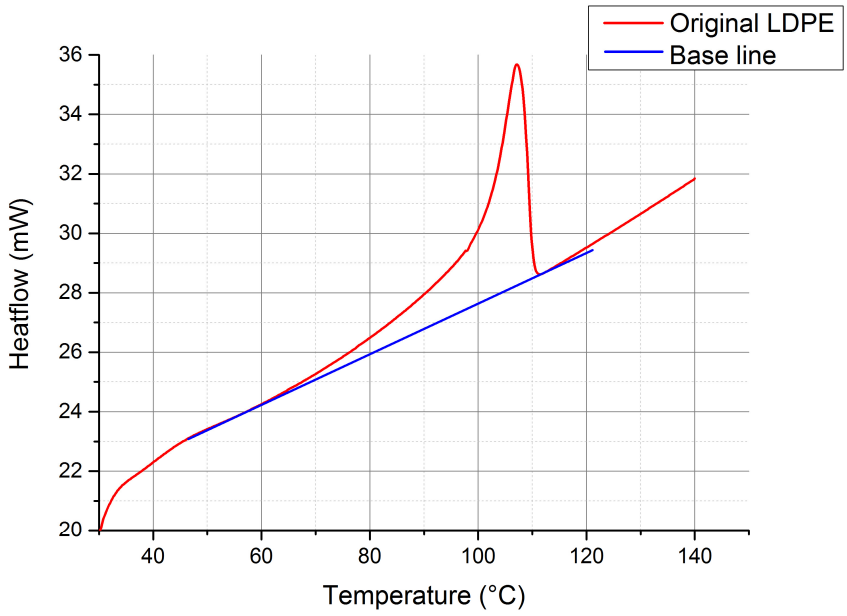

Figure 3.7: DSC results for original LDPE.

Crystallinity is one of the most important properties when dealing with semi-crystalline thermoplastics because it is related to many key properties of this type of polymer, including toughness, brittleness, and long-term stability. Based on the DSC curve, crystallinity can be calculated by the following equation using the baseline shown in Fig. 3.7 [60]:

$$X_c = \frac{\Delta H}{\Delta H_f \times 100\%} \tag{3.2}$$

where ΔH is the sample melting enthalpy, which can be calculated by Pyris software on the basis of the resulting curve and baseline, and ΔH_f is the fully crystalline melting enthalpy (the value for polyethylene is 287.35 J/g) [7]. Therefore, the crystallinity of the virgin LDPE we used was 38.47%.

3.3.2 Results for Air Ageing LDPE

Further measurements were performed on the 90°C and 100°C air thermal ageing LDPE films, and the results are shown in Figs. 3.8 and 3.9, respectively. Typically, the effect of thermal history should be removed by scanning twice when dealing with crystallinity measurements using the DSC technique, for the sake of reflecting the crystallization behaviour of the material itself [60], [61]. This is because the crystallinity of thermoplastic polymer can be impacted by the thermal history introduced by the solidification process and the molecular weight during manufacturing [62]. Therefore, the virgin LDPE sample was scanned twice with the same heating and cooling rate at 10°C/min, and the crystallinity calculated by second scan melting trace was 37.49%, which is less than 1% different from the value measured in the first heating process. Meanwhile, the first DSC curve of the virgin LDPE sample was net and smooth, and did not show any obvious thermal history peak, as seen in Fig. 3.7. Conversely, the samples we tested in other experiments were not melted and cooled twice, which means that the thermal ageing samples were measured with all thermal history. Thus, the DSC curve and crystallinity calculation of specimens were measured without the removal of thermal history and other thermal impacts.

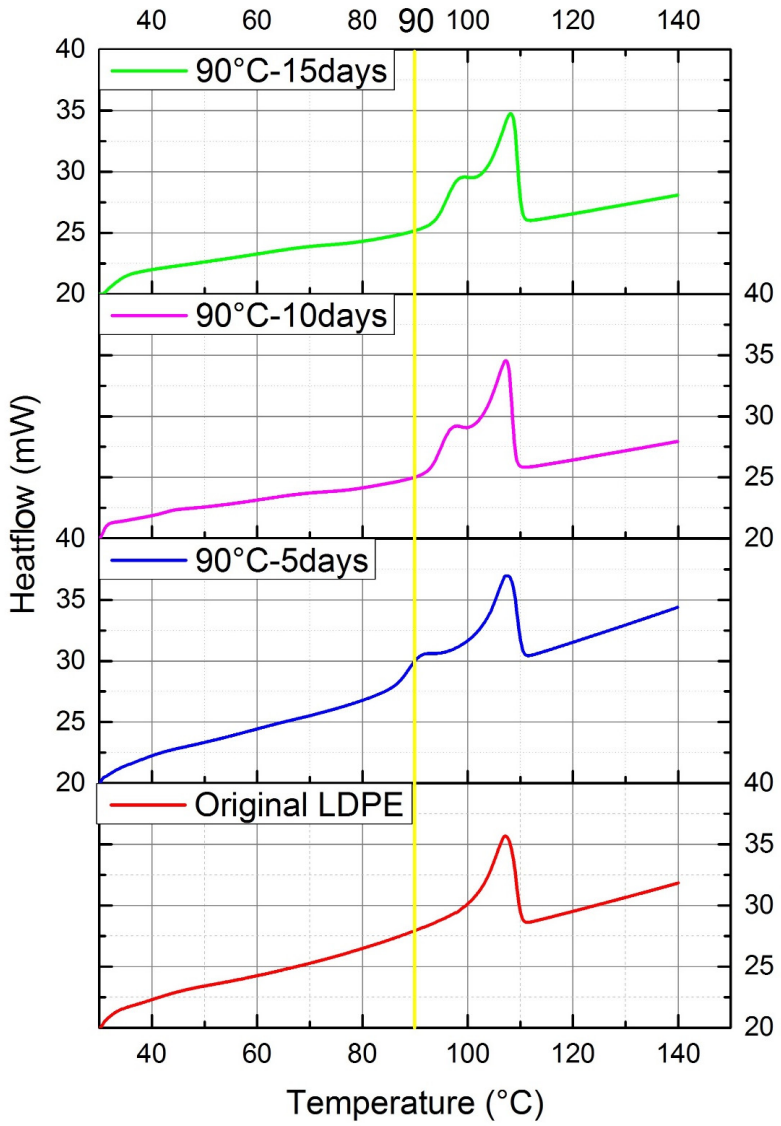

Figure 3.8: DSC curve of original and 90°C air thermal ageing LDPE.

Notably, there is a thermal history peak at 90°C in the curve of the 90°C five-day aged specimen compared with virgin LDPE, and further ageing leads to thermal history peak shifting to the right. Thermal history peak indicates the history of heating, melting, cooling crystallization, and annealing in polymeric material [63]. In the case of thermal ageing, there is a melting peak at the temperature used for ageing, because the crystallization behaviour of the sample could be improved in the ageing temperature range. So the melting peak from 85°C to 95°C in the curve of the 90°C five-day aged specimens indicates the specimens' ageing condition. As for further ageing, regarding the thermal history peak shift to the 90°C to 100°C range, it is supposed that the temperature fluctuation in the oven could be one of the reasons. On the other hand, the change of crystalline structure because of a longer ageing time could result in the melting peak move. In another words, initially, ageing introduces crystallinization, with crystallization temperature (Tc) at around 90°C. But all the crystalline structure is affected by further ageing, so the Tc increases.

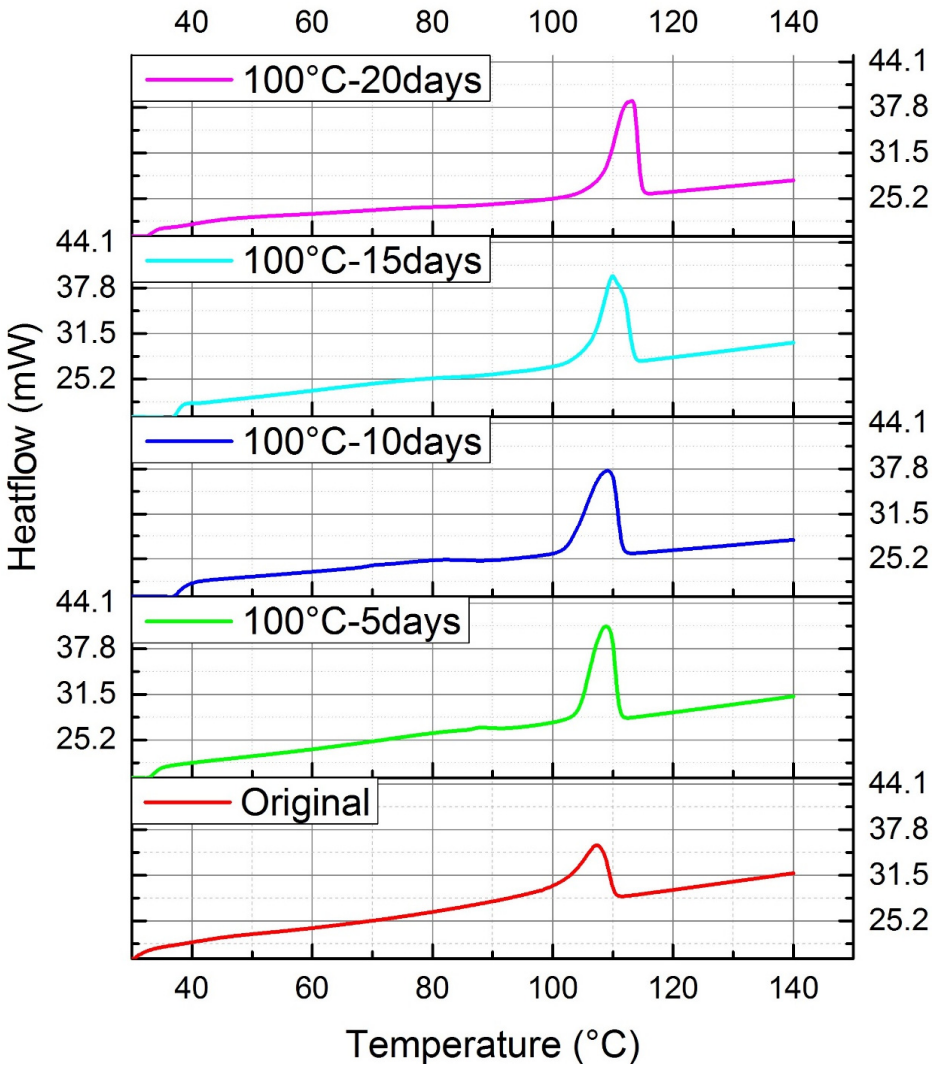

Figure 3.9: DSC curve of original and 100°C air thermal ageing LDPE.

In addition, the DSC melting trace for 100°C ageing LDPE shown in Figure 5.9 represents only one melting peak. Because the ageing temperature is close to the sample melting temperature, the thermal history peak could coincide with the melting peak. As a result, the peak of the ageing samples is narrower and higher. But the peak area can indicate the crystalline condition more clearly, so based on Eq. 3.2, the crystallinity of original, 90°C, and 100°C air thermal ageing LDPE is shown in Table 3.2 and compared in Fig 3.10.

Table 3.3 Crystallinity of original, 90°C, and100°C ageing LDPE.

	Original	**90-5**	**90-10**	**90-15**	
△H（J/g)	110.57	97.00	90.07	94.87	
Crystallinity（%）	38.21	33.52	31.13	32.79	
	Original	**100-5**	**100-10**	**100-15**	**100-20**
△H（J/g)	110.57	70.448	67.29	65.66	63.36
Crystallinity（%）	38.21	24.35	23.26	22.69	21.90

LDPE generally have a crystallinity ranging from 35 to 55% [2], and the data of the commercial sample used in this work is approximately 38.21%. Figure 4.10 shows that thermal ageing can lead to a decrease of crystallinity. Furthermore, the values of 100°C aged LDPE are much lower than those of 90°C aged samples. On the other hand, the crystallinity of samples aged at the same temperature for different times fluctuates within a small range. In other words, the higher ageing temperature has significant impact on the crystallinity of LDPE, but the influence of longer ageing time is limited within a certain range. Hence, the specimens which were aged at a higher temperature and for longer time were tested to investigate if the verdict described above can only be observed in LDPE with limited ageing degree. The LDPE samples aged at 100°C for 30 days and at 110°C for 5, 10, and 15 days were tested, and the results are shown in Fig. 3.11.

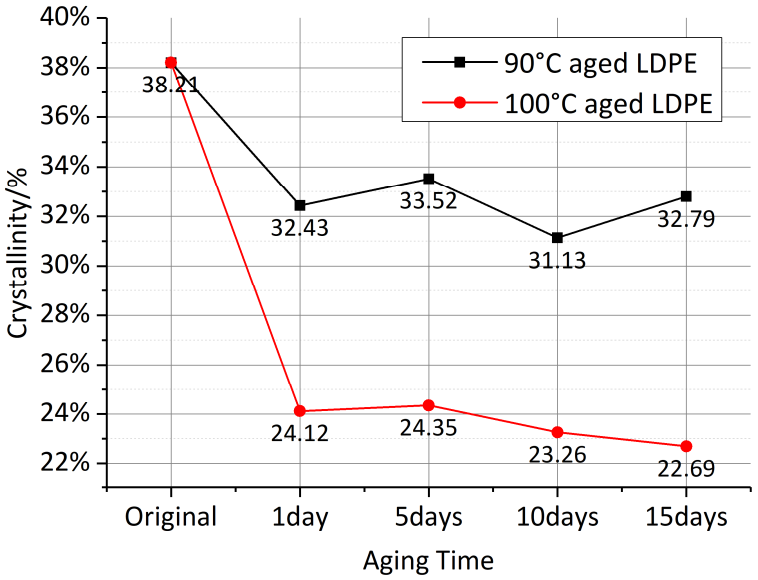

Figure 3.10 Crystallinity of original, 90°C, and100°C ageing LDPE.

Notably, there is not a wide difference between the crystallinity of 100°C 30-day ageing sample and other 100°C ageing samples. Furthermore, the results of 110°C ageing samples show similar traces. Additionally, it can be observed clearly in the last graph in Fig. 3.11 that the crystallinity decreases along with the rise of ageing temperature ranged over 90°C and 110°C.

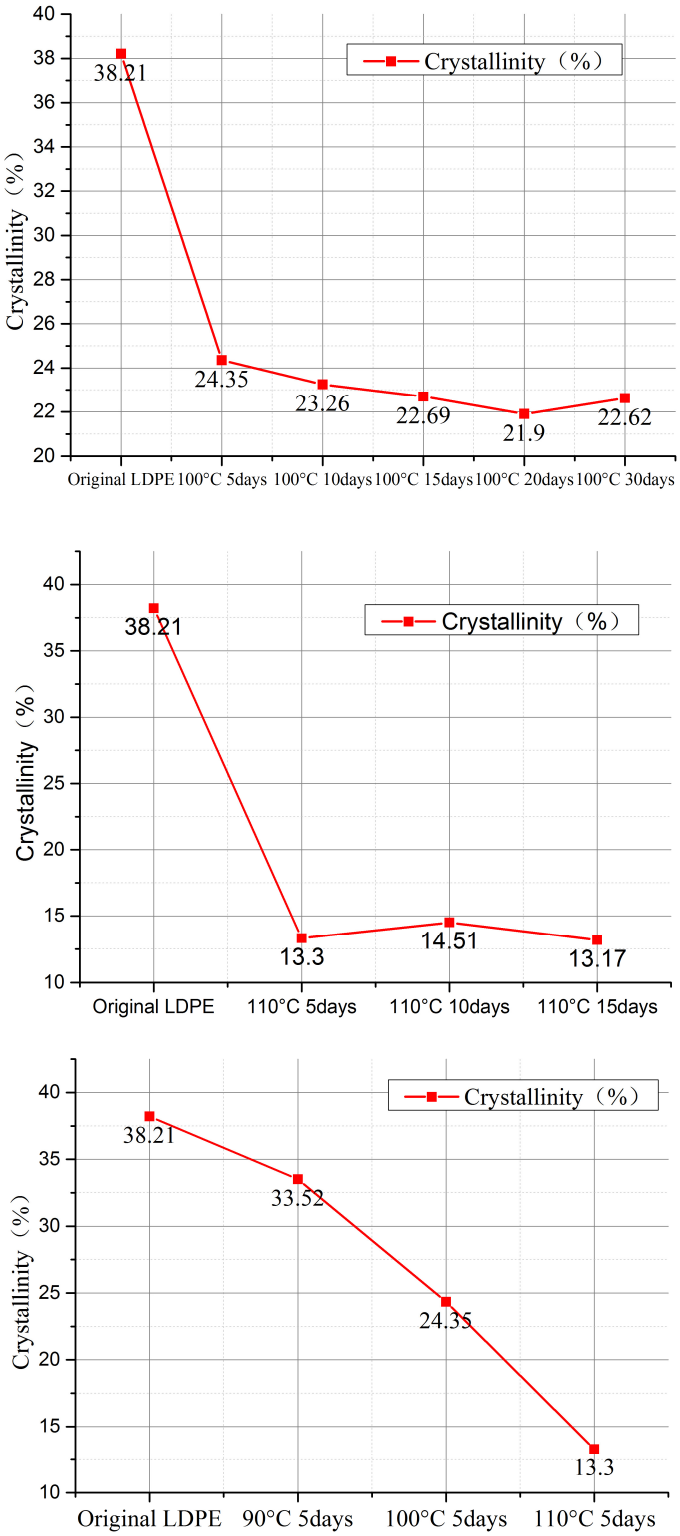

Figure 3.11: Crystallinity comparison among LDPE samples aged at 100°C for 30 days and at 110°C for 5, 10, and 15 days.

In our earlier conjecture, thermo-oxidation may lead to chain scission and reduction in crystallinity in LDPE. However, combining DSC melting trace and crystallinity, it is supposed that the crystallinity is affected by ageing temperature, as crystallization temperature is highly related to historic ageing

temperature. Crystalline structure is affected by both ageing temperature and time, so further experiments to explore the crystalline and chain structure are necessary.

3.3.3 Results for Nitrogen Ageing LDPE

The DSC tests were conducted on LDPE aged in nitrogen, and the curves were recorded as shown in Fig. 3.12. Additionally, the crystallinity of ageing samples was calculated by Eq. 3.2, and is presented in Fig. 3.13.

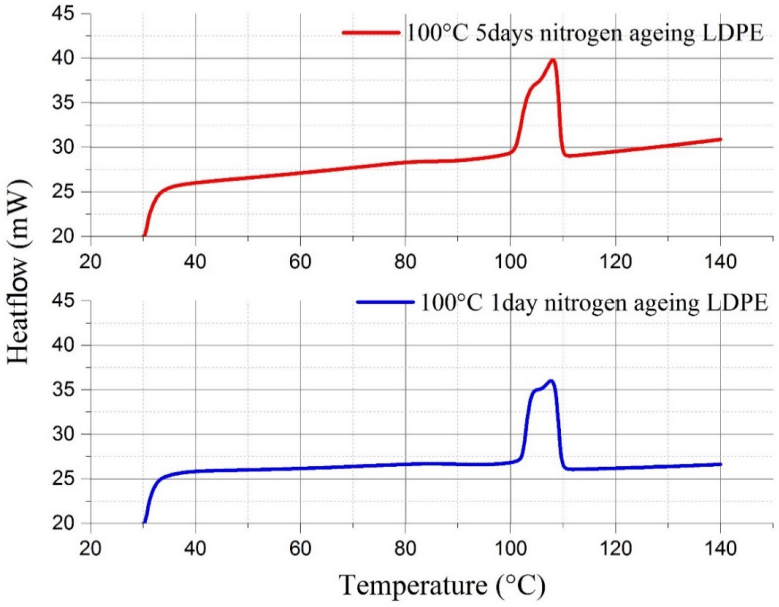

Figure 3.12: DSC curve of 100 °C nitrogen thermal ageing LDPE.

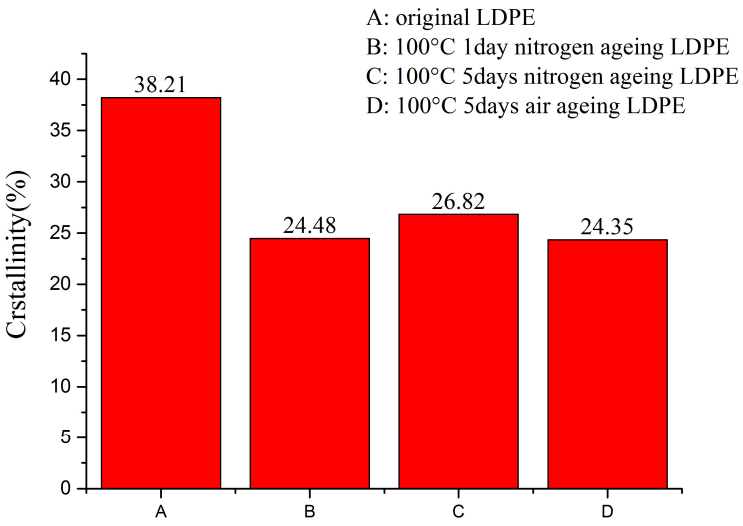

Figure 3.13: Crystallinity of 100°C nitrogen thermal ageing LDPE.

Basically, the graph indicates that the temperature of crystallization in nitrogen ageing LDPE is focused from 100°C to 110°C. Additionally, the heat flow peak shifts right slightly, compared with

the 100°C air ageing sample. This might be due to the temperature instability in the vacuum oven, so that the actual aging temperature of the nitrogen samples is slightly lower than the air aging sample. Hence, the thermal history peak is not completely superimposed with the melting peak of polyethylene. Furthermore, it can be seen in Fig. 3.13 that the crystallinity of nitrogen and air ageing samples does not show a wide difference. So the conjecture made above might be verified, indicating that crystallinity is highly related to ageing temperature.

3.4 Raman Spectroscopy

In other experiment works, it was found that some material features may highly related to the different oxidation degree in different layers. Therefore, the Leica microscope and Raman spectroscopy technique was used to detect the chemical feature especially the thermal-oxidative condition in the sample. A Renishaw Raman RM1000 system was used for ageing LDPE with a 780nm diode laser, and the laser power was set at 25mW. And Peltier cooled charged coupled device (CCD) detector was used in the system. Other setting are consistent with the recommendations of Renishaw in the confocal mode. The microscope with 50 × and 5 × magnification were utilized to focus on the sample from top surface to bottom, which is shown in Figure 3.14 and Figure 3.15. It could be used for positioning the sample film. And the measurements were performed every 10μm inside of LDPE sheet from top surface to bottom. In order to proceed the obtained data, the firstly spike and noises were removed with above 1000 times accumulations and polynomial filters. Then the monitored data was normalised with the normalisation reference peak (1294cm^{-1}). The results of 90°C-5days thermal aged LDPE is shown in Figure 4.16.

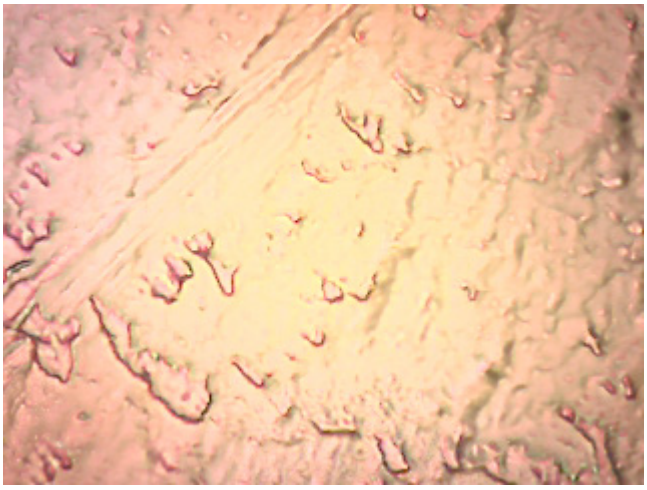

Figure 3.14. The top surface of 90°C-5days ageing LDPE under microscope in Raman system.

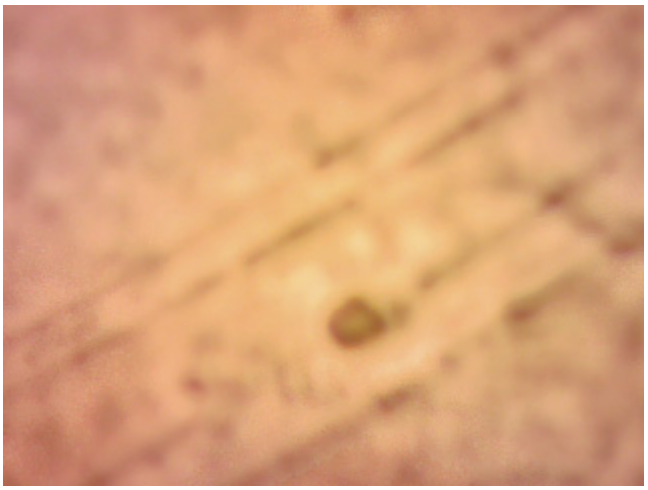

Figure 3.15. The bottom surface of 90°C-5days ageing LDPE under microscope in Raman system.

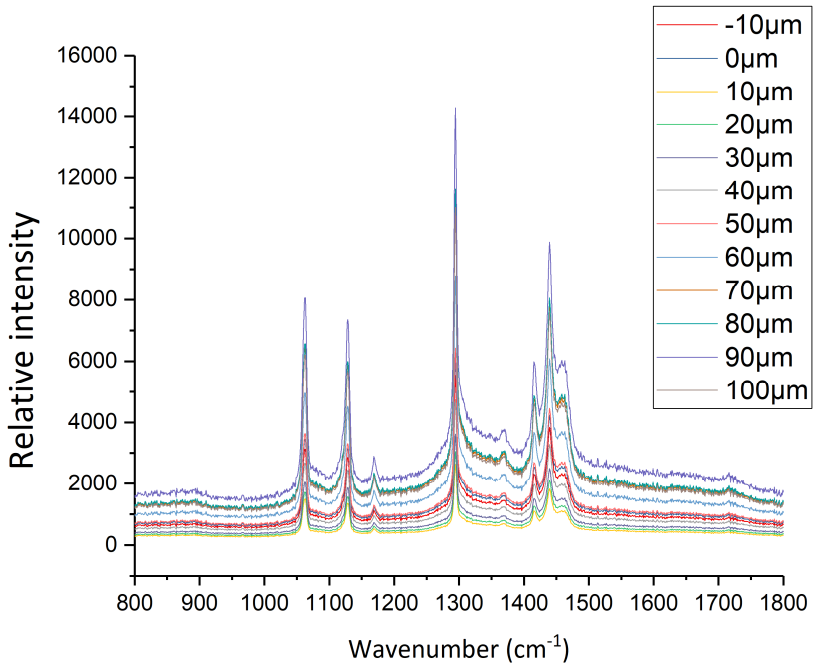

Figure 3.16. Raman spectra of 90-5days thermally aged LDPE film at different focus thickness points (-10μm-100μm)

Table 3.4 shows the peak positions of the main Raman bands of different forms of polyethylene for identifying the chemical structure[64]. It could be found that the peak at 1712 cm^{-1} perform the condition of C=O symmetric stretching which is the carbonyl group. The trends about the C=O group changing v.s. the position inside of original and different thermally aged LDPE films are illustrated in Figure 4.17.

Table 3.4 Raman bands assignment of polyethylene[64][65].

Raman peak position (cm^{-1})	**Assignment**	**Raman peak position (cm^{-1})**	**Assignment**
1083	C-C stretching	1454,1439	C-H bending
1169	C-H rocking	1453	Asymmetric CH_3 deformation

1299	C-H twisting	1605	C=O stretching – aromatic ring
1370	C-H wagging	1712	C=O symmetric stretching - carbonyl

As shown in Table above, the 1712 C=O symmetric stretching group were selected for the analysis, and the results for 90°C thermally ageing LDPE are illustrated in Figure 3.17. And Figure 3.18 shows the results for 100°C ageing samples. It could be found that there is no results for 100°C-15days and 20days thermally ageing LDPE. Because the sample turned yellow with deep ageing, and the worse light transmission makes the search for upper and lower surfaces inaccurate.

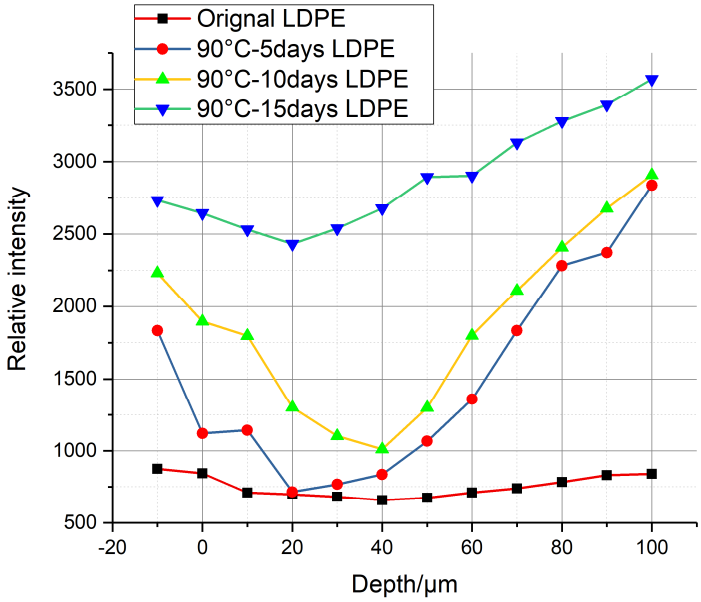

Figure 3.17. Raman spectra of 90°C thermally aged LDPE film at different focus thickness points on oxidation peak

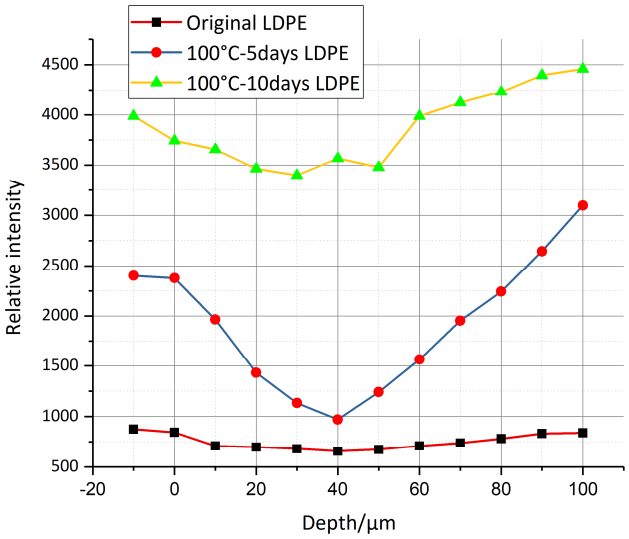

Figure 3.18. Raman spectra of 100°C thermally aged LDPE film at different focus thickness points on oxidation peak

These two figures above illustrate that the oxidative degree near surface is obviously higher than is inside of sample in the slightly ageing LDPE films, such as 90°C-5days, 90°C-10days and 100°C-5days thermally aged specimens. But in deep ageing samples, the oxidative degree is more evenly.

3.5 Conclusion

For the sample preparation and chemical analysis, the commercially available additive-free low-density polyethylene (LDPE), which has less influential factors, was chosen for thermal ageing. LDPE films aged in two different conditions (i.e. air in fan oven, nitrogen in vacuum oven) at different temperatures near melting point for multiple days were prepared. The subsequent chemical changes were monitored with the Fourier-transform infrared (FTIR) technique and differential scanning calorimetry (DSC) method. The results show that thermal ageing in the air leads to a gradual increase in the thermo-oxidative degree of LDPE, and the carbonyl index of sample ageing in the nitrogen environment is prominently reduced. The crystallinity cannot be impacted by oxidation degree, but ageing temperature dominates its change. However, the structure of crystal in ageing LDPE shows a correlation with the degree of ageing. Meanwhile, the LDPE specimens aged in nitrogen performed a notable decrease in crystallinity, with a similar trend with air ageing LDPE. The Raman results show that oxidative degree near surface is higher than it in the mid of sample in slightly ageing LDPE. However, the oxidative degree is more evenly in deep thermally aged samples.

Chapter 4 Space Charge Performance in Thermal Ageing LDPE

In early research, the space charge behaviour was defined as a significantly important electrical property in polymer insulation materials because the distortion of local electric fields which is introduced by accumulated space charges has obvious effect on high field conduction and breakdown phenomena [66]. Space charge impact has been explored in HVDC insulation systems for a long period of time, and its space charge behaviour is highly related to insulation lifetime [67]. Meanwhile, in our research, the space charge behaviour of material is the key that links ageing and electrical performance. As confirmed by the results presented in the previous chapter, thermal ageing has tremendous influence on the chemical properties of polyethylene, and in this part, the space charge behaviour of thermal ageing insulation material is explored. The space charge phenomena of different types of thermal ageing LDPE were measured by the pulsed electroacoustic (PEA) technique, and the results are shown and analysed in this chapter.

4.1 Space Charge Measurement

4.1.1 Overview of Space Charge Measurement Techniques

Researchers attempted to profile accurate space charge distribution in solid dielectrics with an effective method, in order to conduct a comprehensive study of research into space charge behaviour. In earlier studies, destructive approaches were used, and they resulted in significant changes in the charge distribution during the sample preparation before measurement. Two destructive approaches are the Field Probe technique [68] and Dust Figure method [69]. Generally, in these methods, charge behaviour was measured by detecting the surface of slices from cut samples. From the first non-destructive charge measurement method, the transient heating technique, proposed by Collins in the mid-1970s [70], different types of non-destructive measurements have been developed in the past three decades. These methods can be classified into two categories, with two different ultimate principles. The first type consists of thermal methods and includes laser intensity modulation method (LIMM) [71], thermal pulse (TP) method [72], and thermal step pulse (TSP) method [73]. In this case, thermal expansion caused by varied temperature can induce the movement of space charge that accumulated in solid samples and lead to current that contains the charge distribution information [74]. Another type of non-destructive method consists of acoustic methods, including pressure wave propagation (PWP) method [75], laser induced pressure pulse (LIPP) method [76], and pulsed electro-acoustic (PEA) method [77].

The PEA technique is more common than other techniques due to its simplicity in structure, low cost, and ease of implementation. Generally, in the acoustic technique, the displacement of charge caused by an applied pressure wave can lead to an outcome current which reflects the charge distribution. The principles of the widely used PEA method are briefly described in the next section.

4.1.2 Pulsed Electro-Acoustic (PEA) Method

The pulsed electro-acoustic technique was first developed in Japan in the 1980s [77]. This method underwent great development and improvement and become the most common technique to profile charge distribution in solid dielectrics. The principle of the PEA method is represented in Fig. 4.1 [78]. The application of an external pulsed field can perturb the internal space charge, and the resulting Columbic forces then generate acoustic waves, which can be detected by a piezoelectric transducer attached at the ground electrode. Therefore, the acoustic wave signal that contains the information about charge distribution is converted to an electrical signal. After a rational calibration process [79], the charge distribution can be mapped and the charge density can be calculated [80].

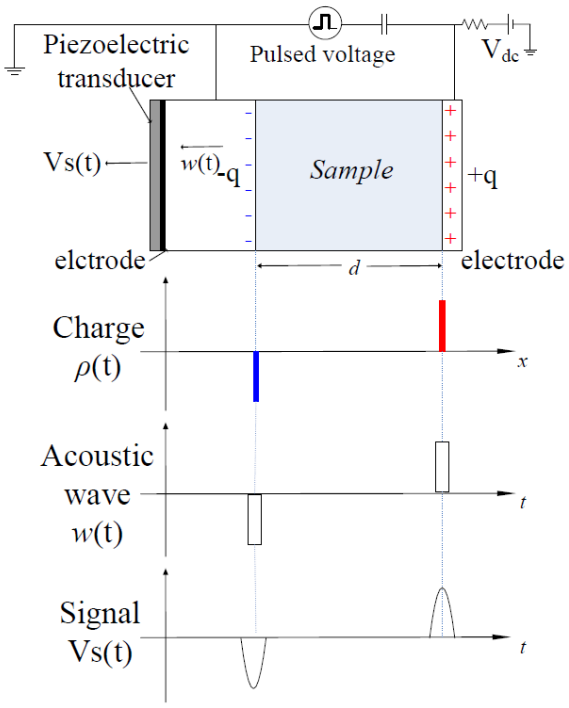

Figure 4.1: Principle of the pulsed electro-acoustic method [78].

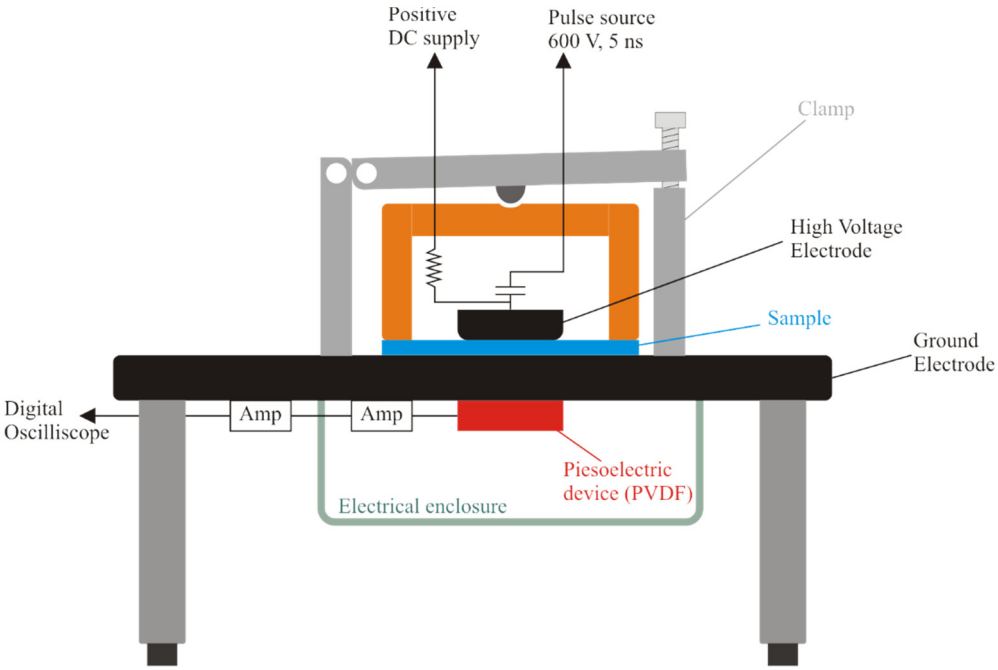

Figure 4.2: Structure of a PEA measurement system.

A common PEA system setup is shown in Fig. 4.2. This setup was employed for space charge measurement detailed in this report. In this system, positive high-voltage direct current (HVDC) voltage can be applied to samples, and the pulse source with 600 V, 5 ns provides the external pulsed electric field, which is coupled with a capacitor to limit the breakdown current [81]. The sample film is sandwiched by high voltage and ground electrode with opportune force; the thickness should be limited to between 0.1 mm and 0.2 mm to obtain a high-resolution output signal. A sample with too thin a thickness will result in a low resolution, and too thick a sample will lead to more noise. The piezoelectric transducer attached on the ground electrode is PVDF film. The converted electrical signal from the piezoelectric device will be magnified with amplifiers and then received by a digital oscilloscope. It should be noted that the piezoelectric transducer and one of the amplifiers are set with an electromagnetic shield for better signal outcome to improve signal-noise ratio.

4.2 Experimental Conditions

Space charge dynamics were measured using the pulsed electroacoustic (PEA) system shown in Fig. 4.2. The thickness of the sample was ~100 µm. A drop of silicone oil was placed between the LDPE film and two electrodes to ensure good acoustic propagation. To subtract the impact of the capacitive charges from the electrodes, a method based on a reference data from a reference voltage was used in the measurements [82]. In this method, first the reference space charge density was measured in a very short period under a lower reference voltage compared with the applied voltage, and an assumption was made that there is no injected charge accumulating in material

under this reference voltage for less than 1.5s volts-on time [83]. The reference voltage is 15kV/mm in this thesis. So the space charge density after subtracting $\rho_{acc}(x)$ is given by [82] the following:

$$\rho_{acc}(x) = \rho_{app}(x) - \frac{V_{app}}{V_{ref}}\rho_{ref}(x) \tag{4.1}$$

where $\rho_{app}(x)$ and $\rho_{ref}(x)$ are space charge density under applied voltage and reference voltage, respectively. V_{ref} and V_{app} represent reference voltage and applied voltage. Meanwhile, the previous work shows that reference subtracted space charge density collected at 2 kV from $180\mu m$ LDPE samples turns out to be nearly zero. Furthermore, the threshold field for charge injection is 8 kV/mm in LDPE samples in PEA measurement [82][84] . In addition, the value threshold field was determined by electroluminescence measurement on LDPE material under DC field, and the threshold is approximately 15~20 kV/mm[85]. Hence, the reference electric field was set at 10 kV/mm to measure capacitive charge, and all types of samples were stressed at an electric field of 40 kV/mm. The PEA data were collected during volts-on for 1800 s and volts-off for 1800 s to explore both the injection and decay behaviours of space charge. Longer volts-on time may lead to more charge neutralisation, and further analysis and simulation could be complicated. Based on the subtraction method, the charge profile of original LDPE before and after processing are shown in Fig. 4.3 (a) and (b), respectively. Compared with original results, the right-side graph shows space charge profile more clearly, and the charge density shown can be defined as injected charge density, so the amount of injected charges can be calculated by integrating the curve.

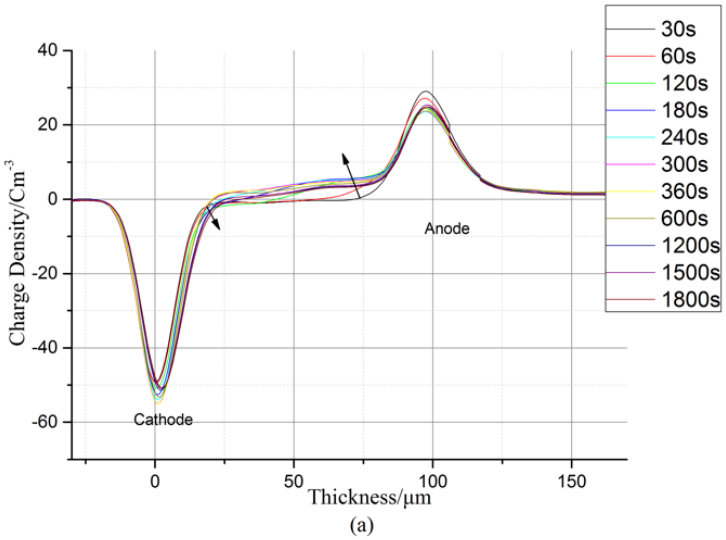

(a)

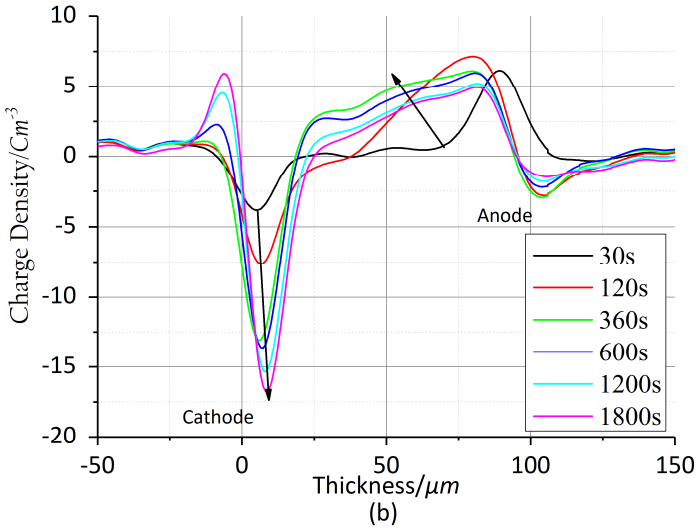

Figure 4.3 The space charge profile of original LDPE before (left) and after (right) data processing.

It can be observed in Fig. 4.3 that the charge injection process during 1800 s DC field application in original LDPE can be divided into three typical parts. Initially, both kinds of charge carriers are injected into the specimen (0 s~360 s), and this is followed by the recombination of electrons and holes (360 s~600 s), as the amount of positive charges decreases. In the last stage, negative charge continues to be injected and moves deep into the bulk to neutralize the positive charge, resulting in the reduction of the amount of positive charge (600 s~1800 s). In other words, positive charges play a key role in early stage (before 360 s), and electrons predominate afterward. The different injection barriers and trap depths between holes and electrons are direct factors in this result. Based on the trapping parameter model [38], the injection barrier of holes in LDPE is lower than electrons, which means that holes can be easily injected. But the depth of both the deep and shallow hole traps is higher than electrons, so a positive charge is harder to trap and accumulate. Meanwhile, the result is that the total charge amount after 1800 s cannot be used to extract the trap density in different samples.

4.3 Space Charge Behaviours in Air Thermal Ageing LDPE

4.3.1 Charge Injection

The volts-on space charge dynamics of LDPE films which were thermally aged at 90°C for 5, 10, and 15 days in fan oven are shown in Fig. 4.4, and the results of 100°C 5, 10, 15, and 20 days of air thermal ageing of specimens are shown in Figs. 4.5 and 4.6. First, comparing the results of the 90°C five-day ageing sample with the original sample, shown in Fig. 4.3, the maximum amount of injected charges in the original sample is obviously higher than the amount of slightly aged LDPE after 1800 s volts-on. This might be for two reasons: the increase of DC conductivity makes the charge carriers

move easily in 90°C five-day ageing LDPE, so the charge neutralization is exacerbated and less charges accumulate. In addition, surface oxidation on the ageing sample may suppress charge injection, as the trap distribution may be changed [86]. These two hypothesises will be discussed in the next chapter, combined with the experimental results of DC conductivity and breakdown strength. However, it can be clearly found in the 90°C 10-day and 15-day ageing samples that both amounts of holes and electrons were increasing over 1800 s, as shown in Fig. 4.4 (a) and (b). So it can be supposed that the neutralization between two varieties of carriers is retarded. Meanwhile, the charge peaks near the electrode are obviously increasing in these further aged LDPE samples, compared with original and slightly aged samples.

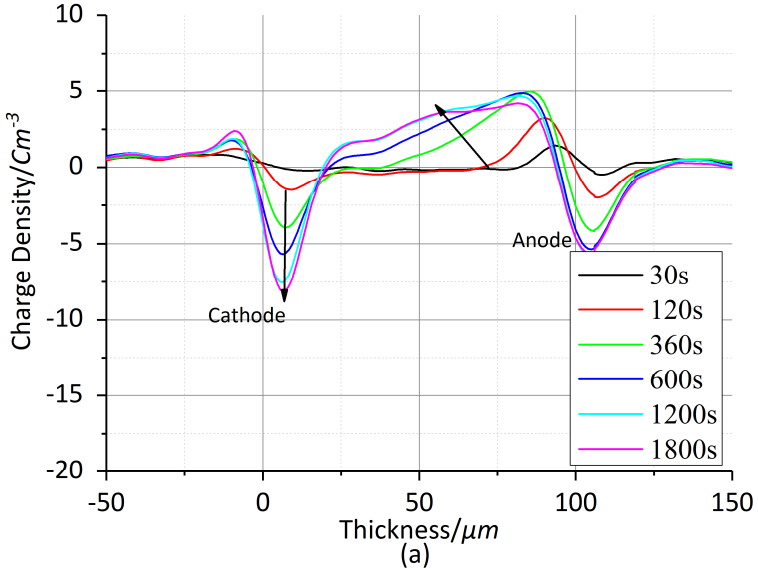

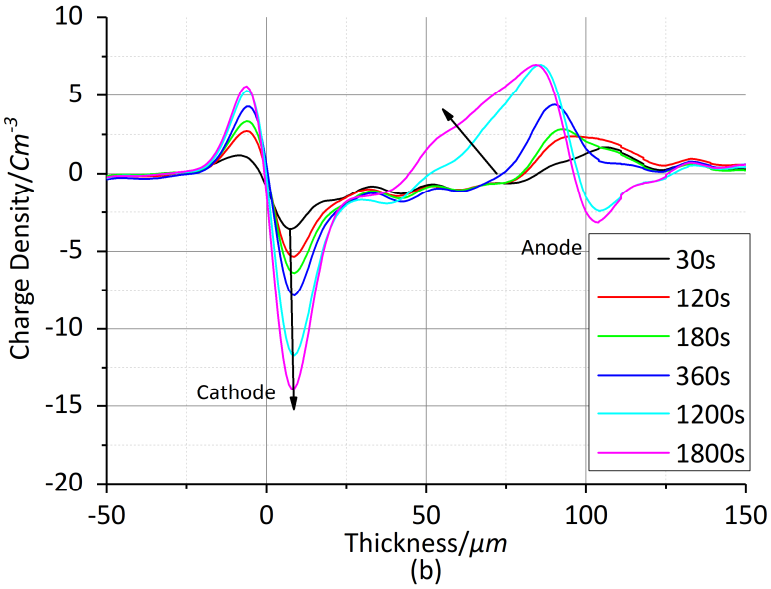

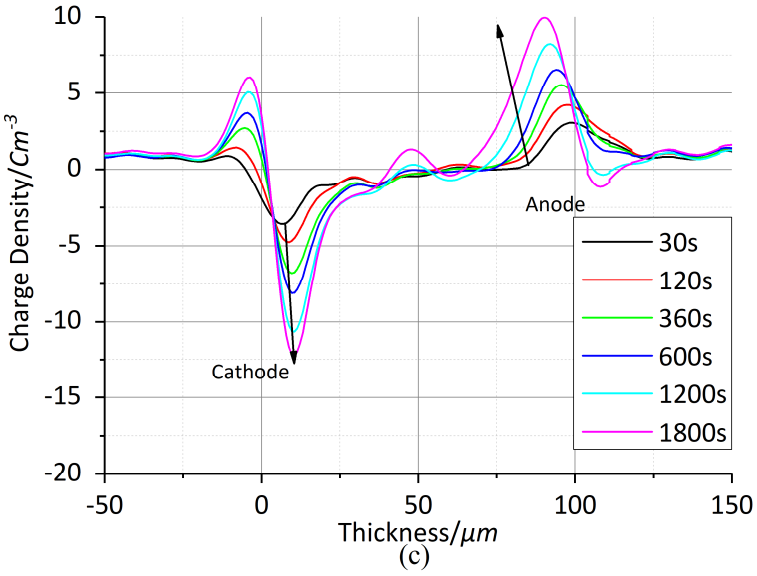

Figure 4.4: Space charge profiles over 1800 s at 40 kV/mm in 90°C 5-day aged LDPE (a), 90°C 10-day aged LDPE (b), and 90°C 15-day aged LDPE (c).

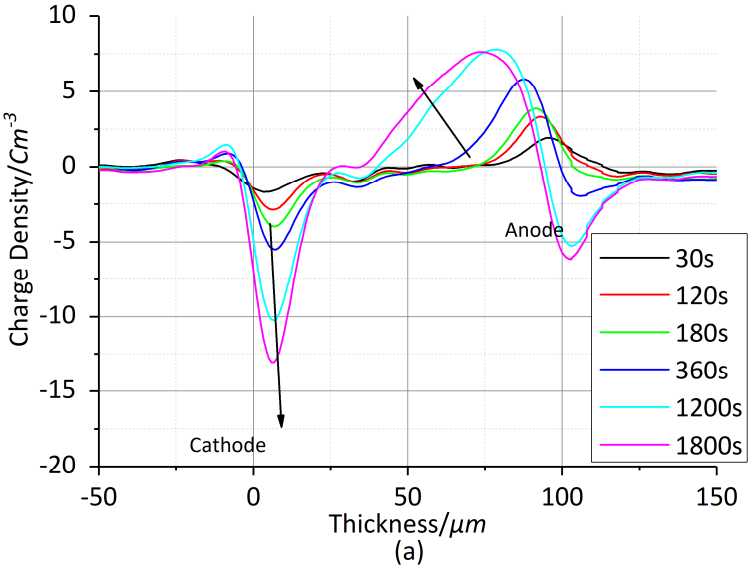

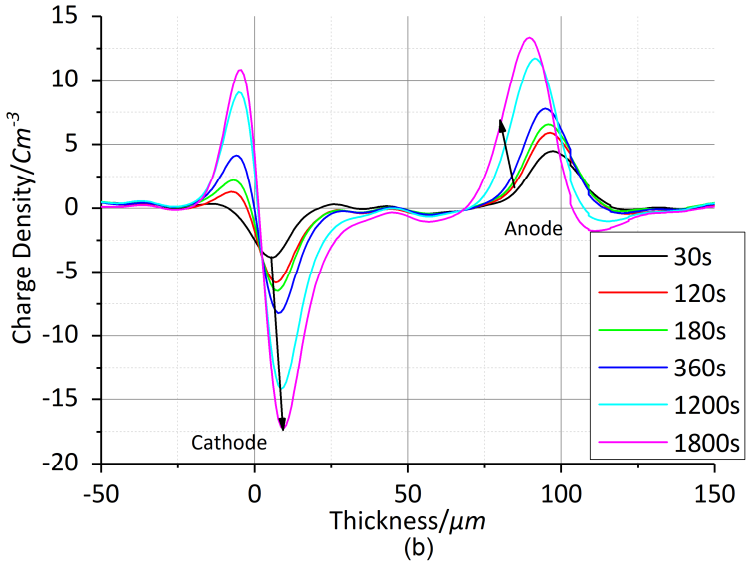

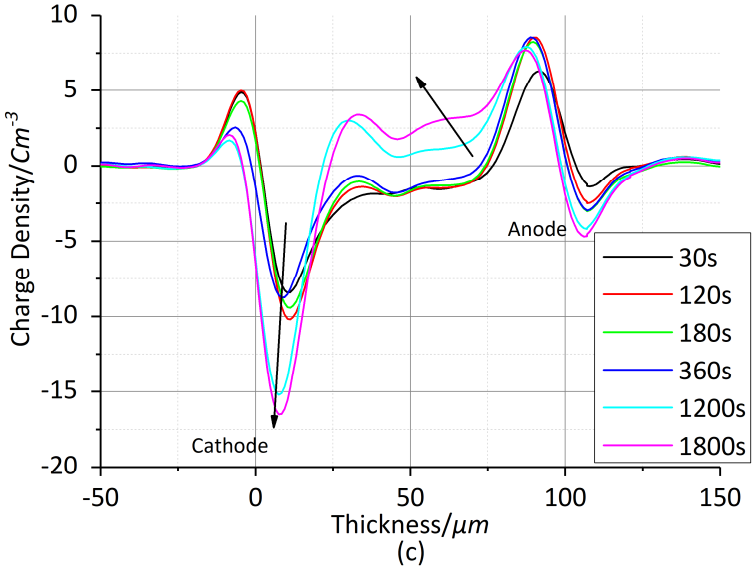

Figure 4.5: Space charge profiles over 1800 s at 40 kV/mm in 100°C 5-day aged LDPE (a), 100°C 10-day aged LDPE (b), and 100°C 15-day aged LDPE (c).

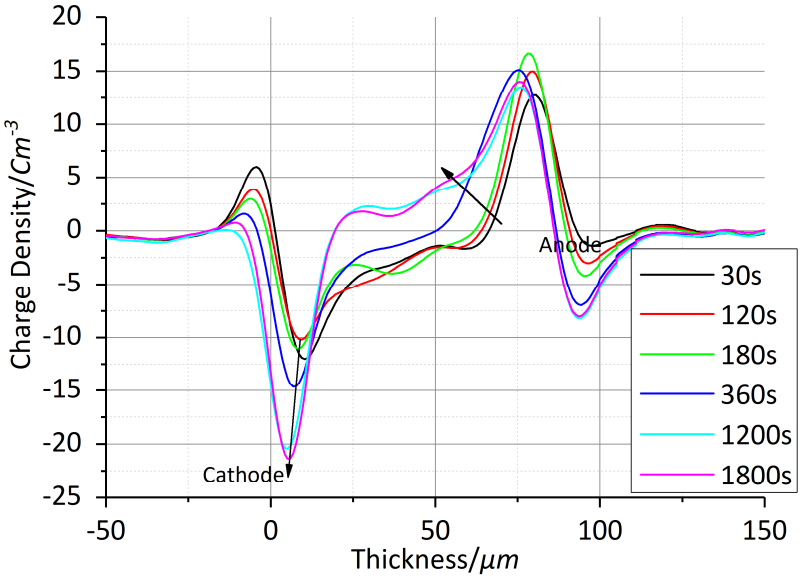

Figure 4.6: Space charge profiles over 1800 s at 40 kV/mm in 100°C 20-day aged LDPE.

The space charge formation in 100°C 5- and 10-day aged LDPE have similar traces with the 90°C 10- and 15-day aged samples, as shown in Fig. 4.5 (a) and (b). In the result of these 100°C ageing samples, hardly any recombination phenomenon can be observed, and the maximum charge densities of both kinds of carriers in the vicinity of the electrodes are enhanced. In addition, the gap between positive and negative charge peaks is increased. It can be inferred that the amount of accumulated charges inside of the bulk of slightly ageing LDPE film is decreased.

As for the specimen ageing at 100°C for 15 and 20 days in air, it is clear that more charges are injected and charges move inside the bulk more easily, especially the positive charge. Meanwhile,

with the increase of the applied field time, the positive carriers gradually dominate, while the injected negative charges shift to the electrode while increasing.

4.3.2 Charge Decay

Then, the volts-off process in different kinds of LDPE films was detected. After removing the external DC field, the space charge profiles for the decay process of original and 90°C aged samples were measured and are shown in Fig. 4.7; Fig. 4.8 shows the 100°C aged sample results. As the influence of external field on charge distribution can be removed, the space charge profile during the decay process can reflect the actual space charge behaviour more clearly, so the charge decay process is commonly used to characterize the spatial charge characteristics of a material and build the relative charge model [24] [87].

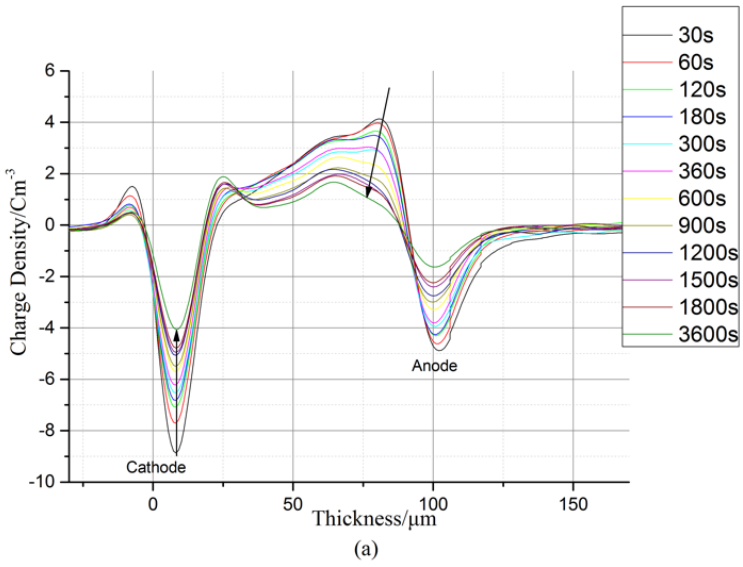

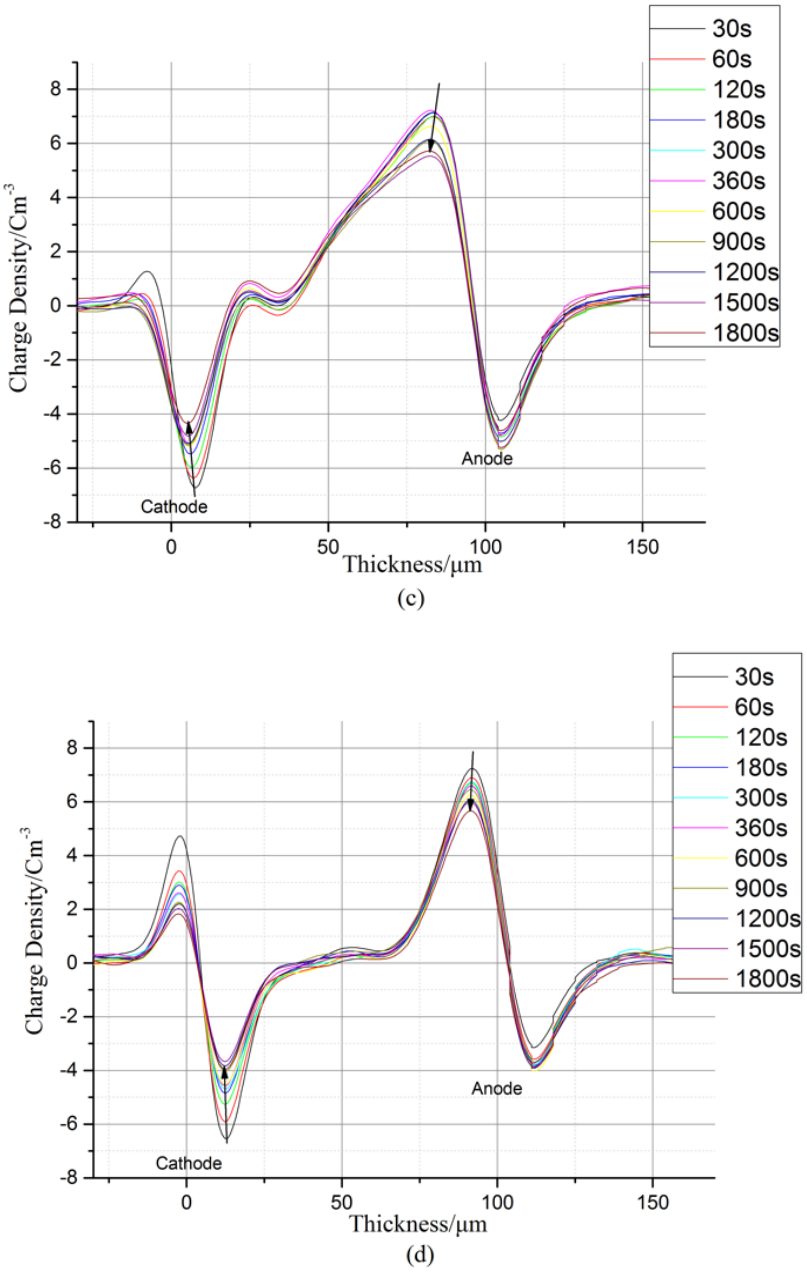

Figure 4.7: Space charge decay after the removal of the applied voltage in original LDPE (a), 90°C 5-day aged LDPE (b), 90°C 10-day aged LDPE (c), and 90°C 15-day aged LDPE (d).

Generally, for the results of original and 90°C ageing polyethylene in Fig. 4.7, it is clear that the charge formation is similar as inferred in the volts-on results. Less charges were injected into the 90°C 5-day specimen, compared with the original LDPE. In addition, it can be observed that charges in the original LDPE decay quicker than in the 90°C 5-day sample, as shown in Fig. 4.7 (a) and (b). Furthermore, with the increase of thermal ageing time, carriers are more difficult to move inside and more easy to accumulate in the vicinity of electrodes, as shown in Fig. 4.7 (c) and (d). In the case of the 100°C ageing specimen, shown in Fig. 5.8, the space charge phenomena of slightly ageing samples are very close to the situation of 90°C LDPE, but deeper ageing samples show quite a different trend. It can be seen in Fig. 4.8 (c) that charge decay is rapid initially, and the amount of

remaining charges is markedly smaller in the 100°C 15-day ageing sample. Furthermore, there is no space charge decay data for the sample aged at 100°C for 20 days, shown here, as charge decays quickly, and the PEA system can only record noise but no charge after 15s.

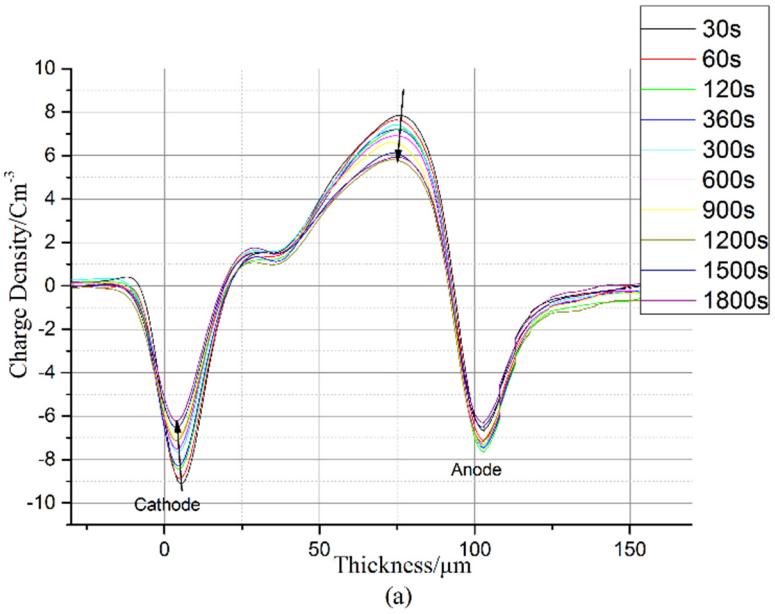

(a)

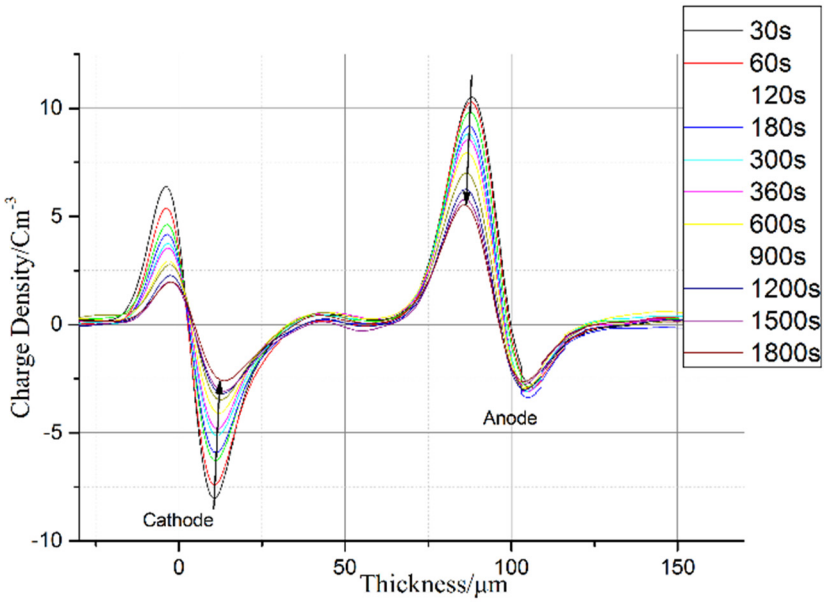

(b)

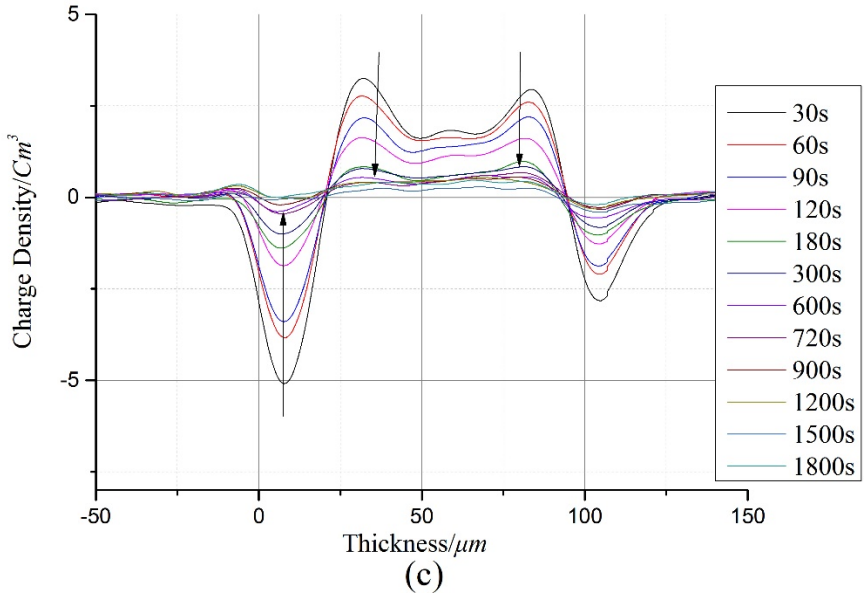

Figure 4.8: Space charge decay after the removal of the applied voltage in 100°C 5-day aged LDPE (a), 100°C 10-day aged LDPE (b), and 100°C 15-day aged LDPE (c).

The total amount of space charge in the bulk is estimated using the following equation:

$$Q = \int_0^d |\rho(x)| \cdot S \cdot dx \tag{4.2}$$

where $\rho(x)$ is the charge density, S is the electrode area, and d is the thickness of the layer. To detect space charge dynamics of ageing samples further, after the total charge amounts were calculated, they were analyzed by the normalization method, shown in Fig. 4.7, to better compare their charge decay rates. Generally, it can be seen in Fig. 4.7 that the total charge in 90°C and 100°C 5-day aged LDPE decays with a slower rate compared with original samples, but charges decay more quickly in 90°C 15-day aged samples. Moreover, the charges in 100°C 15-day aged samples decay much more drastically.

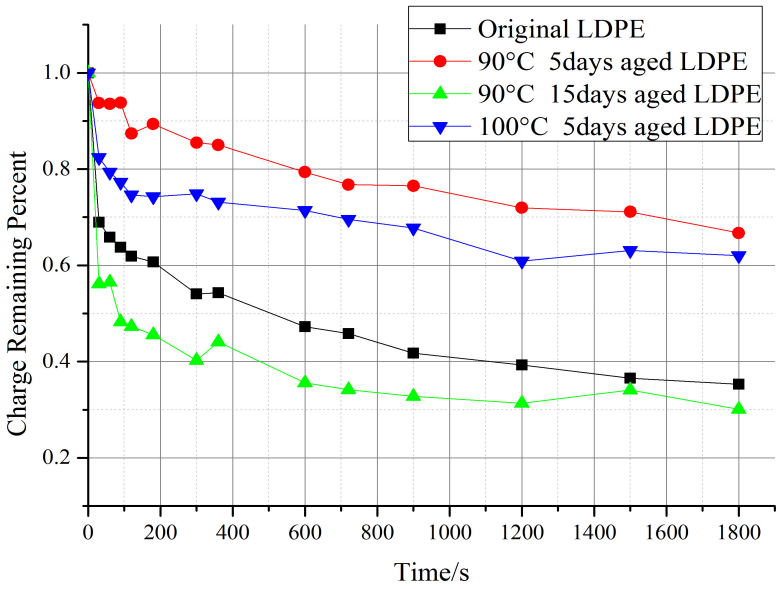

Figure 4.9: The charge decay rate of original, 90°C, and 100°C ageing samples.

In a previous paper which was reviewed in the last section [23], a model based on shallow and deep traps has been proposed to describe space charge dynamics. Moreover, the number density of total trapped charge density during decay is given by the following equation [24]:

$$n(t) = n_1(t) + n_2(t) = n_{10}\exp(-k_{th1}t) + n_{20}\exp(-k_{th2}t) \tag{4.3}$$

where $n_1(t)$ and $n_2(t)$ signify the number density of trapped charges in shallow and deep trap, respectively. The parameters k_{th1}, k_{th2}, n_{10}, and n_{20} are related to microstructure of the material. Changes in parameters may reflect ageing taken place in the material. In detail, k_{th1} and k_{th2} relate to two different trap depths. Consequently, all the values of charge amount vs. time were curve-fitted using the two exponential expressions given in the equation below:

$$Q = a \cdot \exp(-b \cdot t) + c \cdot \exp(-d \cdot t) \tag{4.4}$$

Based on the PEA results, the exponential decay curves of total charge amount in all the samples are found by using the MATLAB curve fitting tool based on Eq. 4.4. The total charge of normal and aged samples and their relationship with time are shown in Fig. 4.10. Meanwhile, the first point of each group shows the total charge collected 30 s after removal of the voltage, which is close to the total charge that was injected into the sample after 1800 s volts-on. In terms of the fitted curve, the decay time of total charge decay to half of the total decay charge during 1800 s can be calculated and is shown in Table 4.1. Generally, it can be observed that the total charge of aged samples decays with a slower rate, compared with the original sample. Exceptions occurred when the sample was aged for a longer time and at a higher temperature, such as the sample aged at 100° C for 15 days. The charge in the sample aged at 100° C for 15 days decays rapidly initially, and the remaining

charge decreases with a much slower rate. Notice that there is no space charge decay data for the sample aged at 100° C for 20 days. This is because charge decays rapidly, and nothing is left after 15s.

Furthermore, Table 4.1 shows that the decay rate of total charge rises from the original to the 90°C 10-day aged sample and from the original to the 100°C 5-day aged sample but reduces from the 90°C 10-days aged sample to the 90°C 15-day aged sample and from the 100°C 5-day aged sample to the 100°C 15-day aged sample. And the results of sample with further ageing time cannot be observed and calculated. Meanwhile, it was observed that the charge peak adjacent to the anode electrode from the aged LDPE sample increases with ageing severity, but the total charge amount inside the sample decreases. This may be due to the recombination effect between positive and negative charges injected from the cathode and anode, respectively.

Table 4.1: The decay time of total charge decay to half of the total decay charge during 1800 s.

Decay time (s)	Original	5 days	10 days	15 days
90°C aged LDPE	404	460	653	583
100°C aged LDPE	404	530	480	120

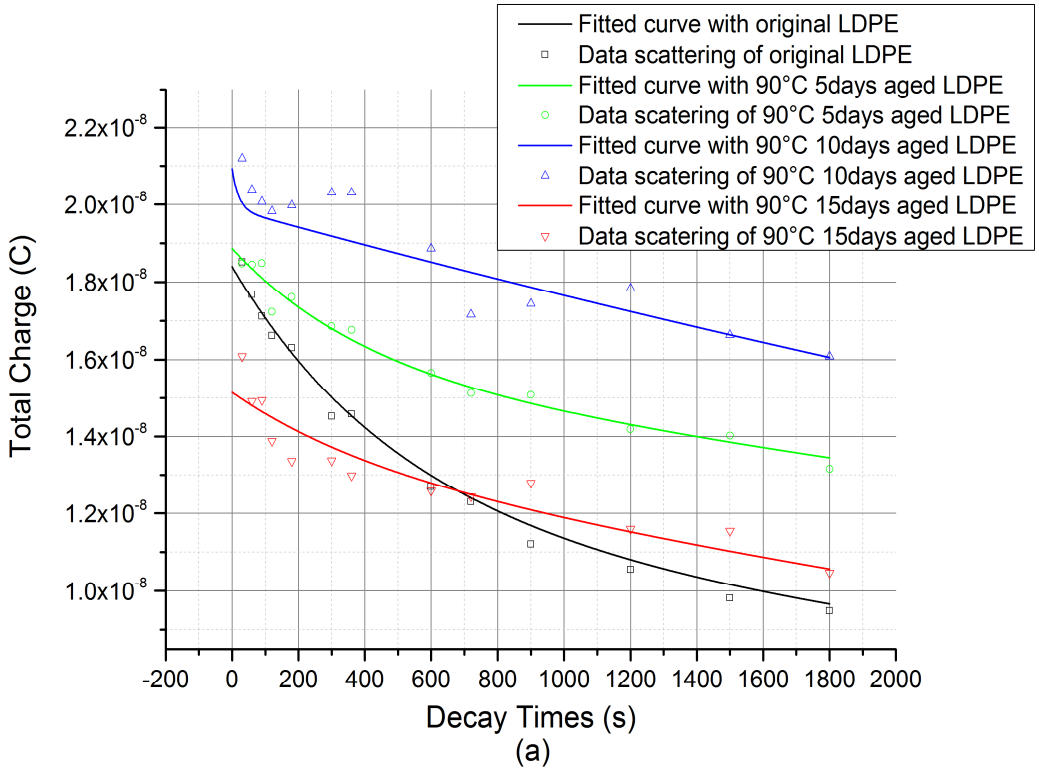

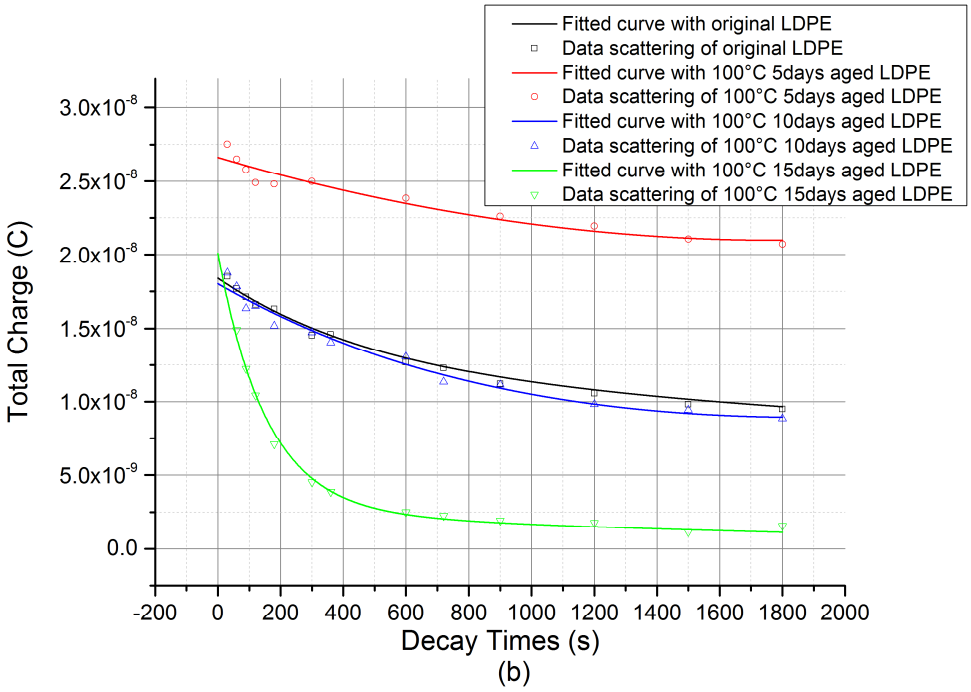

Figure 4.10: Curve fitting results of charge decay after the removal of the applied voltage in original and aged LDPE films.

4.3.3 Discussion

In previous research, shallow and deep traps were proposed to simplify the model and limit charge trapping parameters. Furthermore, the traps with high and low energy level can be related to physical and chemical defects in insulation materials, respectively [23]. Meanwhile, in literature, it has been stated that thermal ageing mainly introduces deep traps into polyethylene [35]. In our results concerning thermal aged LDPE, it seems that the injection of charge carriers becomes harder in the lightly thermal aged samples compared with the original LDPE. This might be explained with deep traps formed after thermo-oxidation. In the slightly aged sample shown, a small amount of deep traps adjacent to the electrodes might be introduced by thermo-oxidation on the surface. Therefore, the average energy of the injection barrier between the electrode and sample might be enhanced, which can suppress charge injection. Conversely, more traps in the vicinity of the electrodes result in nonuniform distribution of space charge, and electric field distortion caused by charge accumulating near the surface may also hinder charge injection, as illustrated in Fig. 4.11. Particularly, for 90°C 5-day aged sample shown in Fig. 4.4, the effect of deep traps in the vicinity of electrodes is not significant, so carriers can still shift inside and be trapped in intrinsic traps. In addition, some carriers can neutralize inside of the sample.

Then, further ageing introduced more deep traps on the surface, which leads to more difficulty in charges moving inside, such as for 90°C 10-day,15-day, and 100°C 5-day, 10-day air thermal ageing

LDPE. More carriers are injected but are trapped in these deep traps near the surface; as a result, smaller amounts of carriers move inside and neutralize. Additionally, it could be verified in the charge decay process, in terms of the theoretical model based on shallow and deep traps, which represents that both trapping and detrapping processes of deep trap charge are slower [23], which was reviewed in chapter 3. For these further ageing samples, a large amount of charges trapped in deep traps did not decay after 1800 s. As shown above in Fig. 4.8(b) for the 100°C 10-day ageing sample, charges are concentrated in the areas close to electrodes in this extreme case. But charges in this specimen decay with a higher rate, compared with slightly aged samples, which might be the reason that electrical conductivity is enhanced by further thermal ageing. The 90°C 15-day aged LDPE shows a similar result, as presented in Fig 4.7 (d). Consequently, the slightly thermal aged samples cannot be used in a trapping parameter model, which requires uniform charge distribution. That is to say, the thermal ageing sample we used to modify trapping model should have a sustainable thermo-oxidation degree, which can be estimated by carbonyl index.

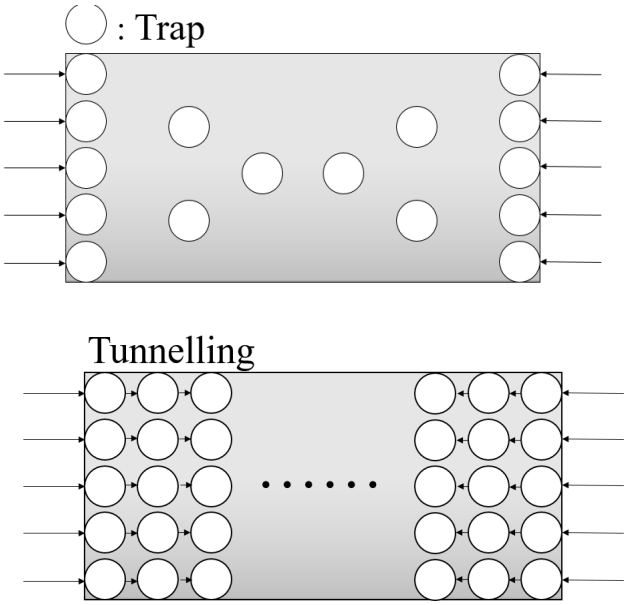

Figure 4.11. Trap distribution diagram in slightly aged sample(left) and further aged sample (right).

Furthermore, as for the samples aged at 100° C for 15 days and 100° C for 20 days, there is a significant chemical change occurring inside of the samples. A huge number of deep traps may be generated inside the entire sample due to further severe thermo-oxidation. Hence, the average deep trap density enhancement and charge tunnelling can easily occur in severely ageing samples. As shown in Fig. 4.5 (c) and Fig. 4.6, a larger maximum charge density and more charges, especially positive charges being trapped during 1800 s volts-on period, can be found, which means that more traps are involved. In other words, carriers can be easily injected inside and more charges are trapped and accumulate in 100° C 15-day and 20-day aged LDPE. Meanwhile, further increase in

electrical conductivity due to thermal aging and quantum tunnelling effect lead to a particularly fast charge decay in these cases. The hypothesis can be verified with DC conductivity measurement, which will be introduced in Chapter 5. The space charge behaviour for nitrogen thermal ageing LDPE can verify that thermo-oxidation primarily generates deep traps. In addition, relative chemical tests should be carried out to explore the thermo-oxidation degree in different depths of these air thermal ageing samples.

4.4 Space Charge Behaviours in Nitrogen Thermal Ageing LDPE

4.4.1 Charge Injection

For the next step, the space charge profiles for nitrogen thermal ageing LDPE films were measured at 40 kV/mm for 1800 s; the charge injection results are shown in Fig. 4.12. First, it can be clearly observed that fewer charges accumulate in the 100°C 1-day nitrogen aged LDPE in comparison with the virgin sample after 1800 s applied electrical field. On the other hand, the positive charge amount is reduced since the time is 540s in the original LDPE, but the time is approximately 120s in this nitrogen ageing specimen, which means that the holes take a shorter time to be injected and move inside the bulk before the recombination process begins. Furthermore, it can be found with the black curve, which represents the charge behaviour after 30 s applied voltage, that positive carriers are more easy to inject. As a result, less accumulated charges might be due to more intense neutralization.

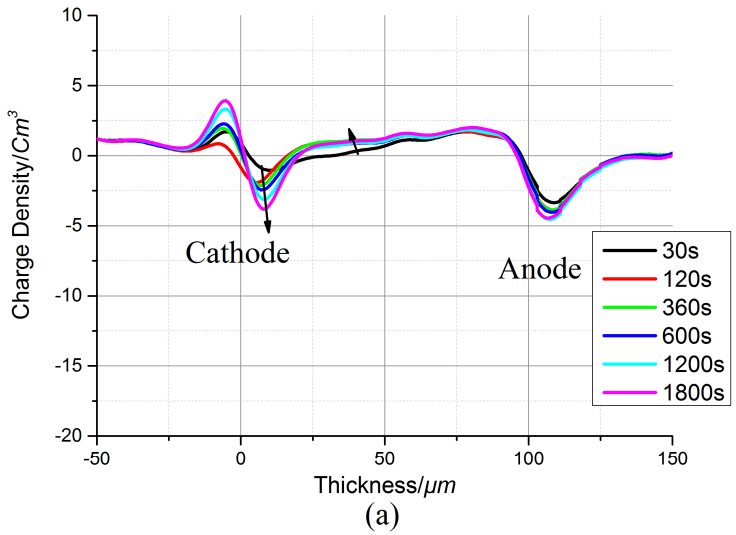

Figure 4.12: Space charge profiles over 1800 s at 40 kV/mm in 100°C 1-day nitrogen aged LDPE.

To clarify, the charge injection behaviour for nitrogen 100°C 5-day aged LDPE is divided into three stages, as shown in Fig. 4.13. First, from the beginning to 90 s, both types of charges are injected

into the bulk. Then, electrons and holes begin to neutralize, and the amount of two varieties of carriers decreases from 90 s to 420 s. Finally, the last graph shows that the negative charges continue to be injected, and it shifts deeper into the bulk while the amount increases, from 420 s. However, the positive charge keeps being recombined, and its density decreases.

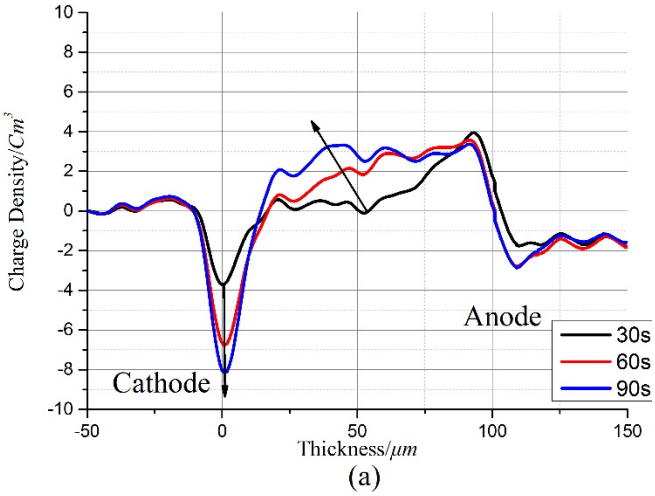

(a)

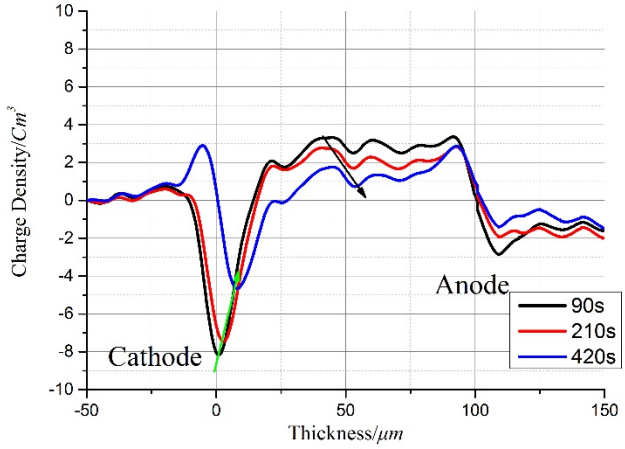

(b)

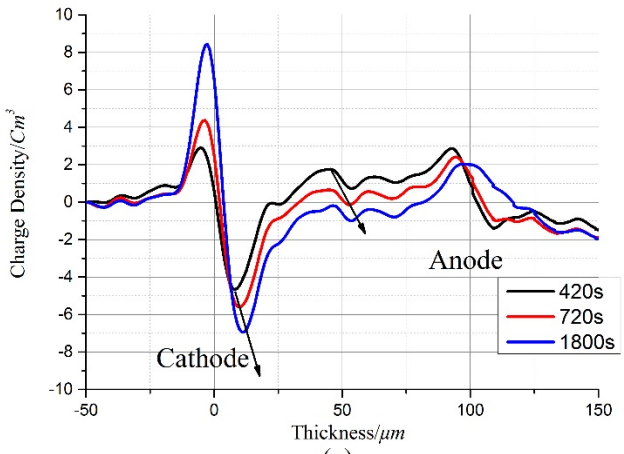

(c)

Figure 4.13: Space charge profiles over 1800 s at 40 kV/mm in 100°C 5-day nitrogen aged LDPE.

In addition, a comparison is made among the virgin LDPE, 100°C 5-day air and nitrogen aged LDPE specimens, as shown in Fig. 4.14. Generally, the specimen aged at 100°C for 5 days in nitrogen has a similar charge injection dynamic compared to the original LDPE. The process starts with hole and electron injection and neutralization, and negative charges predominate in the last stage. But in the nitrogen ageing sample, the recombination process is more drastic, so the amount of the remaining accumulated charges is smaller after the field is applied for 1800 s. On the other hand, compared to the sample aged in air with nitrogen, no clear recombination can be observed, and the charges are slowly injected and accumulate close to the electrode.

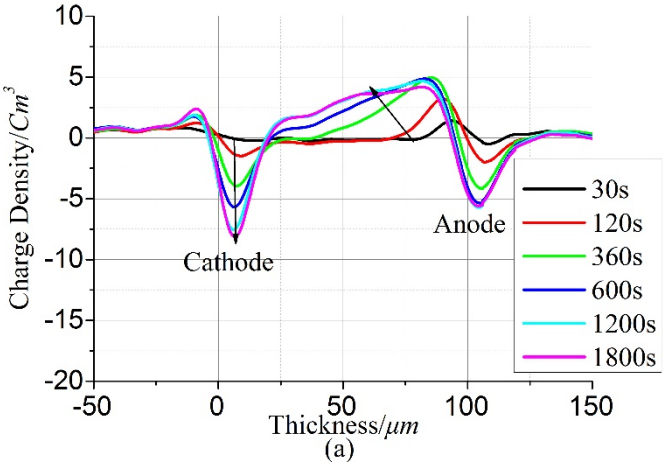

(a)

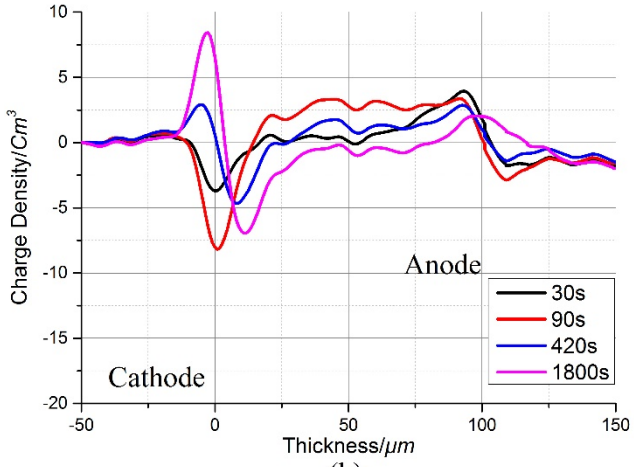

(b)

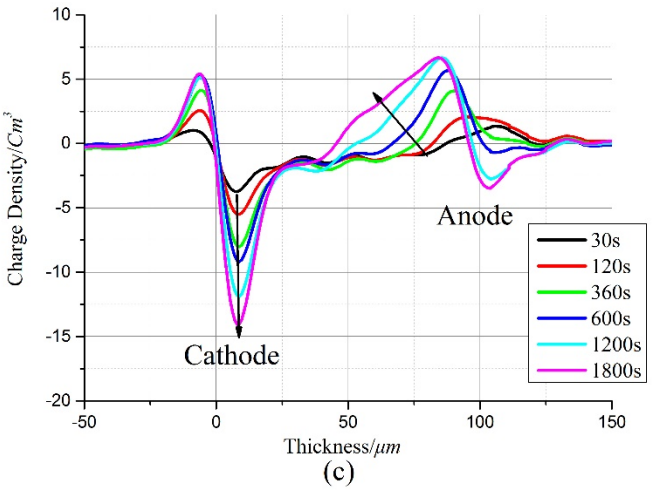

(c)

Figure 4.14: Space charge profiles over 1800 s at 40 kV/mm for original, 100°C 5-day air, and nitrogen aged LDPE.

4.4.2 Charge Decay

After removal of the external voltage, the results of the charge decay dynamics for nitrogen ageing samples are shown in Fig. 4.15. Meanwhile, the amount of charges were calculated with Eq. 4.2, and the results are shown in Fig. 4.16 after processing by the normalization method. Generally, the results of 100°C one-day nitrogen ageing LDPE is close to the original sample decay process, which means there are charges decaying near the electrode and inside the bulk. But in the case of the 5-day nitrogen ageing sample, there is hardly any charge decaying inside the LDPE film. In other words, charges mainly accumulate in the vicinity of the electrode after 1800 s volts-on. Furthermore, it can be found that the remaining charges in both nitrogen ageing specimens are less the charges in the original and air ageing samples. In addition, in Fig. 4.16, a verdict can be made that the original sample decays more slowly than the air ageing sample but more quickly than the nitrogen ageing sample. Besides, charges in the 100°C one-day nitrogen ageing LDPE decay with a uniformly rate, but charges in other samples decay rapid initially, and the remaining carriers decay with a slower rate.

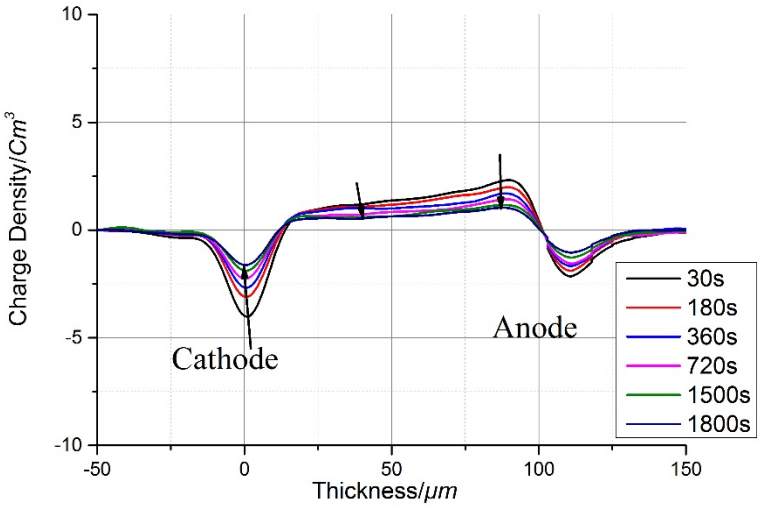

(a)

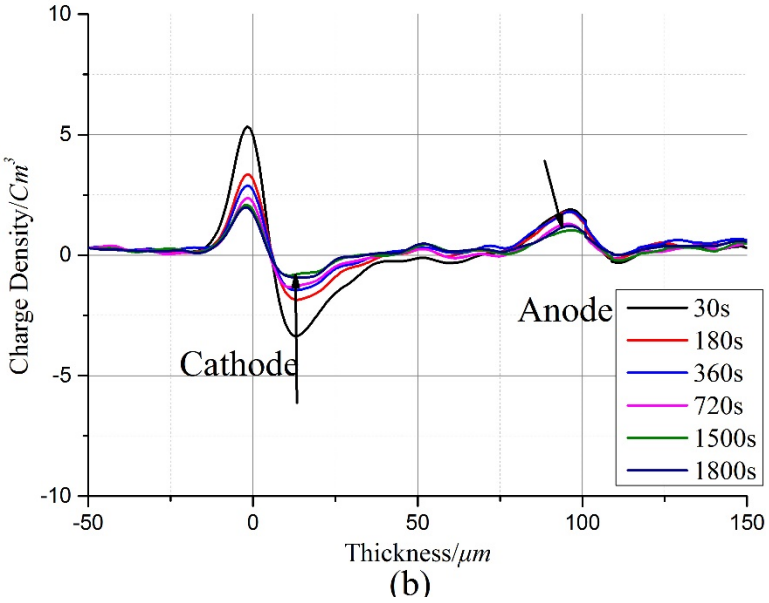

Figure 4.15: Space charge profiles over 1800 s after removal of the electrical field for 100°C 1-day and 5-day air and nitrogen aged LDPE.

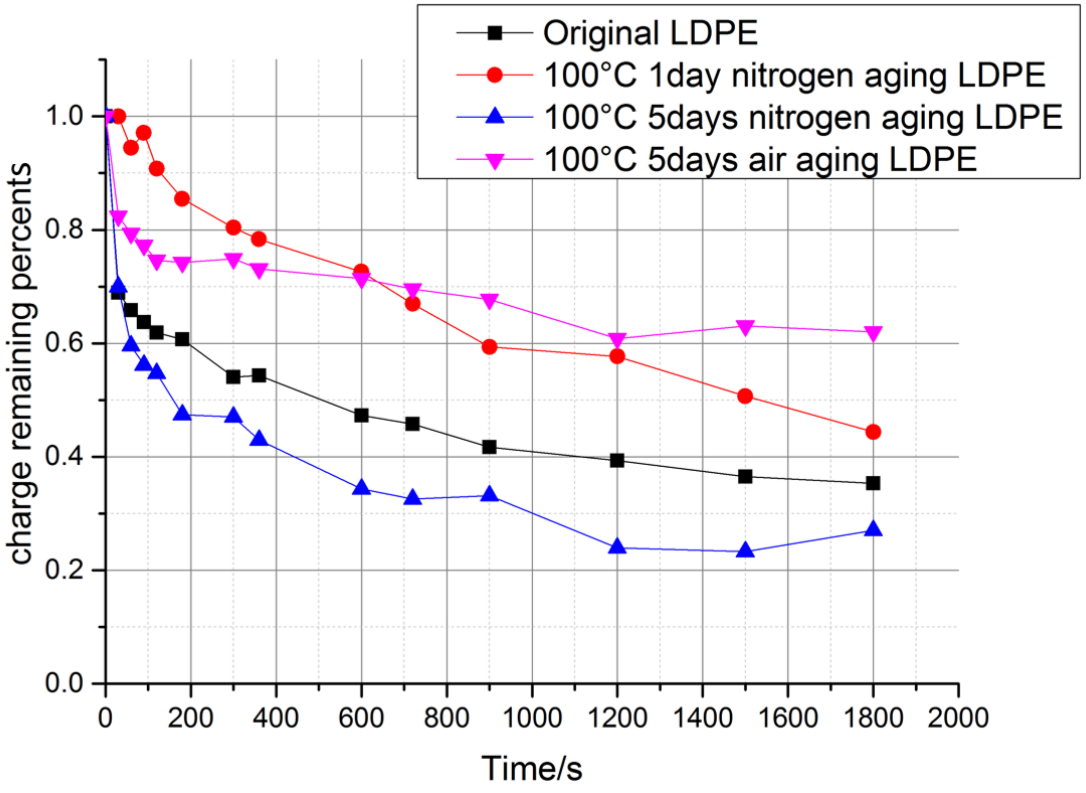

Figure 4.16: Charge decay rate for original, 100°C 5-day air ageing and 100°C 5-day nitrogen ageing LDPE.

4.4.3 Discussion

In the air ageing sample, the deep traps are introduced due to thermo-oxidation, so the charge injects more slowly and moves more slowly. A small number of deep traps near the surface can

hinder charge injection, so the negative charge amount in the slightly air ageing sample is smaller than original one, although there is almost no recombination process. But it can be hardly observed any charge suppression effect in the LDPE aged at 100°C for 5days in nitrogen, compared with sample aged at same temperature and for equally time in air. Furthermore, the distribution of trapped charges is not concentrated in the vicinity of the electrodes. Meanwhile, as shown by the charge decay behaviour in Fig. 4.15, a small fraction of the charge is not attenuated after the removal of the applied field for 1800 s. Hence, it can be inferred that the nitrogen thermal ageing will not introduce deep traps into the sample and there is not any surface feature involved. In other words, the space charge dynamic of LDPE aged in air is highly related to the thermo-oxidation, which can introduce deep traps into the sample.

However, the space charge behaviour of the 100°C 5-day nitrogen ageing LDPE and the virgin sample are still quite different, as shown in Fig. 4.12 to Fig. 4.16. First, it might be explained by the change of crystal structure due to thermal ageing, which may result in the increase of electrical conductivity, so the charges can move easily in the sample. Alternatively, it is supposed that traps introduced by different ageing environments are different; in other words, trap depth is different. The trap introduced by nitrogen thermal ageing is close to the eigen trap (i.e. a shallow trap). As a result, trap density is enhanced, but average trap depth is decreased, so charge can be injected easily and decays more quickly, which is shown above. As the sample is too thin, it also results in a more intense neutralization, so the accumulated trap charge is reduced.

The conjecture about electrical conductivity will be discussed in chapter 6, but the hypothesis about shallow traps involved by nitrogen thermal ageing still needs further experimentation to be verified. Generally, LDPE aged in nitrogen for a longer time should be prepared and tested for space charge behaviour. However, nitrogen ageing samples aged for a longer time cannot be made with the same ageing method, due to the limited air tightness of the vacuum oven we used. Hence, a new nitrogen thermal ageing method should be developed. Then, the charge dynamic of thicker LDPE aged in nitrogen can be used for argumentation.

4.5 Conclusion

Traps are introduced into LDPE samples during thermal ageing in air condition, and deep traps dominate the impact, due to thermo-oxidation. At the early stage of ageing, a small number of deep traps in the vicinity of the electrodes can suppress further charge injection and inhibit inward charge movement. At the late stage of ageing, during the sustainable rise of ageing, more deep traps are brought into the specimen; thus, a large number of charges inject and accumulate. In addition, charge decays significantly more quickly in the severely ageing LDPE. The thermo-

oxidation effect is removed in the nitrogen ageing sample, and more shallow traps may be generated in the nitrogen ageing environment.

Chapter 5 DC Breakdown Strength and DC Conductivity

Commonly, the operational condition and lifetime of insulation materials can be directly reflected by breakdown strength, and electrical breakdown characteristics are typically a key factor in the research on the ageing of dielectric materials. One of the significant parts of my work has been a focus on explaining the effect of thermal ageing on electrical properties by space charge behaviours. Conductivity measurement is required to be conducted to verify the hypothesis proposed in the last chapter. Consequently, the DC breakdown strength and DC conductivity were measured, and the results are introduced and discussed in this chapter.

5.1 DC Breakdown Strength Tests

5.1.1 Experimental Details

DC electrical breakdown strengths of the normal and aged samples were measured. In the experiment, the prepared sample was sandwiched between two spherical electrodes of 6.5 mm diameter. Moreover, to avoid flashover during the rise of the external field, the sample and the two spherical electrodes were fully immersed in silicone oil. The specimens were tested at room temperature (~20°C). The external voltage was increased with a ramp rate of 100 V/s from zero. The testing protocol and procedure follow ASTM standard D3755-97 [88]. For each type of sample, approximately 20 measurements were made to reduce statistical error.

To analyse and describe DC breakdown behaviours, the breakdown data were processed using the Weibull distribution, which is the most common method to describe stochastic behaviours [89]. The Weibull distribution was introduced by Waloddi Weibull in the 1950s [90], and its probability density function is given by [91]

$$f(x,\alpha,\theta) = \begin{cases} \frac{\alpha}{\theta^{\alpha}} x^{\alpha-1} \exp\left[-(x/\theta)^{\alpha}\right], \ x>0; \ \alpha,\theta>0 \\ 0, \ elsewhere \end{cases} \tag{5.1}$$

where α and θ are the shape parameter and the scale parameter, respectively. Application of the Weibull distribution on the mechanical and electrical failure mechanism is based on a physical model known as the “weakest-link-hypothesis” [92]. In this model, it is supposed that there is a chain formed with a series of tandem rings, and the strength or lifetime of this chain depends on the weakest ring, which is similar to the electrical breakdown process (i.e. the weakest link

dominates). In statistics, the 95% confidence interval is calculated to indicate the electrical failure possibility, and the slope reflects the dispersibility of the results.

5.1.2 Results and Discussion

Figure 5.1 shows the Weibull plots of the cumulative probability of breakdown vs. breakdown voltages for 90°C aged, and Fig. 6.2 presents the results of 100°C aged samples. Moreover, upper (E_{upper}) and lower (E_{lower}) 95% confidence bounds for each sample and corresponding slopes are given in Table 6.1, based on the characteristic values of breakdown strength (E_c) which have 63.2% failure probability.

Table 5.1: Breakdown strength for 90°C aged and 100°C aged samples with 95% confidence bounds with unreliability at 63.2%

	E_{lower}/kVmm^{-1}	E_c/kVmm^{-1}	E_{upper}/kVmm^{-1}	Slope β
Original LDPE	481.486	495.723	509.558	15.2383
90°C 1-day aged LDPE	514.659	527.726	540.351	17.7377
90°C 5-day aged LDPE	550.017	565.616	580.747	16.6098
90°C 10-day aged LDPE	557.534	569.985	581.974	22.7266
90°C 15-day aged LDPE	501.914	520.015	537.653	13.1475
100°C 1-day aged LDPE	506.930	517.333	527.489	25.0000
100°C 5-day aged LDPE	574.565	586.501	597.780	25.0001
100°C 10-day aged LDPE	409.583	429.395	448.773	12.6263

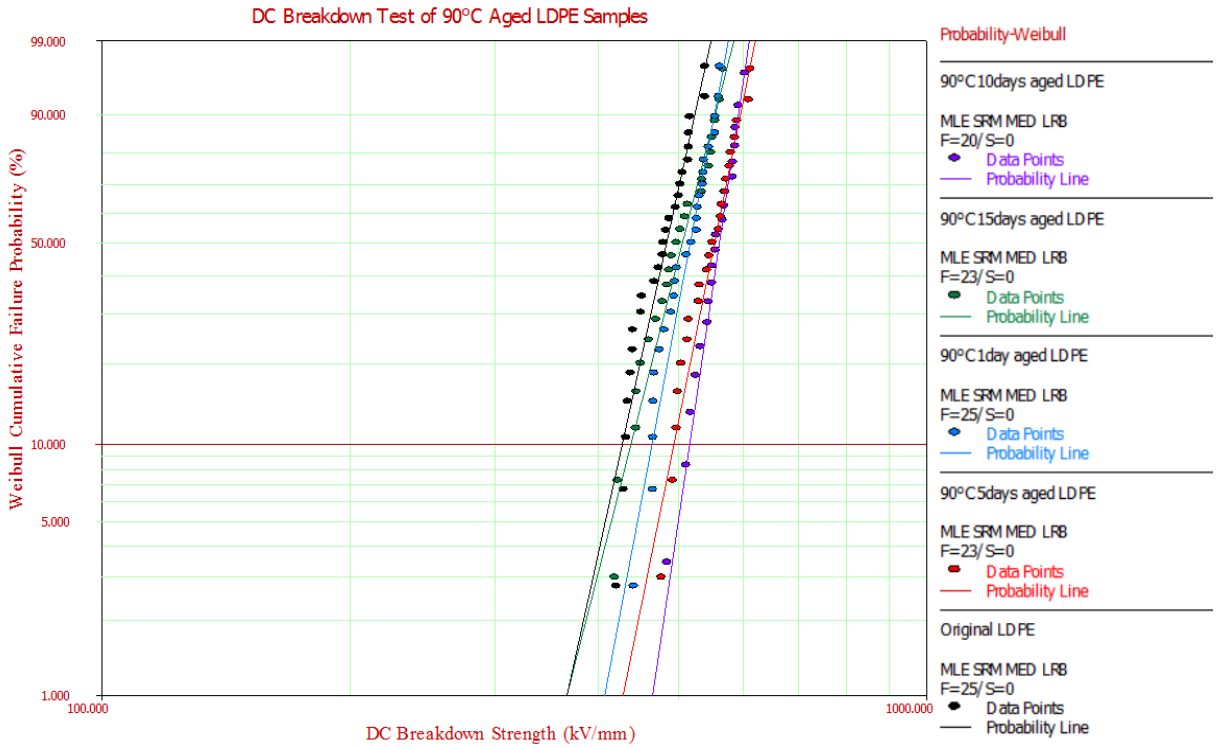

Figure 5.1: The Weibull plots of the cumulative probability of breakdown vs. breakdown voltages for 90°C ageing LDPE.

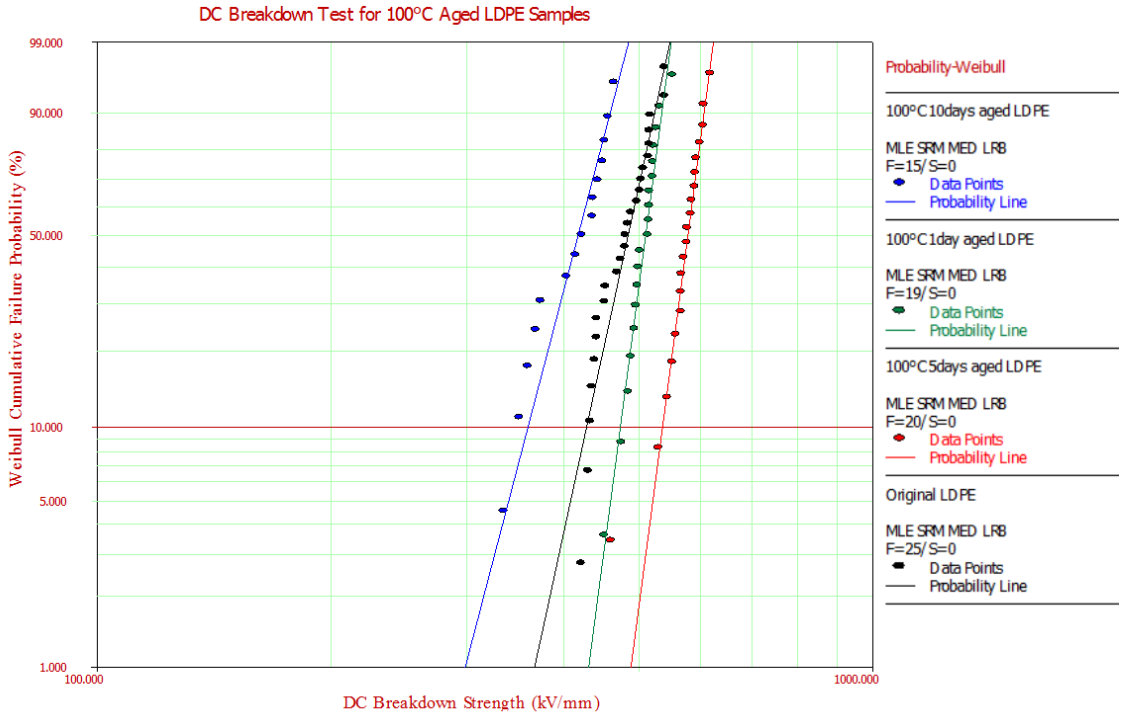

Figure 5.2: The Weibull plots of the cumulative probability of breakdown vs. breakdown voltages for 100°C ageing LDPE.

The thermo-oxidation has a strong impact on the electrical performance of LDPE insulation. The changes in electrical breakdown strength are closely associated with the concentration of carbonyl groups when the samples are aged below the melting temperature (112°C) [93]. Normally, in the

earlier model of the breakdown behaviour of thermal aged LDPE, the breakdown strength of aged LDPE decreases with the ageing degree when compared with the original LDPE [94]. Nevertheless, Figs. 6.1 and 6.2 show that the breakdown strength of both 90°C and 100°C ageing samples increases initially up to 10 days at 90°C and 5 days at 100°C. Any further ageing will lead to a decrease in the breakdown strength.

Specifically, the breakdown strength of all the 90°C ageing LDPE samples are higher than that of the original sample. Combined with the space charge behaviour, it can be found that these sample are affected by surface thermo-oxidation, which means that charges are hindered by deep traps in the vicinity of electrodes. Hence, it can be inferred that fewer charges trapped in the bulk lead to lower amplification of electric field, and this might be the reason why these slightly aged LDPE have higher DC breakdown strength. Moreover, for further-aged samples, more deep traps resulted in plenty of charges injecting and accumulating in the bulk. However, the 90°C 15-dayageing sample with less charges accumulating has a lower DC breakdown strength than the 90°C 10-day ageing sample with more charges. In addition, the situation is the same when comparing the 100°C 5-day and 10-day ageing LDPE. As I reviewed the correlation between space charge and breakdown phenomena, it was found that the local electrical field is affected by applied field and field distortion generated by the accumulation of space charge. Furthermore, as the local electrical field surpasses the intrinsic breakdown strength of the insulation material, the dielectric breaks down [43]. But the present results show that there should be another factor involved.

Combining the DC conductivity results, it is supposed that there might be two reasons why these samples have lower DC breakdown strength. First, a large number of charges trapped inside of materials introduces more serious electric field distortion, and high electrical conductivity introduced by tunnelling effect between charges and the breakdown of chemical structure could be another factor. Consequently, the equation for breakdown strength might be inferred:

$$E_b = E_i - E_{sc} \tag{5.2}$$

where E_b means the actual breakdown strength of dielectric, E_i indicate the intrinsic breakdown strength, which is affected by electrical conductivity, and E_{sc} is the field distortion introduced by trapped charges. The electrical conductivity is highly related to chemical structure, which can be changed by thermal ageing.

Furthermore, the Weibull plots of the cumulative probability of breakdown vs. DC breakdown voltages for LDPE aged at 100°C for one day and five days in nitrogen are shown in Fig. 5.3, with comparison between virgin and 100°C 5-day air ageing LDPE. Table 5.2 shows the relative corresponding slope, and upper (E_{upper}) and lower (E_{lower}) 95% confidence bounds.

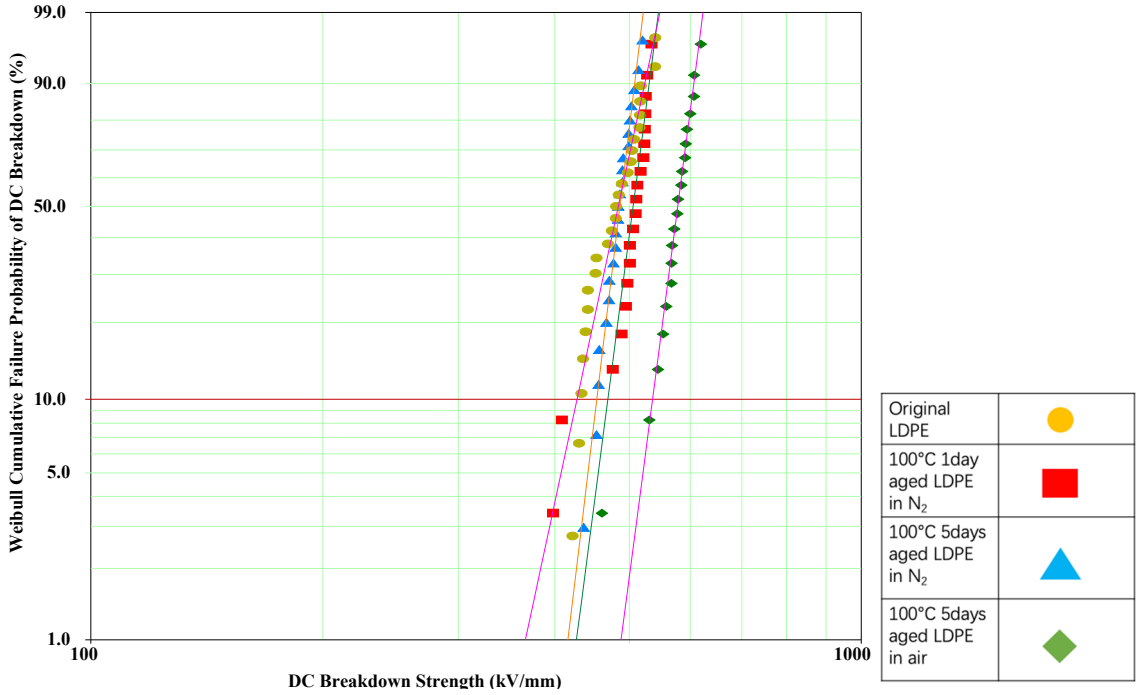

Figure 5.3: The Weibull plots of the cumulative probability of breakdown vs. breakdown voltages for 100°C 1-day and 5-day nitrogen ageing LDPE.

Table 5.2: Breakdown strength for 100°C nitrogen ageing LDPE with 95% confidence bounds and unreliability of 63.2%.

	E_{lower}/kVmm^{-1}	E_c/kVmm^{-1}	E_{upper}/kVmm^{-1}	Slope β
100°C 1-day nitrogen ageing LDPE	502.812	513.201	523.309	25.0000
100°C 5-day nitrogen ageing LDPE	483.507	492.790	507.669	25.0001

In Figure 5.3, it can be observed that the DC breakdown strength of 100° C 1-day and 5-day nitrogen ageing LDPE have similar situations with respect to the virgin specimen. But the value of the 100° C 5-day fan oven ageing LDPE is notably higher, so the hypothesis proposed above can be verified: thermo-oxidation is the main reason that leads to higher DC breakdown strength in slightly thermal aged samples. The FTIR and CI results could be used to relate the ageing sample with the insulation under in-service conditions. However, if surface oxidation dominates, the effect still needs to be explored in future work.

5.2 DC Conductivity Measurements

5.2.1 Experimental Details

To verify the hypothesis that states that the substantial growth of conductivity in seriously aged LDPE is the reason why rapid charge decay rate and much lower DC breakdown strength were observed in these samples, DC conductivity measurements were performed on the original and

aged LDPE samples. The tests were carried out at room temperature. Before measurements, both sides of all the samples were gold coated to obtain a better surface connection between samples and electrodes. A semi-automatic gold coater was used for the coating of ageing LDPE films. The coating current is on 25 mA; coating time is 3 minutes and coating diameter is 20 mm. As for DC conductivity measurement condition, the supply field was selected as 40 kV/mm due to space charge volts-on voltage, which is the same as for the space charge measurement conditions. On the other hand, current was measured by a Keithyley 6487 picoammeter, and the current flowing through the sample was recorded every 10 s for 7200 s. After several tests, the results showed that the conductivity can be stable after 7200 s applied voltage in LDPE in the conditions of our DC conductivity tester.

5.2.2 Results and Discussion

The DC conductivity results of the original and 90° C ageing LDPE are shown in Fig. 6.4, and the abscissa time and vertical conductivity are shown as logarithms. In addition, the results of 90°C 10- and 15-day aged samples were processed with the moving average method to smooth out fluctuations due to too-low measurement currents.

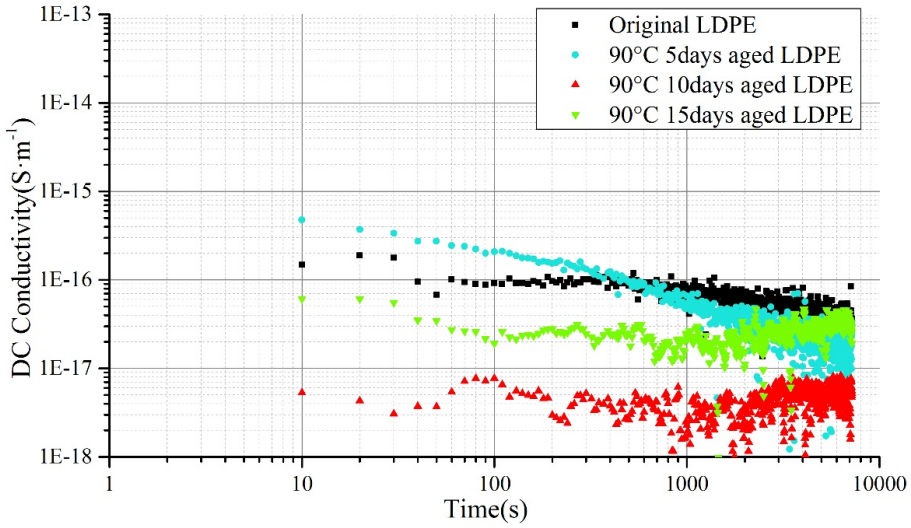

Figure 5.4: DC conductivity under 40 kV/mm of original and 90°C 5-,10-, and 15-day aged LDPE.

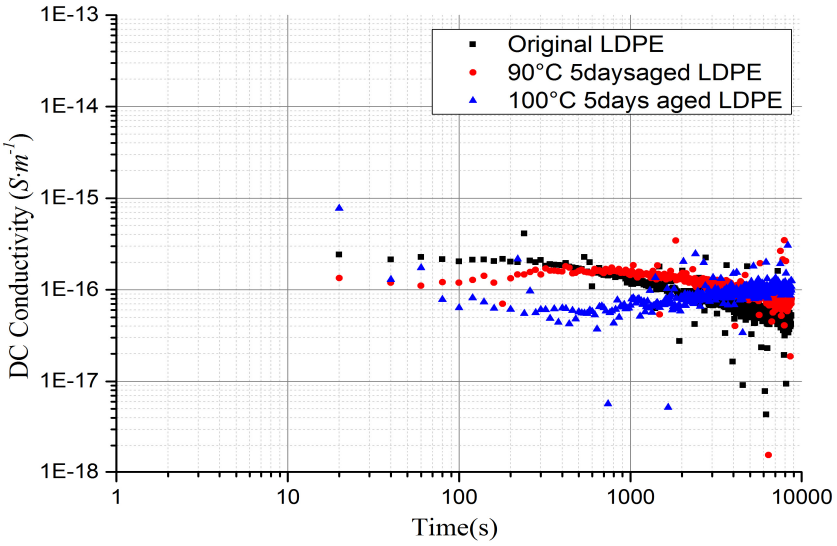

Figure 5.5: DC conductivity under 60 kV/mm of original, 90°C, and 100°C 5-day aged LDPE.

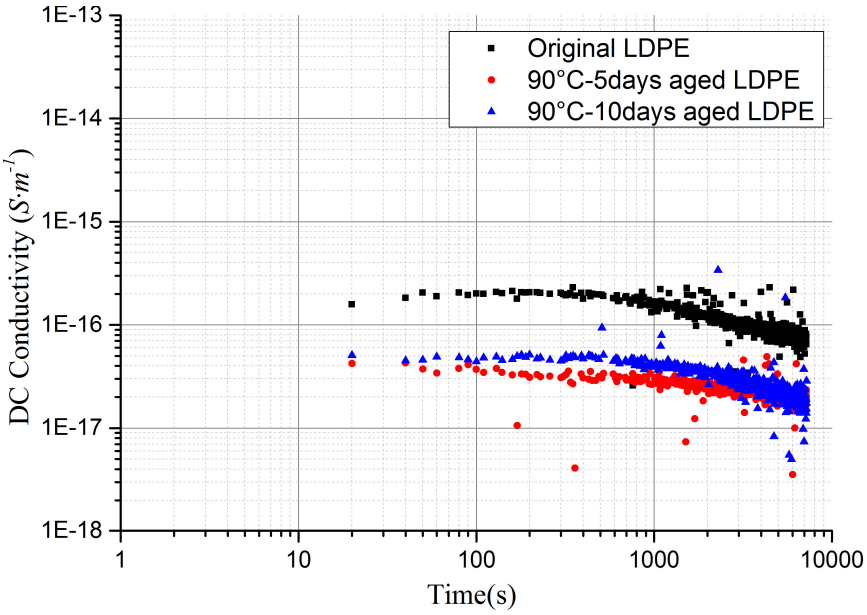

Figure 5.6: DC conductivity under 80 kV/mm of original and 90°C 5- and10-day aged LDPE.

It can be observed in Fig. 5.4 that the conductivity of all the 90°C air ageing LDPE are lower than original sample, but there is no clear gap and boundary among them. In addition, the results for 90°C ageing samples show a large spread of the data. Generally, it is due to the limited detected current of our picoammeter. To obtain clearer results, the external field was raised up to 60 kV/mm and 80 kV/mm; the results are shown in Figs. 5.5 and 5.6. But the results shown in Fig. 5.5 are still too discrete. Furthermore, it is clear in Fig. 5.6 that the DC conductivity of 90°C 5-day and 10-day ageing LDPE is lower than that of the original specimen. Moreover, 90°C 20-day ageing LDPE was measured, as shown in Fig. 5.8, and the electrical conductivity increased.

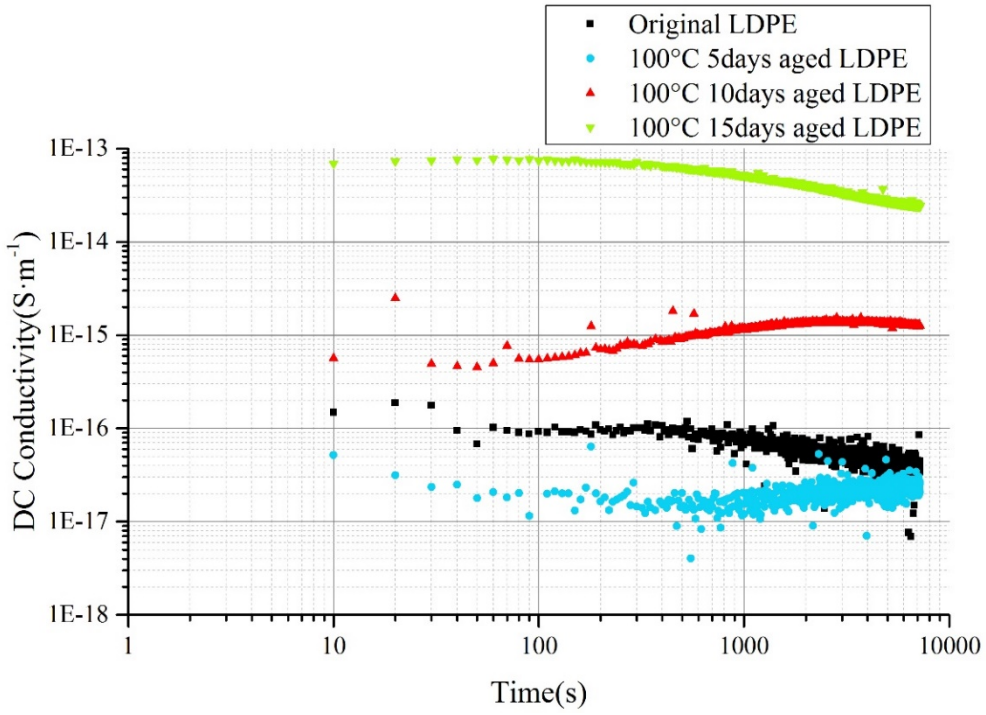

Figure 5.7: DC conductivity under 40 kV/mm of original and 100°C 5-, 10-, and 15-day aged LDPE.

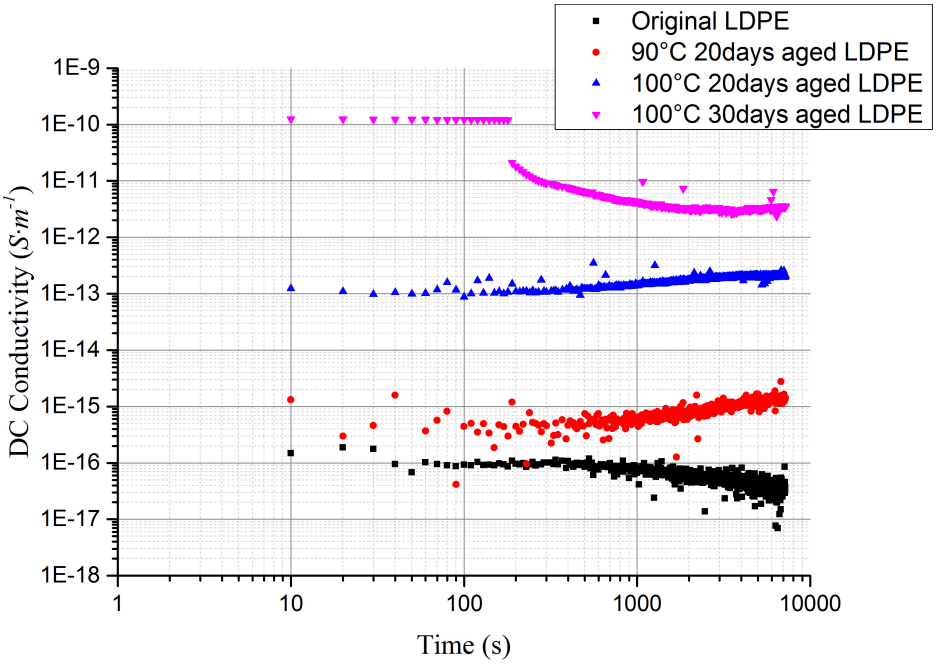

Figure 5.8: DC conductivity under 40 kV/mm of original, 90°C 20-day, and 100°C 20- and 30-day aged LDPE.

The DC conductivity profiles tested under 40 kV/mm for 100°C ageing specimens are shown in Figs. 5.7 and 5.8, which represent the results for slightly and severely aged samples, respectively. For 100°C ageing LDPE, the DC conductivity decreased initially in 100°C 5-day ageing film, and further ageing will result in an upward tendency.

Polyethylene is a type of wide band-gap insulator material, and the carrier in the valence band can be motivated under sufficient electrical field or higher temperature (i.e. enough supporting energy).

Therefore, the conducting current that is measured in DC conductivity generally comes from mobile charges which are injected into dielectrics with Schottky injection. In addition, other current flow which is detected may be generated by ion current [1]. Moreover, the capture of the injected charge by deep traps adjacent to the electrode will suppress further charge injection [95]. Hence, lower DC conductivity in slightly ageing samples could be the effect of deep trapped charges in the vicinity of electrodes, which lead to less charges being injected and can hinder charges from moving toward the sample. These deep traps are introduced by surface thermo-oxidation, which can be supported with space charge behaviour, as described in chapter 5. Moreover, combined with the space charge behaviour, larger amounts of deep traps can be generated by further thermal ageing. As a result, enhanced tunnelling effect between traps makes the carriers move easily, so the space charge distributes more uniformly instead of concentrating close to the electrode. Consequently, increase in current flow is detected as the hindering effect of deep trapped charge is attenuated and more charges inject into the material. Thus, the LDPE aged at 90°C for 20 days and 100°C for 15, 20, and 30 days show higher DC conductivity performance. Alternatively, defects introduced by thermal ageing may lead to the enhancement of ionization, which would increase electrical conductivity due to larger ion current. This factor could be the reason why the DC conductivity of the 100°C 10-day ageing specimen goes up while trapped charges gather near the electrode. In particular, with the 100°C 30-day ageing sample shown in Figure 7.8, a discontinuous breakpoint occurred at 120 s, which means that electrical breakdown happened at that moment and a hole across the sample formed, so further measured current decreased.

Furthermore, Fig. 5.9 describes the DC conductance characteristic of the LDPE aged at 100°C in nitrogen for one day and five days. It can be seen that the one-day aged specimen shows a lower electrical conductivity compared with the virgin sample, and the value of the five-day ageing sample is clearly greater. The conductivity behaviour of the one-day LDPE might be due to the instability of the device at low current, as the result is dispersive. Another cause could be slight oxidation introduced by leaking of the vacuum oven. As for the five-day nitrogen ageing specimen, its PEA results show a higher charge mobility, which is verified by the DC conductivity. This result might be the effect of more shallow traps introduced by oxygen-free thermal heating. Hence, it can be inferred that oxidation brings deep traps into LDPE, but thermal heating generates shallow traps during thermal ageing.

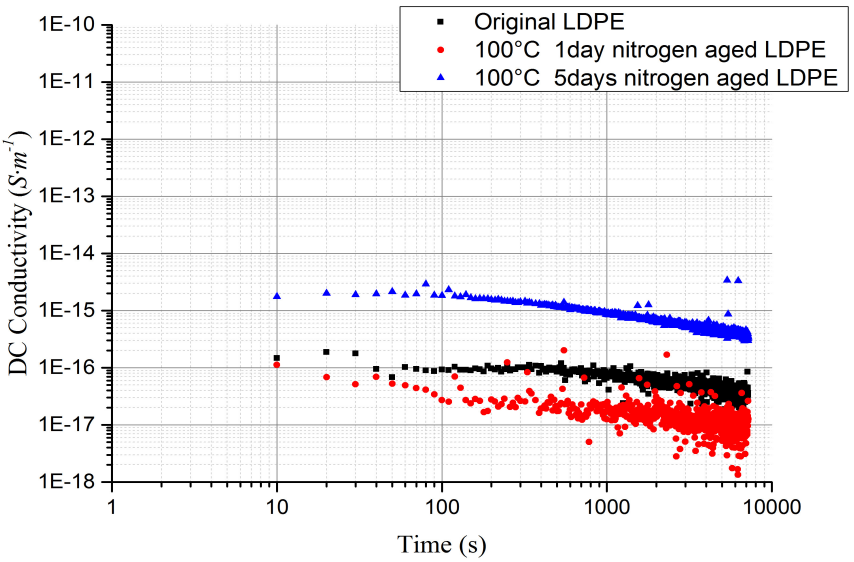

Figure 5.9: DC conductivity under 40 kV/mm of original, 100°C one-day, and five-day nitrogen aged LDPE.

5.3 Conclusion

In general, slightly air aged LDPE samples achieve lower DC conductivity and higher DC breakdown strength, and further ageing results in the reduction of breakdown strength and increase of conductivity. But the LDPE aged in nitrogen have similar DC breakdown behaviour and slightly larger values of electrical conductivity in comparison with original sample.

Traps are introduced into samples during thermal ageing in the fan oven, and deep traps dominate the impact. At the early stage of ageing, a small amount of deep traps in the vicinity of the electrodes can suppress further charge injection, which results in the increase of breakdown strength and reduction of DC conductivity. Meanwhile, deep traps are involved in LDPE by thermo-oxidation, and shallow traps are generated by heating in thermal ageing. During the sustainable rise of ageing, more deep and shallow traps are brought into the sample; thus, higher DC conductivity and lower breakdown strength are detected due to a large amount of charge injection.

Chapter 6 Thermal Ageing and Its Impact on Charge Trapping Parameters

In recent years, the space charge behaviour has been defined as a significantly important electrical property in the insulation materials, especially in HVDC systems, because the distortion of local electric fields caused by accumulated charges has obvious effect on high field conduction and breakdown phenomena[66][43]. Besides, in past decades, plenty of works on the ageing of insulation materials have been done and many efforts have been made to establish a “standard” relationship between ageing and lifetime[36][96]. And in our research, the space charge phenomena of material could be considered as the key that link ageing, electrical performance and lifetime[86][97][25]. We aim to describe the space charge dynamics with trapping parameters and use the initial parameters to infer the space charge properties of polymer insulation after ageing. Thus, the change in charge traps of dielectrics can be used to characterize electrical performance of the material, and therefore, the ageing status.

There are three primarily factors need to be solved: the estimation of trapping parameters, the influence of ageing on the trapping parameters and the relation between charge dynamics and other electrical performance such as breakdown strength, dielectric loss and conductivity. The early trapping parameters evaluation model proposed by Chen[23] has been used in different normal and ageing samples in previous research[7][9]. Furthermore, an improved trapping parameters model has been established, which considered the neutralization process and double trap energy depth[38], which has been reviewed in Chapter 2. In this Chapter, the trapping parameters of original and ageing LDPE samples will be estimated by the improved model.

6.1 Space Charge Profile and Data Processing

As shown in Chapter 4, based on the subtraction method, the charge profile of original LDPE before and after processing are displayed in Fig 6.1(a) and (b), respectively. And the charge amount can be calculated by Equation 4.2. Based on the measured data on several samples with same condition, the charge amount of original LDPE during applying and removal external field has been averaged as shown in Fig.6.2 with error bars. The black line in 1800s shows the volts-off point.

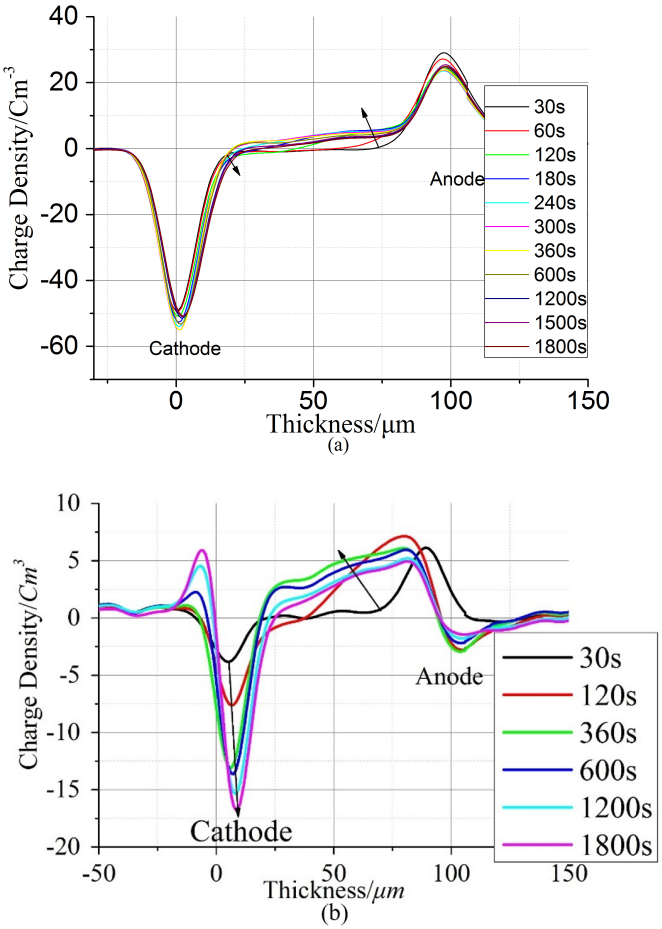

Fig. 6.1. The space charge profile of original LDPE before(a) and after(b) subtraction.

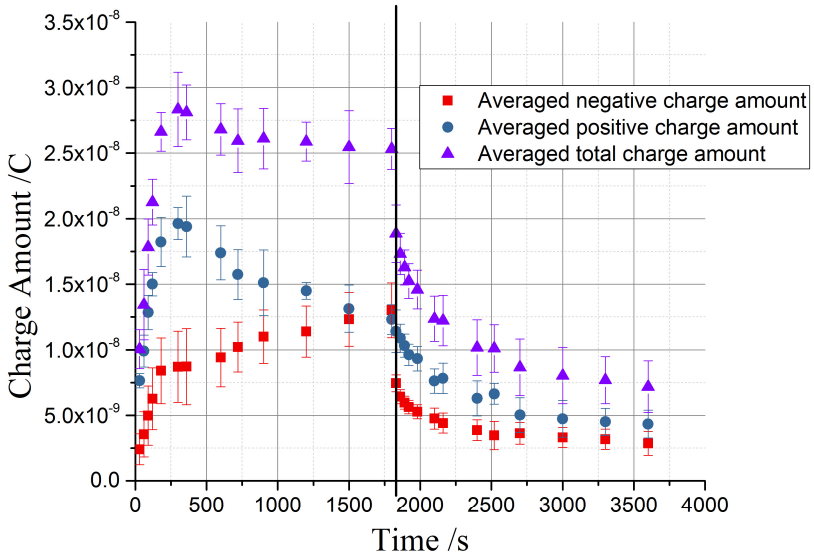

Fig 6.2. The averaged negative, positive and total charge amount of original LDPE samples.

6.2 Trapping Parameters Estimation

The thickness of two charge regions in different samples is shown in following Table 6.1. It can be found that there is no great change for the width of negative charge region, but the hole area reduces by almost half between 90°C 5days and 15days LDPE specimens. Based on the mean value of charge amount in samples and the charge region thickness, the numerical solutions of parameters were found with MATLAB software through the Euler's Method. Fig.6.3 indicates the best fitting curve with the improved model for original and ageing LDPE. The scatter shows the averaged charge density measured by the PEA system, and the red and black lines represent the condition for electron and holes, respectively. Furthermore, full lines show the simulated net charge profiles, and dash-dotted lines refer to mobile charge behaviour in the sample. Meanwhile, the condition of charges trapped by shallow and deep traps can be obtained with the dashed and dot lines. And the R-square values and trapping parameters results are shown in Table 6.2.

Table 6.1 Thickness of charge region for each type of samples

Type of LDPE sample	Negative Charge region thickness/μm	Positive Charge region thickness/μm
Original	22	60
90°C 5days	19.4	64.1
90°C 15days	26.3	33.3

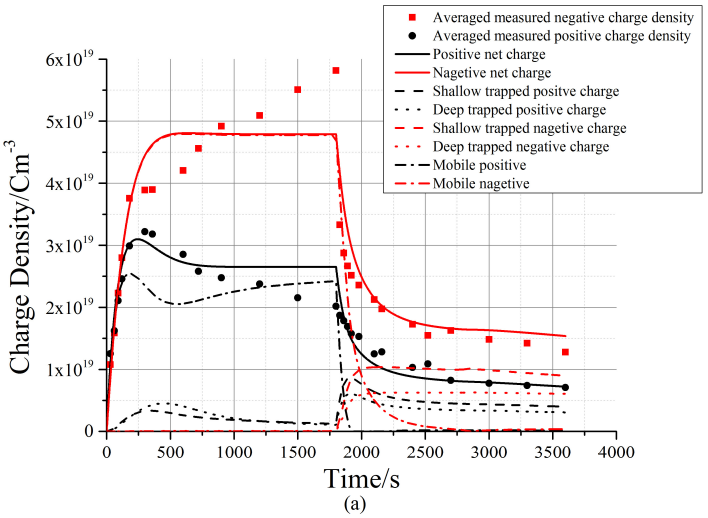

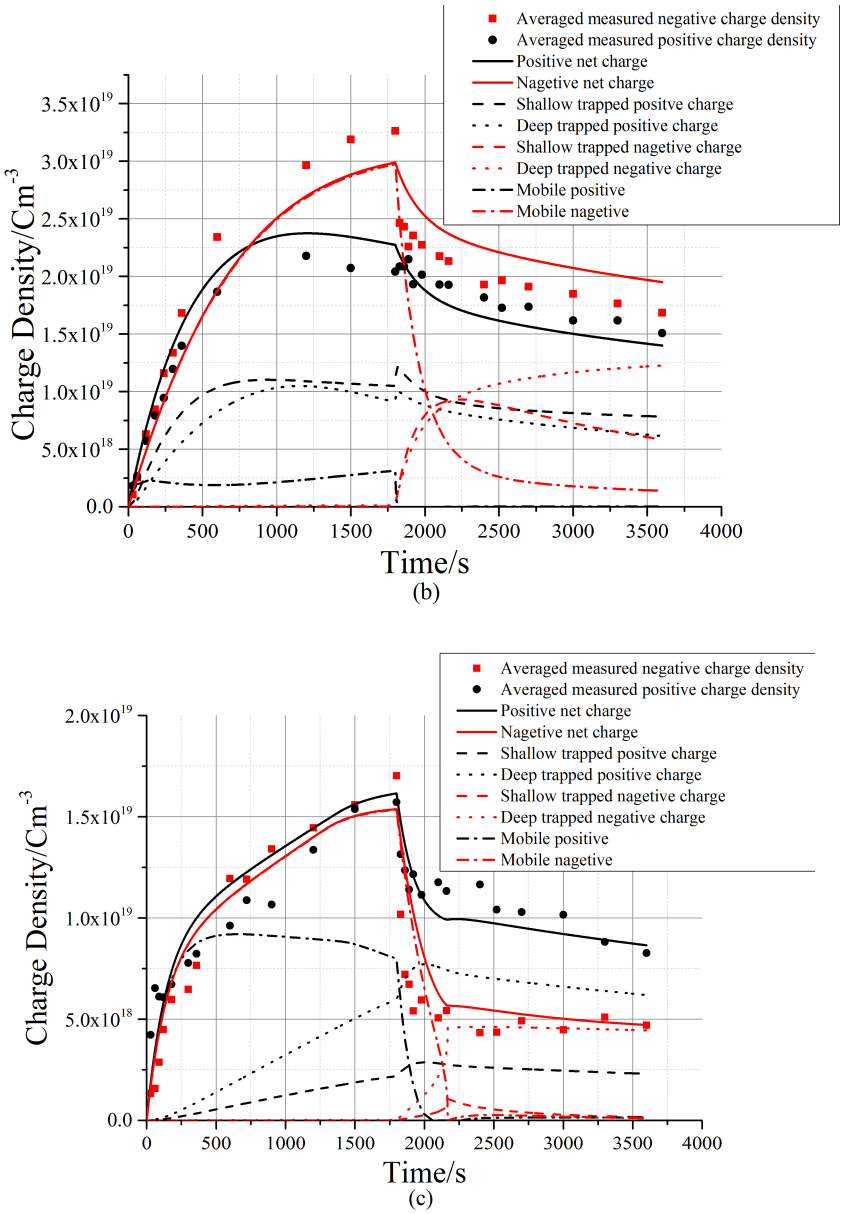

Fig. 6.3. The trapping parameters for original (a), 90°C 5days (b) and 90°C 15days(c) LDPE films.

Table 6.2. Trapping parameters for each type of LDPE samples

Type of LDPE sample	Original		90°C 5days		90°C 15days	
	Shallow traps	Deep traps	Shallow traps	Deep traps	Shallow traps	Deep traps
R-square Value	0.9520		0.9508		0.9199	
P_e/s^{-1}	0.005		0.0013		0.0035	
P_h/s^{-1}	0.0035		0.0011		0.0058	
w_e/eV	1.17		1.225		1.2071	

w_h/eV	1.135		1.183		1.1986	
N_{te}/m^{-3}	1.1E+19	6.5E+18	3.3E+19	2.6E+19	2.0E+18	4.8E+18
N_{th}/m^{-3}	2.0E+21	1.5E+21	5.0E+22	2.0E+22	3.0E+20	1.0E+21
E_{te}/eV	1.025	1.055	0.99	1.044	0.96	1.06
E_{th}/eV	1.049	1.111	1.08	1.12	1.15	1.31

In Fig. 6.3 (a), it can be found that the measured density of positive net charge in original LDPE increase in the first 300s with the external electrical field, and decrease in the remaining time. But the number of electrons keep growing. Meanwhile, the Fig.6.2. shows that the total charge amount gradually become stable after volts-on for 300s. This could be used to confirm the existence of significant charge neutralization, while the fitting results of both carriers also show this point. However, in 90°C 5days specimen, this phenomenon is weakened, and it could hardly be observed any reduction of net carrier density in 15days ageing sample while applying voltage.

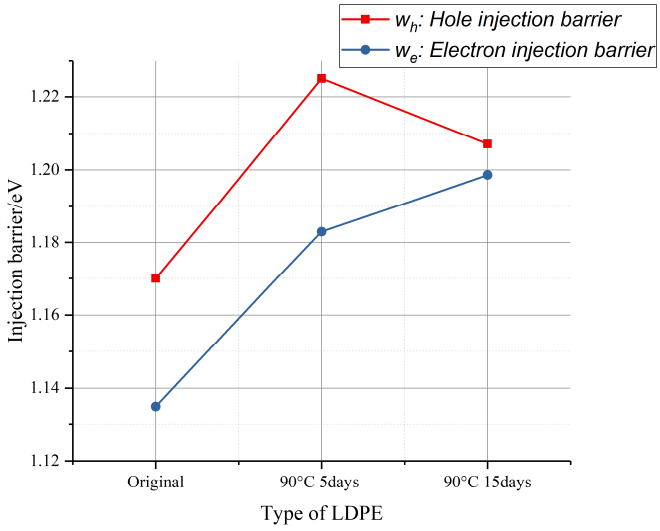

Figure 6.4. Injection barrier.

Regarding trapping parameters shown in Table 6.2, three typical trapping parameters were selected and shown in Figure 6.4 to Figure 6.6. Firstly, it can found in Figure 6.4 that the value increases compared with the normal sample at the early stage of thermal ageing. And positive charge injection barrier decreases in further ageing but negative one keeps increase. Hence it can be accounted by higher electrical conductivity according to our previous research on ageing LDPE films[97]. For slightly aged LPDE, a small number of deep traps in the vicinity of the electrodes,

which were introduced by thermo-oxidation on the surface, can suppress further charge injection and inhibit charge inward movement. In another word, higher injection barrier can be introduced by thermo-oxidation on the surface. And for deeply ageing specimen, more traps are introduced and the average distance between adjacent traps reduces, so the quantum tunnelling might be easily to occur[1]. Moreover, the higher electrical conductivity in 90°C 15days aged LDPE could make the dynamic balance between positive and negative charge easier to be established [97]. Thus, this part of charges can hardly be detected by the PEA technique. Furthermore, it could be presumed that trapping parameters evaluated by space charge characteristics, which dynamic balance has been built, can reflect trap conditions better. Hence, space charge for aged sample with longer press time will be measured in our future work.

On the other hand, the mobile negative charge profiles, shown with dashed-dot line in Fig. 6.3, for all the sample equal to the negative net charge. It should noticed that the mobile charge described in this model represents the charge that is moving between the traps by hopping conduction [98], which can be detected by the PEA technique. This could be caused by the higher mobility for electrons in polymer dielectrics, and the domination of negative charge in original LDPE can confirmed this deduction.

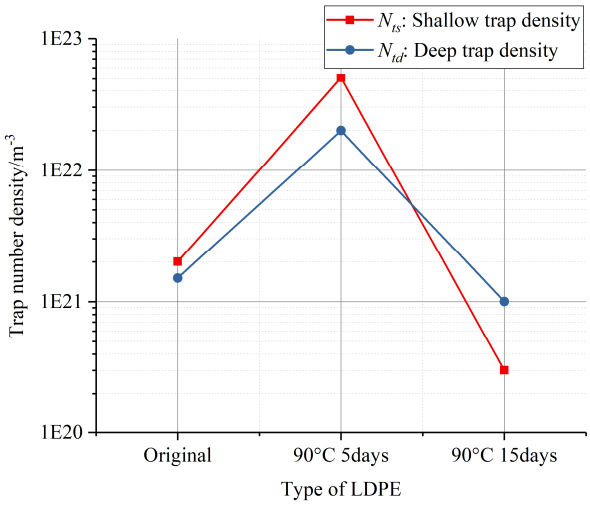

Figure 6.5. Trap density.

Then it can be observed that the shallow and deep trap density of both kinds of carriers in 90°C 5 days ageing LDPE, compared with original sample, shown in Figure6.5. That means more traps can be generated by thermal ageing in air, especially deep traps. Further ageing will lead to the decrease of trap density. As the deduction proposed before, it might due to the high DC conductivity, which can result in charge decay in a higher rate. Meanwhile the charge that move between traps by tunnelling cannot be calculated by this model, if the tunnelling current forms between electrodes. Thus, the trap density in this deep ageing LDPE may not be evaluated accurately.

Furthermore, Figure 6.6 represents that the energy level of deep trap is deepened and shallow trap has lower depth in LDPE samples after thermal ageing. These could be the reason why charges in ageing sample decay quicker in advance, and the remaining charges decrease with a much slower rate, compared with the original LDPE.

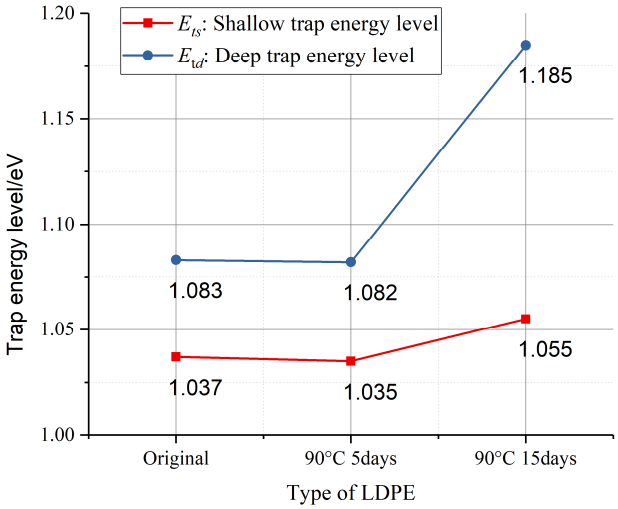

Figure 6.6. Trap energy level.

6.3 The Limitations of the Model.

As introduced in Chapter 2, this trapping parameters estimation model have a basic assumption: the distribution of traps is uniform. However, combined with the previous experiment results, the traps introduced by thermal ageing are concentrated near the surface in the slightly aged sample. And it is clearly in the Raman results that oxidation degree of these lighty aged sample is not evenly. As a result, the trapping parameters estimated with this model may not reflect the actual trap properties in 90°C- 5days, 90°C-10days and 100°C-5days aged LDPE films.

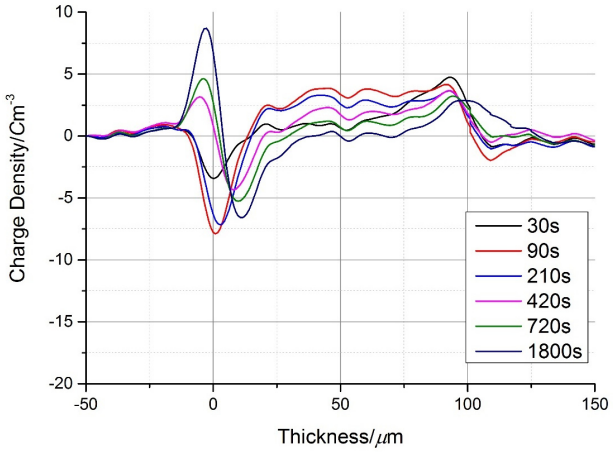

Figure 6.7. Space charge injection profile after subtraction on 100°C 5-days nitrogen thermally aged LDPE.

Meanwhile, in this model, two clearly charge fronts area need to be defined as shown in Figure 2.16. In original, 90°C-5days, 90°C-10days and 90°C-15days ageing samples, there is a clear gap between positive and negative charge peak. However, it's hard to distinguish two charge peak with the same charge region in the space charge results of nitrogen thermally aged LDPE, shown in Figure 6.7. Because the charge region is changing during charge accumulate or decay. There is the same situation in 100°C-15days sample.

In addition, in 90°C-15days thermally aged films, higher DC conductivity and more deep traps are introduced by thermal ageing. So the charge move quicker in the sample, and a lot of mobile charges recombined in volts-on part, and mobile charges decay in a much higher rate. As the results, charges detected by our PEA systems may not reflect the trap properties clear. Meanwhile, in the mid area of the sample, holes and electrons may be trapped in the same time and same area. However, the PEA systems might "think" charges in this area are neutralized and detect no charges accumulated. Hence the trapping parameters estimated in this kind of sample may be not accurate. In further research, thicker sample and related PEA systems might be useful, and different space charge measurement could be used as well.

6.4 Conclusion

An improved trapping parameters model has been used to evaluate the trap conditions in original and thermal ageing LDPE. In this model, space charge characteristics during both volts-on and volts-off process are utilized to estimate trapping parameters. Meanwhile, the space charges are treated as trapped and mobile charges, respectively, and the charge neutralization has been taken into consideration. However, there still be limitations of this trapping parameters estimation model in thermally aged LDPE samples.

The injection barrier could be enhanced by thermal ageing due to surface oxidation. And thermal-oxidation in LDPE can introduce shallow traps with lower energy level and deep traps with deeper energy depth. Furthermore, the dynamic balance between carriers is harder to be estimated in LDPE films with a higher thermal ageing degree.

Chapter 7 Conclusion and Future work

7.1 Conclusions

This thesis focuses on space charge behaviour and its impact on other chemical and electrical properties in insulation polymeric materials, especially in LDPE. The trap properties were introduced to explain the electrical performance (electrical breakdown and conductivity). The literature review in early stage have been done in three parts: the structure of PE and its properties, the thermal ageing in polymer insulation, and the mechanisms of charge injection and transport in insulation materials. Some previous space charge studies and space charge models were also discussed. It can be summarized as:

- PE, as a wide band gap insulator, has been used as cable insulation for many years because of its good electrical performance, which is closely related to the structure of a chain. In different categories of PE, XLPE is more commonly used in electrical cables due to its unique crosslinking structure resulting in a higher operating temperature, however, the additive in XLPE may alter its charge behaviours.
- Thermal ageing could introduce a C=O (carbonyl) structure and crosslinking plays a secondary role in thermal ageing in LDPE. Thermally aged LDPE has lower breakdown strength, which is closely associated with oxidation.
- Space charge accumulation can enhance the local electrical field, which may lead to dielectric failure under a smaller applied field than breakdown strength.
- The electrode materials and various kinds of ageing have significant effects on space charge formation. Generally, the impact of ageing is explained by the change in trap distribution.
- An improved trapping parameters estimation model and its three unique advantages were introduced: i) both polarisation and depolarisation processes of charge dynamics are used; ii) the space charges are treated as mobile and trapped charges, and iii) the charge neutralisation is taken into consideration.

In experiments, a commercially available additive-free LDPE with the thickness of ~100μm was chosen as the sample for thermal ageing. The LDPE films were aged in two different conditions, air in a fan oven and nitrogen in a vacuum oven, and at different temperatures near melting points for different lengths of time. The subsequent chemical changes were monitored with the FTIR technique, DSC method, and the Raman technique. Moreover, the space charge dynamics in aged specimens were observed using the PEA technique. In addition, DC breakdown strength and DC

conductivity measurements were performed in order to investigate the impact of thermal ageing on insulating properties. Based on the experiment results, the following conclusions may be drawn:

- Thermal ageing in air leads to a gradual increase in the thermal oxidative degree of LDPE and the carbonyl index of the sample aged in the nitrogen reduced significantly. The crystallinity was not impacted by the thermal ageing time and environment, but the ageing temperature dominated the change. Besides, the structure of the crystal in the ageing LDPE showed a correlation with the degree of oxidation and the heating environment.
- The degree of oxidation near the surface is higher than in the middle of the sample in slightly ageing LDPE. However, the oxidative degree is more even in deep thermally aged samples.
- Traps are introduced into LDPE samples during thermal ageing in air conditions and deep traps dominate the impact due to thermo-oxidation. At the early stage of ageing, a small number of deep traps in the vicinity of the electrodes can suppress further charge injection and inhibit charge inward movement, which results in the increase of breakdown strength and reduction of DC conductivity.
- During the sustainable rise of the degree of ageing, more deep and shallow traps are brought into the sample, thus higher DC conductivity and lower breakdown strength were detected due to a large number of charges being injected and trapped.
- The LDPE aged in nitrogen had similar DC breakdown behaviour and a slightly larger value of electrical conductivity in comparison with the original sample. The thermo-oxidation effect is removed in the oxygen-isolated thermal ageing sample, and more shallow traps may be generated. Hence, it is supposed that oxidation mainly introduces deep traps and shallow traps are generated by the thermal effect.

Furthermore, the trapping parameters of thermally aged LDPE were estimated by the improved model and some conclusions may be made:

- The injection barrier could be enhanced by thermal ageing due to surface oxidation. Thermal oxidation in LDPE can introduce shallow traps with lower energy levels and deep traps with increased energy depth. Furthermore, the dynamic balance between carriers is harder to estimate in LDPE films with a higher degree of thermal ageing.
- There are still three limitations to the model when it is used in thermally aged LDPE: the trap distribution in the slightly aged sample, unstable charge region, and the limitation of the PEA technique.

7.2 Future Works

Based on the previous review and experiments, future work will focus on the following:

- **Further nitrogen thermal ageing.** Due to the limit of the gas tightness of the vacuum oven, the nitrogen aged samples were made with short ageing times. For the sake of investigating the impact of oxygen-illustrated thermal ageing on LDPE, a new ageing system should be developed.

- **Trapping parameters model further modified.** In the Chapter 7, three key limitations of the current model were described. In order to achieve the initial aim of connecting ageing, trap properties, and space charge dynamics, the use scenarios of the model need to be divided and more trapping parameters might need to be introduced. Meanwhile, the improved space charge test method could help with the trapping parameters estimation.

- **Numerical connection between the degree of ageing and trapping parameters.** After collecting enough accurate trapping parameters for LDPE with different degrees of ageing, a numerical model could be built and combined with chemical analysis.

List of References

[1] J. . Fothergill and L. . Dissoldo, “Electrical degradation and breakdown in polymers,” 1992.

[2] A. J. Peacock, *Handbook of Polyethylene: Structure, Properties an Applications*. Marcel Dekker, Inc., 2000.

[3] R. Bartnikas, “Performance characteristics of dielectrics in the presence of space charge,” *IEEE Trans. Dielectr. Electr. Insul.*, vol. 4, no. 5, pp. 544–557, 1997, doi: 10.1109/94.625644.

[4] D. I. Bower, *An Introduction to Polymer Physics, Cambridge University Press, 2002;* 2007.

[5] D. I. Bower, *An Introduction to Polymer Physics*. Cambridge University Press, 2007.

[6] David I. Bower, “An introduction to Polymer Physics,” 2002.

[7] J. Mark, *Polymer Data Handbook*. Oxford Universit, 1999.

[8] G. F. Moore, *Electric Cables Handbook*. 1997.

[9] E. F. P. Argaut, H. Auclair, “Development of 500kV low density polyehtylene insulated cable,” pp. 77–81.

[10] M. S. Khalil, “International research and development trends and problems of HVDC cables with polymeric insulation,” *Electr. Insul. Mag. IEEE*, vol. 13, no. 6, pp. 35–47, 1997, doi: 10.1109/57.637152.

[11] C. Guo, L. Zhou, and J. Lv, “Oxidation and Crosslinking Processes During Thermal Aging of Low-Density Polyethylene Films,” *Polym. Polym. Compos.*, vol. 21, no. 7, pp. 449–456, 2013, doi: 10.1002/app.

[12] J. a Tireau, L. a Van Schoors, K. Benzarti, and X. Colin, “Environmental ageing of carbon black-filled polyethylene sheaths employed in civil engineering,” *J. Nanostructured Polym. Nanocomposites*, vol. 5, pp. 94–100, 2009.

[13] S. Ilie and R. Senetscu, “Polymeric Materials Review on Oxidation , Stabilization and Evaluation using CL and DSC Methods,” 2009, [Online]. Available: http://cds.cern.ch/record/1201650/files/Ilie_TE_Technical_Notes.pdf?version=1%5Cnhttp://cds.cern.ch/record/1201650/.

[14] A. Tzimas, S. Rowland, L. Dissado, M. Fu, and U. Nilsson, “Effect of long-time electrical and thermal stresses upon the endurance capability of cable insulation material,” *IEEE Trans. Dielectr. Electr. Insul.*, vol. 16, no. 5, pp. 1436–1443, 2009, doi: 10.1109/TDEI.2009.5293958.

[15] J. P. Crine, “On the interpretation of some electrical aging and relaxation phenomena in solid dielectrics,” *IEEE Trans. Dielectr. Electr. Insul.*, vol. 12, no. 6, pp. 1089–1107, 2005, doi: 10.1109/TDEI.2005.1561789.

[16] A. Tzimas, S. M. Rowland, and L. A. Dissado, “Effect of electrical and thermal stressing on charge traps in XLPE cable insulation,” *IEEE Trans. Dielectr. Electr. Insul.*, vol. 19, no. 6, pp. 2145–2154, 2012, doi: 10.1109/TDEI.2012.6396975.

[17] K. C. Kao, *Dielectric phenomena in solids: with emphasis on physical concepts of electronic processes*. 2004.

[18] J. Li, Y. Zhang, Z. Xia, X. Qin, and Z. Peng, “Action of space charge on aging and breakdown of polymers,” *Chinese Sci. Bull.*, vol. 46, no. 10, pp. 796–800, 2001, doi: 10.1007/BF02900426.

[19] D. R. Wolters and J. J. Van Der Schoot, “Kinetics of charge trapping in dielectrics,” *J. Appl. Phys.*, vol. 58, no. 2, pp. 831–837, 1985, doi: 10.1063/1.336152.

[20] L. Boukezzi, A. Boubakeur, and M. Lallouani, “Effect of artificial thermal aging on the crystallinity of XLPE insulation cables: X-ray study,” *Annu. Rep. - Conf. Electr. Insul. Dielectr. Phenomena, CEIDP*, pp. 65–68, 2007, doi: 10.1109/CEIDP.2007.4451517.

[21] S. Katakai and K. Yahagi, “Effect of thermal aging on breakdown strength of polyethylene,” *Jpn. J. Appl. Phys.*, vol. 24, no. 4 R, pp. 441–445, 1985, doi: 10.1143/JJAP.24.441.

[22] G. Chen and A. E. Davies, “Effect of thermo-oxidative ageing on electrical performance of low density polyethylene,” in *Proceedings of 1995 IEEE 5th International Conference on Conduction and Breakdown in Solid Dielectrics*, 1995, pp. 651–655, doi: 10.1109/ICSD.1995.523067.

[23] G. Chen and Z. Xu, “Charge trapping and detrapping in polymeric materials,” *J. Appl. Phys.*, vol. 106, no. 12, pp. 1–5, 2009, doi: 10.1063/1.3273491.

[24] T. C. Zhou, G. Chen, R. J. Liao, and Z. Xu, “Charge trapping and detrapping in polymeric materials: Trapping parameters,” *J. Appl. Phys.*, vol. 110, no. 4, pp. 1–6, 2011, doi: 10.1063/1.3626468.

[25] N. Liu, G. Chen, and Y. Xu, “Trapping Parameters And Their Relation To Insulation Status of XLPE Cables,” *High Volt. Eng.*, vol. 41, no. 2015, pp. 1154–1166, 2015.

[26] M. Bussac, D. Michoud, and L. Zuppiroli, “Electrode Injection into Conjugated Polymers,” *Phys. Rev. Lett.*, vol. 81, no. 8, pp. 1678–1681, 1998, doi: 10.1103/PhysRevLett.81.1678.

[27] R. H. Fowler and L. Nordheim, “Electron Emission in Intense Electric Fields,” *Proc. R. Soc. London*, vol. 119, no. 781, pp. 173–181, 1928.

[28] M. A. Grado-Caffaro and M. Grado-Caffaro, “Electrical conductance from the Fowler-Nordheim tunneling,” *Optik (Stuttg).*, vol. 116, no. 6, pp. 299–300, 2005, doi: 10.1016/j.ijleo.2005.01.011.

[29] D. K. Das-Gupta and K. Doughty, “Dielectric and conduction processes in polyetherether ketone (PEEK),” *IEEE Trans. Electr. Insul.*, vol. EI-22, no. 1, pp. 1–7, 1987, doi: 10.1109/TEI.1987.298955.

[30] D. Street, “Space Charge and Dielectric Polarization in Polymers,” pp. 24–29, 2000.

[31] J. Brunson and D. Peak, “Hopping Conductivity and Charge Transport in Low Density Polyethylene,” 2010.

[32] K. Kato and H. Okubo, “DEPENDENCE OF CHARGE BEHAVIOR ON ELECTRIC FIELD DISTRIBUTION AROUND GIS SPACER UNDER HVDC APPLICATION,” pp. 23–28, 2015.

[33] N. Liu, G. Chen, and Y. Xu, “Trapping parameters comparison between cable sections from different service conditions by a new trapping-detrapping model,” 2014, vol. 0, no. 2, pp. 449–452, doi: 10.1109/CEIDP.2014.6995737.

[34] G. Chen, Y. Tanaka, and T. Takada, “Electrodes and charge injection in low-density polyethylene using the pulsed electroacoustic technique,” *IEEE Trans. Dielectr. Electr. Insul.*, vol. 8, no. 6, pp. 867–873, 2001.

[35] C. Xiang, Q. Zhou, W. An, and N. Wu, “Effect of Thermal Ageing on Space Charge Characteristics of Cross-linked Polyethylene,” pp. 9–12.

[36] D. H. Mills, P. L. Lewin, and G. Chen, “Ageing of high voltage cable insulation,” *2011 Electr. Insul. Conf. EIC 2011*, no. June, pp. 439–443, 2011, doi: 10.1109/EIC.2011.5996194.

[37] M.FU, G.Chen., and L.A.Dissado, “The Effect of Gamma Irradiation on Space Charge Behaviour and DIelctric Spectroscopy of Low-density Polyethylene,” pp. 442–445, 2007.

[38] N. Liu *et al.*, “An improved model to estimate trapping parameters in polymeric materials and its application on normal and aged low-density polyethylenes,” *J. Appl. Phys.*, vol. 118, no. 6, p. 064102, 2015, doi: 10.1063/1.4928182.

[39] M. Fu, G. Chen, and X. Liu, “Space charge behaviour in LDPE after AC electrical ageing,” *Proc. 2004 IEEE Int. Conf. Solid Dielectr. 2004. ICSD 2004.*, vol. 1, 2004, doi: 10.1109/ICSD.2004.1350329.

[40] G. Chen, M. Fu, X. Z. Liu, and L. S. Zhong, “Ac aging and space-charge characteristics in low-density polyethylene polymeric insulation,” *J. Appl. Phys.*, vol. 97, no. 8, pp. 1–7, 2005, doi: 10.1063/1.1868880.

[41] I. Ieda and N. Nawata, “DC Treeing Breakdown Associated with Space Charge Formation in Polyethylene,” *IEEE Trans. Electr. Insul.*, vol. EI-12, no. 1, pp. 19–25, 1977, doi: 10.1109/TEI.1977.298002.

[42] Y. Zhang, J. Lewiner, C. Alquié, and N. Hampton, “Evidence of strong correlation between space-charge buildup and breakdown in cable insulation,” *IEEE Trans. Dielectr. Electr. Insul.*, vol. 3, no. 6, pp. 778–783, 1996, doi: 10.1109/94.556559.

[43] G. Chen and J. Zhao, “Space charge and thickness dependent dc electrical breakdown of solid dielectrics,” *ICHVE 2012 - 2012 Int. Conf. High Volt. Eng. Appl.*, pp. 12–15, 2012, doi: 10.1109/ICHVE.2012.6357154.

[44] G. Chen and Z. Xu, “Space charge dynamics in low density polyethylene under dc electric fields - art. no. 012008,” pp. 1–4, 2009, doi: 10.1088/1742-6596/142/1/012008.

[45] K. Matsui *et al.*, “Space charge behavior in low-density polyethylene at pre-breakdown,” *IEEE Trans. Dielectr. Electr. Insul.*, vol. 12, no. 3, pp. 406–415, 2005, doi: 10.1109/TDEI.2005.1453444.

[46] L. A. Dissado, V. Griseri, W. Peasgood, E. S. Cooper, K. Fukunaga, and J. C. Fothergill, “Decay of space charge in a glassy epoxy resin following voltage removal,” *IEEE Trans. Dielectr. Electr. Insul.*, vol. 13, no. 4, pp. 903–916, 2006, doi: 10.1109/TDEI.2006.1667752.

[47] A. Tzimas, S. M. Rowland, L. A. Dissado, M. Fu, and U. H. Nilsson, “The effect of dc poling duration on space charge relaxation in virgin XLPE cable peelings,” *J. Phys. D. Appl. Phys.*, vol. 43, no. 21, p. 215401, 2010, doi: 10.1088/0022-3727/43/21/215401.

[48] N. Liu and G. Chen, “Changes in charge trapping/detrapping in polymeric materials and its relation with aging,” *Annu. Rep. - Conf. Electr. Insul. Dielectr. Phenomena, CEIDP*, pp. 800–803, 2013, doi: 10.1109/CEIDP.2013.6747077.

[49] G. Chen, Y. Tanaka, T. Takada, and L. Zhong, “Effect of Polyethylene Interface on Space Charge Formation,” *IEEE Trans. Dielectr. Electr. Insul.*, vol. 11, no. 1, pp. 113–121, 2004, doi: 10.1109/TDEI.2004.1266324.

[50] M. Ieda, G. Sawa, and S. Kato, “A consideration of Poole-Frenkel effect on electric conduction in insulators,” *J. Appl. Phys.*, vol. 42, no. 10, pp. 3737–3740, 1971, doi: 10.1063/1.1659678.

[51] H. Marsacq, D. ; CEA, Centre d’’Etude du Ripault, Monts, France ; Hourquebie, P. ; Olmedo, L. ; Janah, “effects of physical and chemical defects of polyethylene on space charge behaviour,” pp. 672–675, 2011.

[52] G. Mazzanti and M. Marzinotto, *Extruded Cables for High-Voltage Direct-Current Transmission: Advances in Research and Development*. Wiley, 2013.

[53] E. N. Coker, “The oxidation of aluminum at high temperature studied by Thermogravimetric Analysis and Differential Scanning Calorimetry,” no. October, 2013.

[54] S. D. Tables, “Infrared Tables (short summary of common absorption frequencies),” *Spectroscopy*, vol. 2620, 2010.

[55] a. L. Andrady, J. E. Pegram, and Y. Tropsha, “Changes in carbonyl index and average molecular weight on embrittlement of enhanced-photodegradable polyethylenes,” *J. Environ. Polym. Degrad.*, vol. 1, no. 3, pp. 171–179, 1993, doi: 10.1007/BF01458025.

[56] C. F. William Brown, Brent Iverson, Eric Anslyn, “Organic Chemistry,” p. 165, 2013.

[57] W. D. Callister and J. Wiley, *Materials science and engineering an introduction*. .

[58] P. Komitov, G. Kostov, and S. Stanchev, “Ageing of LDPE: Structural changes,” *Polym. Degrad. Stab.*, vol. 24, no. 4, pp. 303–312, 1989, doi: http://dx.doi.org/10.1016/0141-3910(89)90040-2.

[59] M. P. Stevens, “Polymer chemistry an introduction,” pp. 3–4, 2003.

[60] W. Sichina, “DSC as problem solving tool: measurement of percent crystallinity of thermoplastics,” *Perkin Elmer Instruments, and PETech*, 2000, [Online]. Available: http://scholar.google.com/scholar?hl=en&btnG=Search&q=intitle:DSC+as+Problem+Solving+Tool+:+Measurement+of+Percent+Crystallinity+of+Thermoplastics#0.

[61] N. I. Nikonorova, N. F. Bakeyev, S. K. Fakirov, and V. A. Kargin, “Influence of thermal history of polyethylene crystallization from solution,” *Polym. Sci. U.S.S.R.*, vol. 11, no. 10, pp. 2503–2511, 1969, doi: http://dx.doi.org/10.1016/0032-3950(69)90144-0.

[62] C. ALbano and R. Sciamanna, “Effects of thermal history on the properties of semicrystalline thermoplastics: Polypropylene.”

[63] W. G. Harland, M. M. Khadr, and R. H. Peters, “High-density polyethylene: thermal history and melting characteristics,” *Polymer (Guildf).*, vol. 13, no. 1, pp. 13–19, 1972, doi: http://dx.doi.org/10.1016/0032-3861(72)90029-8.

[64] C. Augusto, F. De Oliveira, M. Tadeu, T. Pacheco, K. Lednev, and L. Silveira, “Raman spectroscopy in forensic analysis : identification of cocaine and other illegal drugs of abuse,” no. November 2015, pp. 28–38, 2016, doi: 10.1002/jrs.4864.

[65] A. M. M. A. C. Donald, A. S. Vaughan, and P. W. Yeth, “On Confocal Raman Spectroscopy of Semicrystalline Polymers : The Effect of Optical Scattering,” vol. 57, no. 12, 2003.

[66] T. Mizutani, “Space charge measurement techniques and space charge in polyethylene,” *IEEE Trans. Dielectr. Electr. Insul.*, vol. 1, no. 5, pp. 923–933, 1994, doi: 10.1109/94.326659.

[67] D. Fabiani *et al.*, “Polymeric HVDC cable design and space charge accumulation.,” *IEEE Electr. Insul. Mag.*, vol. 23, no. 6, pp. 11–19, 2007, doi: 10.1109/MEI.2007.4389975.

[68] M. S. Khalil and B. S. Hansen, “Investigation of space charge in low-density polyethylene using a field probe technique,” *IEEE Trans. Electr. Insul.*, vol. 23, no. 3, pp. 441–445, 1988, doi: 10.1109/14.2385.

[69] N. Ando and F. Numajiri, “Experimental Investigation of Space Charge in XLPE Cable Using Dust Figure,” *Electr. Insul. IEEE Trans.*, vol. 75, no. February, 1979.

[70] R. E. Collins, “Analysis of spatial distribution of charges and dipoles in electrets by a transient heating technique,” *J. Appl. Phys.*, vol. 47, no. 11, pp. 4804–4808, 1976, doi: 10.1063/1.322521.

[71] T. Pawlowski, R. J. Fleming, and S. B. Lang, “LIMM study of Space Charge in Crosslinked Polyethylene,” pp. 196–199.

[72] H. Von Seggern, “Thermal-pulse technique for determining charge distributions: Effect of measurement accuracy,” *Appl. Phys. Lett.*, vol. 33, no. 2, pp. 134–137, 1978, doi: 10.1063/1.90282.

[73] P. Notingher, S. Agnel, and A. Toureille, “Thermal step method for space charge measurements under applied dc field,” *Dielectr. Electr. Insul. IEEE Trans.*, vol. 8, no. 6, pp. 985–994, 2001, doi: 10.1109/94.971455.

[74] N. H. Ahmed and N. N. Srinivas, “Review of space charge measurements in dielectrics,” *IEEE Trans. Dielectr. Electr. Insul.*, vol. 4, no. 5, pp. 644–656, 1997, doi: 10.1109/94.625650.

[75] J. L. F. Chapeau, C. Alquie, “The pressure wave propagation method for the analysis of insulating materials: application to LDPE used in HV Cables,” no. 3, pp. 405–410, 1986.

[76] G. M. Sessler, J. E. West, and G. Gerhard, “High-resolution Laser-pulse Method for Measuring Charge Distributions in Dielectrics,” *Phys. Rev. Lett.*, vol. 48, no. 8, pp. 563–566, 1982, doi: 10.1103/PhysRevLett.48.563.

[77] T. Takada and T. Sakai, “Measurement of Electric Fields at a Dielectric/Electrode Interface Using an Acoustic Transducer Technique,” *IEEE Trans. Electr. Insul.*, vol. EI-18, no. 6, pp. 619–628, 1983, doi: 10.1109/TEI.1983.298700.

[78] J. Zhao, “Dynamics of space charge and electroluminescence modelling in polyethylene,” p. 136, 2012.

[79] N. O. Copying, W. Bsi, P. Except, A. S. Permitted, and B. Y. Copyright, *PD IEC / TS 62758 : 2012 BSI Standards Publication Calibration of space charge measuring equipment based on pulsed electroacoustic (PEA) measurement principle*. 2012.

[80] G. Chen, Y. L. Chong, and M. Fu, “Calibration of the Pulsed Electroacoustic Technique in the Presence of Trapped Charge,” vol. 1974, 2006, doi: 10.1088/0957-0233/17/7/041.

[81] Z. Xu, “Space charge measurement and analysis in low density polyethylene film,” 2009.

[82] N. Liu, C. Zhou, G. Chen, and L. Zhong, “Determination of threshold electric field for charge injection in polymeric materials,” *Appl. Phys. Lett.*, vol. 106, no. 19, p. 192901, 2015, doi: 10.1063/1.4921050.

[83] Z. An, J. Cang, X. Chen, and Y. Liu, “Method for investigating threshold field of charge injection at electrode/dielectric interfaces by space charge observation,” *Appl. Phys. Lett.*, vol. 101, no. 17, pp. 1–5, 2012, doi: 10.1063/1.4757985.

[84] E. Measurements, “Investigating dc polyethylene threshhold by space charge,” vol. 7, no. December, pp. 797–803, 2000.

[85] G. C. Montanari, F. Palmieri, G. Mazzanti, C. Laurent, and G. Teyssedre, “AC charge injection investigated by means of space charge measurements: threshold and frequency dependence,” *Proc. 7th Int. Conf. Prop. Appl. Dielectr. Mater. (Cat. No.03CH37417)*, vol. 3, no. 2, pp. 895–899, 2003, doi: 10.1109/ICPADM.2003.1218566.

[86] Z. Li *et al.*, “Thermal ageing and its impact on charge trap density and breakdown strength in ldpe 1,” pp. 23–28, 2015.

[87] T. Y. G. Tay, C. Science, Y. Tanaka, and T. Takada, “Electrodes and Charge In j ection in U sing the Pulsed Electroacoustic Technique,” *IEEE Trans. Dielectr. Electr. Insul.*, vol. 8, no. 6, pp. 867–873, 2001.

[88] E. Testing, “Standard Test Method for Dielectric Breakdown Voltage and Dielectric Strength of Solid Electrical Insulating Materials Using Impulse Waves,” *Test*, vol. 97, no. Reapproved 2012, pp. 2–5, 2015, doi: 10.1520/D3426-97R12.2.

[89] M. S. Khalil, “The role of BaTiO3 in modifying the dc breakdown strength of LDPE,” *IEEE Trans. Dielectr. Electr. Insul.*, vol. 7, no. 2, p. 261, 2000, doi: 10.1109/94.841819.

[90] W. Weibull, “A Statistical Distribution Function of Wide Applicability,” *Journal of Applied Mechanics*, vol. 103. 1951.

[91] Y. Wang, Y. C. Chan, Z. L. Gui, D. P. Webb, and L. T. Li, “Application of Weibull distribution analysis to the dielectric failure of multilayer ceramic capacitors,” *Mater. Sci. Eng. B-advanced Funct. Solid-state Mater.*, vol. 47, no. 3, pp. 197–203, 1997, doi: 10.1016/S0921-5107(97)00041-X.

[92] S. L. Fok and J. Smart, “The accuracy of failure predictions based on Weibull statistics,” *J. Eur. Ceram. Soc.*, vol. 15, no. 9, pp. 905–908, 1995, doi: 10.1016/0955-2219(95)00061-X.

[93] A. E. Chen, G. Davies, “Effect of thermo-oxidative ageing on electrical performance of low density polyethylene,” pp. 1–5, 2005, doi: 10.1002/pen.20231.

[94] L. a. Dissado, S. J. Urban, and P. a. Norman, “Breakdown statistics of the space-charge ageing model for polymericinsulation,” *Proc. Conf. Electr. Insul. Dielectr. Phenom. - CEIDP ’96*, vol. 1, 1996, doi: 10.1109/CEIDP.1996.564615.

[95] L. S. and Z. L. George Chen, “Space charge in nanodielectrics and its impact on electrical performance,” in *IEEE 11th International Conference on the Properties and Applications of Dielectric Materials, Sydney*, 2015, pp. 1–6, doi: 10.1520/E0948-09.2.

[96] P. Hahn, R. Polansky, C. Republic, and C. Republic, “LIFETIME ESTIMATION OF THERMOPLASTICS COMPOUNDS FOR CABLE SHEATHING USING ARRHENIUS EQUATION k = Ae,” no. 1, 2015.

[97] Z. Li, N. Liu, S. Gabriel, and G. Chen, “Thermal Ageing and Its Impact on Charge Trap Density and Breakdown Strength in Polyethylene,” 2016.

[98] J. Brunson, “Hopping Conductivity and Charge Transport in Low Density Polyethylene Hopping Conductivity and Charge Transport in Low Density Polyethylene,” 2010.